Universitetet
i Stavanger

FACULTY OF SCIENCE AND TECHNOLOGY

MASTER'S THESIS

Study programme: Mathematics and Physics	Spring / Autumn 2017 Open/Confidential
Author: **Seyedeh Shahrzad Rasouli**	Shahrzad Rasouli (signature)

Supervisor: Professor Dr. Steinar Evje (UiS)

Co-supervisors: Dr. Helmer André Friis (IRIS) and Dr. Ingunn W. Jolma (IRIS)

Title of master's thesis:

Tumor Interstitial Fluid Pressure Distribution – Analytical and Numerical Study

Credits: 60 ECTS

Keywords: Interstitial fluid pressure Cancer Numerical simulations	Number of pages: 103 Stavanger, 27.11.2017

Title page for Master's Thesis
Faculty of Science and Technology

In the Name of Allāh, the Most Gracious, the Most Merciful

Tumor Interstitial Fluid Pressure Distribution - Analytical and Numerical Study

by

Seyedeh Shahrzad Rasouli

Thesis submitted in fulfillment of
the requirements for degree of
MASTER OF SCIENCE
(MSc)

Faculty of Science and Technology
Department of Mathematics and Physics
2017

Preface

This dissertation is submitted in fulfillment of the requirements for degree of MSc. (Master of Science) Mathematics and Physics at the Faculty of Science and Technology (Department of Mathematics and Physics), University of Stavanger (UiS), Norway. The research work presented in this thesis is conducted mainly at International Research Institute of Stavanger (IRIS). The outcome of this work together with new findings from an ongoing research work will hopefully result in a journal publication.
A relevant background information and literature review to this work, followed by the work objectives and problem statement is given in Chapter 1, the introduction. Chapter 2 discusses in details two of the main models related to the work. The main results and related discussions are presented in Chapter 3. Finally, conclusions and recommendations are given in Chapter 4.

Acknowledgements

All glory and honour to Allah for his grace, encouragement and guidance.
I would like to address my utmost thanks and gratitude to my main thesis advisor, Dr. Helmer André Friis for his excellent guidance and supervision during the entire period of this research.
I wish to express my thanks to Dr. Ingunn Westvik Jolma, research scientist at Medtech, for her very helpful technical support, specially with regards to biological concepts related to this work. Her time for reviewing this thesis is also highly appreciated.
My great appreciation goes to my academic advisor, Professor Dr. Steinar Evje for the insightful and encouraging discussions we had.
My thanks are also to the Medical Technology research group (Medtech), and especially the manager, Dr. Thor Ole Gulsrud, for this unique research opportunity at Medtech research group.
Mr. Erich Christian Suter was an indispensable help in some technical parts of the research work.
My sincere thanks are also directed to the IT department at IRIS, especially Mr. Geir Magne Sande for the great arrangements and IT supports.
I am greatly thankful to the happy and encouraging faces, whom I met at IRIS every day for including me in their nice and friendly community at IRIS.
Finally, I would like to express my sincere gratitude to my dear parents for all their supports and their kindness. I am most grateful for the encouragements of my dear husband, Reza; and, I am thankful to our dear son, Mohammad, for his patience and all the joy he brings.

Abstract

Cancer is one of the deadliest diseases in the world and although huge research efforts have been applied to improve survival rates, there are still great challenges in treatment of the disease. Many factors contribute in the process of drug delivery and its absorption in tumor cells. Inside the tumor, the high interstitial fluid pressure (IFP) is one of the main barriers for drug penetration. In this work, interstitial fluid pressure is analytically investigated for homogeneous (without necrotic core) and heterogeneous (with necrotic core) tumor by considering the periphery region as a region between necrotic core and tumor edge. This is performed by adjusting a constant value of interstitial hydraulic conductivity for tumor and a lower constant value of interstitial hydraulic conductivity for normal tissue. Then, we focus on a heterogeneous tumor surrounded by normal tissue with the categorization of the necrotic core, periphery and intermediary regions and analytically investigate the tumor interstitial fluid pressure distribution for periphery and intermediary regions in some limiting cases. As the interstitial fluid pressure deeply correlates with the interstitial hydraulic conductivity, for further investigation, it is assumed that the interstitial hydraulic conductivity adopts a constant value in the central region and normal tissue; while it is changing radially continuously throughout the periphery and intermediary regions. In order to study such problems, more generally it is necessary to apply numerical methods. The numerical approach used in this work helps to investigate the tumor interstitial fluid pressure distribution for all regions. The effect of the necrotic core size on the maximum interstitial pressure is investigated. Moreover, the influence of the sizes of periphery and intermediary regions is inquired. From our numerical simulations, it is found that the abundance of blood vessels inside the periphery region influences the distribution of the interstitial fluid pressure; in such a manner that, increasing numbers of well-functional blood vessels causes a higher maximum value of the interstitial fluid pressure. A better understanding of interstitial fluid pressure distribution within a tumor, and methods to describe this in numerical terms, can be used in combination with imaging tools in order to gain insights in cancer cells aggressiveness and treatment planing. We also consider a more real model of a tumor where an asymmetric distribution of blood vessels is considered by including areas with variable arterial hydraulic conductivity in the periphery region. In this situation, the maximum interstitial fluid pressure is not observed in the center of the tumor, unlike the symmetric cases.

Contents

List of Figures

List of Tables

Chapter 1

Introduction

1.1 An insight into cancer biology

In this section some general, but important, terms related to cancer are introduced and defined. A simple overview of the mechanism through which abnormal cell division occurs and how and why tumors grow to to become a cancerous tumor is provided. Finally, a brief section about cancer diagnosis and treatment is presented.

1.1.1 What is cancer?

The word cancer comes from the word for crab because, like a crab, they "grab on and don't let go" [43]. Our body is made up of billions of cells which are the microscopic pieces of our tissues and organs [23] . Normally, every day, millions of cells are destroyed inside our body because of senility or injuries. Meanwhile, successor cells come instead. Sometimes, and for reasons we do not fully understand, a cell has been deformed and changes to a cancerous cell which is not similar to the normal cells of the body. An abnormal new growth of cells is defined as a *neoplasm*. This abnormal growth of cells is usually more rapid than that of normal cells and will continue if not treated. If a neoplasm forms a mass it is commonly referred to as a *tumor* [28]. According to [13], in general, neoplasms are categorized into four main groups: benign neoplasms, in situ neoplasms, malignant neoplasms, and neoplasms of uncertain or unknown behavior. Here, brief definitions and specifications for the benign and malignant are provided. *Benign* neoplasms (or tumors) grow relatively slowly and don not spread into the surrounding tissue and they are made up of cells that are quite similar to normal cells. On the other hand, *malignant* neoplasms (or tumors), also called cancerous neoplasms, grow significantly faster than benign ones and spread into and hurt the surrounding tissues. Gradually, aimless and fast divisions of the cancerous cells in any origin creates tumor lumps. This lump can discharges some hormones or it can apply pressure to the surrounding tissue. It causes huge disruptions in the body. They can also spread throughout the body into other organs. While, most benign tumors respond well to treatment, malignant neoplasms are often resistant to treatment, may spread to other parts of the body and they sometimes recur after they are removed.

1.1.2 Tumor growth and cancer development

Our life starts with a single cell. Each type of normal cells has specific tasks and set of knowledge or instructions, known as *genes*, in their DNA. Consequently, they know when to stop replicating and die; the phenomenon by which cells die after a period of time is called *apoptosis*. When a cell divides, it splits into two daughter cells (a process known as 'replication'), smaller versions of the original cell (the mother cell). Each daughter cell gets a complete copy of all the DNA instructions that its parent had. The daughter cells can then become mother cells to their own daughter cells, passing along the same genes they inherited from their mother, and the process continues [35]. Although cells die after a period of time, division certifies that new cells take the place of dead ones. Cells are guided by hormones and catch messages from them. Through vascular system, blood carries these messages in addition to carrying waste fluid and oxygen (according to

the function of the arterioles and venules, described in the following sections). On the other hand, the lymphatic system, as a part of our body's defense (immune) system, drains excess fluid [23].
In case the DNA of cells becomes damaged, the cells replication process is disordered and negatively affected by the damage happened in the DNA; therefore, this may result in the development of cancerous cells; i.e. the cells can not anymore distinguish when to start dividing and when to die. When these cells start to divide abnormally, leading to formation and growth of lumps, a neoplasm or tumor forms. Fig.(1.1a) illustrates the formation and dividing of cancerous cells within an area; cancerous cells have not yet spread to the surrounding tissue. Similar to normal cells, cancerous cells cannot live without oxygen and nutrients. To continue growing, a tumor needs to start creating its own blood vessels to get sufficient nutrition such as oxygen to stay alive and continue getting larger. The process of developing a new blood-supply system is called *angiogenesis*. In such situation, it is quite probable for the cancerous cells to invade the surrounding tissue, as shown in Fig.(1.1b). Moreover, as it is shown in Fig.(1.1b), active cancerous cells can enter vessel or lymphatic capillaries and move to other organs of the body and create a tumor there; invasion of cancerous cells to the surrounding tissue and other organs of body is called *metastasize*. According to the UK Cancer Research, [42], as the cancer grows, it will squeeze and block small blood vessels in the area; this leads to low blood and oxygen levels that can eventually cause some of the normal tissue will begin die off.

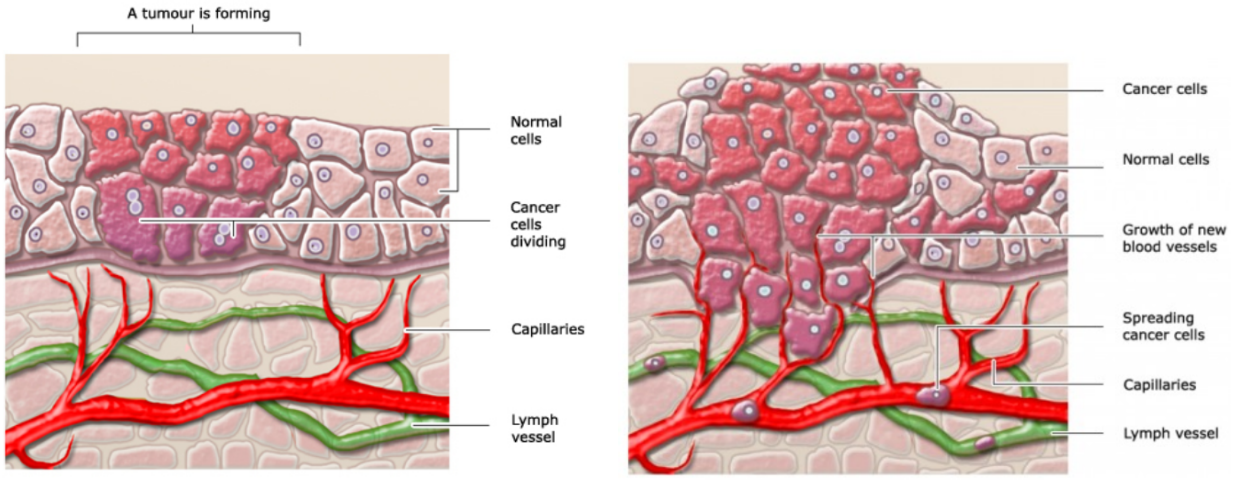

(a) (b)

Figure 1.1: (a) Cells start to divide abnormally, leading to formation and growth of lumps, (b) The cancerous cells invade surrounding tissue and enter vessel or lymphatic capillaries through which can move to other organs of the body and create a tumor there.

For a tumor to grow, availability of blood supply is a vital factor. As the tumor gets bigger in size, the distance between center of tumor and blood vessels becomes greater; therefore, less oxygen and nutrition are delivered to the center of tumor. As a result, a *necrotic core* develops in the central region. Once a cancer can stimulate blood vessel growth, it can quickly grow bigger. It will stimulate the growth of many new blood vessel capillaries from the nearby blood vessels to get nutrients and oxygen. Compared to the regular vasculature of normal tissues, blood vessels in tumors are often highly abnormal. These physiological differences can cause problems in cancer treatment [5].

1.1.3 Diagnosis and treatment of cancer

There are over 200 different types of cancer. The characteristics of the cancer are distinguished by where in the body it appears [30]. In addition, different factors in the environment and style of life, target different organs of our body to create cancerous cells. For example, the UV radiation from the sun targets the skin or smoking targets the lungs [30]. The first step in treating tumor is to get information about symptoms and the stage of the cancer (i.e. how much it has spread throughout the body); this gives us information to better

recognize the type of the tumor. Some methods such as X-rays, CT scans, MRI scans and PET traces are applied to discover the position of a tumor and discover the organs which can be affected by that. The only clear method to diagnose cancer is to look at the extracted cancerous tissue under a microscope (known as biopsy), blood test is a good alternative [42]. Generally, the main aims of different types of treatment are to remove the cancerous tissue by surgery, radiation or chemical method and stop the replication of cancerous cells, reduce the abundances of blood vessels in the tumor tissue and consequently, decrease the growth and spread of cancerous cells [31][26][10][38][45]. Sometimes an operation to take the tumor out of the organ can be effective. For some types of tumor, chemotherapy drugs or radiotherapy are used to shrink the tumor before and after operation to prevent growing back. More details about the treatment of various types of cancer is out of scope for this research work and can be found in the above-mentioned selected references.

1.2 Fluid flow in porous media

In this section, first, the Darcy law, one of the most fundamental laws of fluid flow in porous media together with further developments based on this law are presented and important parameters are defined and discussed. in addition, fundamentals and basic concepts related to fluid flow in biological systems and governing parameters are provided.

1.2.1 Darcy Law

Normally, whenever there is a discussion of the flow of fluid(s) through porous media, one of the very first topics to acknowledge is the outstanding experimental work by Henry Philibert Gaspard Darcy [8] that resulted in the following equation while he was investigating the flow of water through sand filters for water purification in Dijon, a city in France:

$$Q = \frac{c \cdot A \cdot \Delta h}{L}$$

In this equation c, the constant of proportionality, was introduced to be a characteristic parameter of the sand. Later, it was Muskat (1937) who first refined Darcy's equation for single-phase flow by including viscosity in the single (fluid) phase equation of Darcy; this change made it suitable, specially for the petroleum industry. Therefore, the original Darcy equation is transformed to the current well-known version (presented below) which instead of Darcy equation seems fairer to be called "Darcy-Muskat" equation:

$$v = \frac{k}{\mu}\frac{dp}{dx}$$

Where v is the superficial velocity (cm/s) or also well known as Darcy velocity, dp/dx (atm/cm) is the pressure gradient in the flow direction, μ is the fluid viscosity (cp), and k (D) is the new proportionality constant called "permeability" (which completely defines dynamically the porous medium as the carrier of a homogeneous fluid in viscous motion) with the following definition according to Muskat [19]:
The formal definition of the permeability of a porous medium may, therefore, be stated as the volume of a fluid of unit viscosity passing through a unit cross section of the medium in unit time under the action of a unit pressure gradient. It is thus a constant determined only by the structure of medium in question and is entirely independent of the nature of the fluid.
Another format of the "Darcy-Muskat" equation is presented below:

$$q = \frac{k \cdot A}{\mu}\frac{dp}{dx}$$

Where q is the flow rate of the fluid passing the porous medium (cc/s) and A (cm2) is the total cross section of the porous medium perpendicular to the flow direction. Note that the above-mentioned units for different parameters are commonly used in petroleum industry and for flow in biological systems, more relevant consistent units are used.

1.2.2 Flow in biological systems

Our body is mostly made up of fluid which is inside or outside of the cells. Thus, fluid in our body is divided into two original areas, intracellular and extracellular. The intracellular (IC) compartment contains the fluid that bathes the inside of the cells of the body. The extracellular (EC) compartment is the fluid that lies outside of the cells. Consequently, the extracellular compartment is separated into two areas of intravascular (fluid inside the blood capillaries) and interstitial (fluid outside the blood vessels) [17]. Although the fluid in intracellular and extracellular is constant, it moves inside and outside cells. The existence of cell membrane affects the getting in or out of the cells. The cell membrane can be less permeable, semipermeable or high permeable. It means that the permeability of the membrane determines how much fluid can pass through the membrane [17]. The fluid composition and the hydraulic conductivity are the main properties that govern fluid transport in a biological system.
Interchanges between the cells in the tissue and the blood build up the composition of tissue fluid. So, In different areas of the body there are different compositions of tissue fluid. Some contents of blood such as red blood cells can not pass through the capillary walls. Therefore, they can not enter into the tissue fluid. Hydraulic conductivity, symbolically represented as K (cm^2/mmHg.sec), is a property that describes the ease with which a fluid (usually water) can move through pore spaces or fractures. It depends on the intrinsic permeability [1] of the material [14].

1.3 Review of some relevant publications

Nowadays, showing the principle of the tumor growth and clarifying how it manifests through cancer types are defined by large-scale molecular profiling data which is an important benefit for computational biologists. Mathematical modeling has an exclusive role to show the physical development of cancer [25]. Many factors play roles in treating tumors. In the following, a review of related mathematical modeling research works from literature is provided.

Tumor properties (e.g. tumor size) have an important effect on drug transport and its absorption by tumor cells. 3-D models reconstructed from magnetic resonance images (MRI) can be utilized as a powerful tool to study the influence of tumor properties on drug delivery and uptake. Through a numerical method, Zhan et al. [47] simulated the physical processes to study the drug transport in 3-D tumor models of different sizes. Using a pharmacodynamics model [2], they tried to evaluate the therapeutic influence of each tumor, according to anticipated intracellular drug concentration. Results show that changing the size of tumor causes non-linear changes of interstitial fluid pressure. In addition, the distribution of tumor vasculature, could vary depending on the particular tumor type, size and growth stage. MRI determines the effect of tumor size on drug transport and its uptake by tumor cells. Zhan et al. [47] argue that there is nonlinear relationship between spatial-mean interstitial fluid pressure and tumor volume. Moreover, transvascular transport is more efficient in small tumors, because of the low spatial-mean interstitial fluid pressure and dense micro-vasculature.

Recently, Soltani et al. [37], modeled the distribution of positron emission tomography tracer (PET tracer) [3] uptake by considering a general equation which is used for solute transport modeling. in their model they could incorporate the combined effect of transport parameters of solid tumor such as hydraulic conductivity togethr with transvascular permeability. Using a mathematical model for angiogenesis process, they produced the capillary network of a solid tumor and normal tissues. In addition, pressure distribution was calculated by a mathematical method, which solved for blood flow in the vessels and fluid flow in the

[1] vascular permeability: the movement of fluids and molecules between the vascular and extravascular compartments.

[2] Pharmacodynamic modeling is based on a quantitative integration of pharmacokinetics, pharmacological systems, and (patho-) physiological processes for understanding the intensity and time-course of drug effects on the body. Application of such models to the analysis of meaningful experimental data allows for the quantification and prediction of drug–system interactions for both therapeutic and adverse drug responses.[11]

[3] positron emission tomography (PET)[1] is a nuclear medicine functional imaging technique that is used to observe metabolic processes in the body. The system detects pairs of gamma rays emitted indirectly by a positron-emitting radionuclide (tracer), which is introduced into the body on a biologically active molecule. Three-dimensional images of tracer concentration within the body are then constructed by computer analysis.

interstitum, simultaneously. Afterwards, spatiotemporal distribution model was exerted to model distribution of PET tracer uptake. They calculated convention and diffusion from vessel to tissue and in the tissue. Moreover, they investigated the efficiency of convection an diffusion on tracer transport; these results showed that convection terms have negligible effect on tracer transport.

Liu et al. (2016)[22] presented the theoretical basis to approximate the absolute value of tumor interstitial fluid pressure (TIFP). Moreover, a method was developed to measure TIFP, noninvasively. By paying attention to the specific boundary and continuity conditions in addition to using the MRI technology, theoretical variables were transformed into measurable variables. They showed that an analysis of the changes of tissue fluid flow in the tumor rim and surrounding tissue gives the approximate TIFP in the center of the tumor. These come from three noninvasive measurable parameters: (i) a guess of the velocity of the tumor interstitial fluid at the tumor surface, which has the maximum value, (ii) size of the distance from the tumor surface to the absorption region of the tumor exudates, and (iii) an assessment of the hydraulic conductivity of the interstitium through which the tumor exudate travels. The non-uniform fluid flow in the rim of the tumor was experimentally investigated; they showed that the fluid flow within the tumor rim, even for round-shaped tumors, was not uniform.

One of the reasons that cause the fall of cancer therapy is the complicated capillary network of angiogenesis. To investigate the effect of capillary network structure on drug delivery, a simulation (multi-scale mathematical method) of drug delivery to a solid tumor was applied by Sefidgar et al. (2015) [33]; In this research work it was suggested that the mathematical model contains blood flow through vessels, solute and fluid diffusion, convective transport in extracellular matrix and extravasation from blood vessels. The effect of heterogeneous dynamic capillary network on interstitial fluid flow and drug transportation and absorption was shown by a multi-scale method. In addition, drug delivery was simulated by convection-diffusion equation. Drug transport was simulated by three approaches: without using a vascular network, using a static vascular network, and using a dynamic vascular network. Uniform and higher drug concentration of avascular approach than that of vascular approaches was one of the outcomes of implementing this method. In The dynamic vascular network, more real case occurred with more irregular blood vessels, high interstitial pressure, and more heterogeneity in drug distribution than other two approaches.

The delivery efficiency of anti-cancer drug and its absorption by cancerous cells was determined by an important factor of interstitial fluid transport [24]. Charjoui et al.(2015) [24] performed a general numerical simulation of the interstitial fluid transport which builded 3D models of tumor and its surrounded normal tissue assuming constant interstitial hydraulic conductivity. Moreover, the effect of some factors on interstitial fluid pressure (IFP) such as tumor radius, size of normal tissue, tissue hydraulic conductivity, and presence of the necrotic core are investigated. The main aim here [24] was to test the effects of the geometrical properties of tumor and its surrounding normal tissue on IFP. It was verified that the tumor size had a considerable effect on IFP distribution; increasing the size of the tumor causes increased IFP. In contrast, different shapes and volumes of surrounding normal tissue had a moderate effect on IFP inside the tumor and its surrounding normal tissue. Moreover, increase in hydraulic conductivity of the interstitium caused decrease in IFP inside the tumor. It was shown that applying treatment methods that increase the hydraulic conductivity of the interstitium can improve the drug delivery. Additionally, presence of necrotic core inside the tumor exposed considerable effects on IFP. Consequently, formation of the tumor and its surrounded normal tissue affected IFP distribution inside the interstitium. Moreover, bigger tumors produced higher IFP. The size of the normal tissue had negligible effects on IFP; however, presence and location of necrotic core inside the tumor interstitium changed the IFP [24].

Computational methods are strong tools for the investigating the drug delivery process. Sefidgar et al. (2015) [32] studied the mechanism of transportation of anti-cancer drug from the injection part to absorption by tumor. They presented a numerical solution in which fluid flow and solute transport equation were solved together to study the effect of shape and size of the tumor on drug delivery. They figured out that drug delivery in prolate shape of the tumor was effectively better than other shapes of tumor. In addition, increasing the size of the tumor showed a decrease in drug concentration in interstitial fluid. They observed that the drug concentration in interstitial fluid did not depend on osmotic and interavascular pressure. More-

over, among diffusion and convection mechanisms of drug transport, diffusion was better in most different tumor shapes and size. In the tumors that convection had remarkable effect, the drug concentration was larger than that of other tumors at the same time post injection. The reason of the fact that systematic performance causes nonuniform drug distribution was investigated by the computational methods defined by [32].

The interstitial hydraulic conductivity has an important role on determining interstitial fluid pressure. Commonly, both in a tumor and normal tissue, the hydraulic conductivity has been considered as a constant. Liu et al. (2015) [21] claimed that the hydraulic conductivity and the curvature of the tumor interstitial fluid pressure (TIFP) are not continuous at the surface of the tumor. They assumed avascular or poorly vascularized tumor surrounded by normal tissue; therefore, they argued that it was reasonable to divide a tumor into three regions of necrotic core (in which tumor interstitial fluid pressure and interstitium structure are uniform), periphery, and intermediary (the region between periphery and normal tissue) regions. Through periphery and intermediary regions, fluid composition and tumor cells vary. They showed that the hydraulic conductivities of the necrotic core and normal tissue were constant with the difference that the hydraulic conductivity of the necrotic core was higher than that of the normal tissue. In addition, the hydraulic conductivity of periphery region was monotonically decreasing by increasing the distance from the center of the tumor. In contrast, the hydraulic conductivity of intermediary was increasing to the value of the normal tissue, by increased radial position. As a result, according to the relation between tumor interstitial fluid pressure and the hydraulic conductivity, they suggested a method to approximate the actual TIFP distribution.

In 1988, Baxter et al. [3] developed a general theoretical framework for transvascular exchange and extravascular transport of fluid in tumors. For the sake of simplicity, they assumed a homogeneous tumor with no lymphatics and no extravascular binding. According to their numerical solution, in a uniformly perfused tumor, the important reason for heterogeneous distribution of nonbinding macromolecules was the high interstitial fluid pressure. The interstitial pressure was anticipated by defined models. It was observed that the highest interstitial fluid pressure occurred at the center of the tumor and it had the lowest value in the periphery of the tumor, while the steep gradient of pressure was anticipated in the periphery. The outcomes of their work showed that although factors such as heterogeneous distribution of blood supply and hindered interstitial transport determined the permeation of macromolecules into tumors, high interstitial pressure had a significant role on drug delivery and its absorption by cancerous cells.
In 1990, Baxter et al. [4] considered a more real case by assuming nonuniform perfused tumor and applied the same theoretical framework. In the model, the effect of presence of lymphatics was examined. One of the consequences was that the interstitial pressure in the center of the tumor did not decrease by the presence of the necrotic core. In contrast, if lymphatic presents in the tumor, it caused reductions in interstitial fluid pressure inside the tumor.

1.4 Problem statement

The TIFP influences the effectiveness of drug delivery to cancerous tissue. The need for a proper understanding of fluid interstitial pressure inside a tumor and its surrounding normal tissue serves as one of the main motivations for this work. In this work, first, I have examined the work by L.T. Baxter and R. Jain [3][4], which is one of the highly cited publications in this field, and present analytical solutions for some specific cases of tumor; such as, homogeneous and heterogeneous tumor. Then, I focus on the model by L.J. Liu and M. Schlesinger [21], in which a tumor surrounded by normal tissue is categorized to three regions of necrotic core, periphery and intermediary regions. In addition analytical investigation of the interstitial pressure for regions of periphery and intermediary are provided in two limiting cases. Further, in this study, the impact of different important contributing biological properties of a typical tumor on TIFP is investigated, by using computational methods, and also we compare the models described by Baxter and Liu in some relevant cases. Moreover, in this work, we will focus on a numerical investigation of the TIFP distribution. It is predicted that high pressure is an indicator of cancer cell aggressiveness and consequently creates the barrier on treating tumors. While, low TIFP is related to a high permeable interstitial which caused the facility of drug delivery.
Relevant questions that will be investigated by using a numerical model, are:

- How does the size of the necrotic core affect the tumor interstitial fluid pressure distribution?
- How will the arterial, venous and lymphatic hydraulic conductivity influence on the distribution of tumor interstitial fluid pressure?
- How is the pressure distribution affected by an asymmetric distribution of blood vessel capillaries?

Chapter 2

Mathematical Formulation

Tumor interstitial fluid pressure has been investigated by using different approaches over the years. Here, we focus on two mathematical models,

1. Models presented by L.T. Baxter and R.K. Jain in 1988 [3] and 1990 [4], where they considered the constant interstitial hydraulic conductivity throughout a tumor and lower constant interstitial hydraulic conductivity in a normal tissue.

2. A model based on Baxter models, but improved, published by L.J. Liu and M. Schlesinger in 2015 [21], where they categorized a tumor surrounded by normal tissue in three different regions (necrotic core, periphery and intermediary regions) and defined a continuous variation of the interstitial hydraulic conductivity; such that, it gets the constant value in the necrotic core and it is decreasing throughout the periphery region and then it should be monotonically increasing up to the constant value of interstitial hydraulic conductivity in the normal tissue.

In this chapter, the first part (section (2.1)) is a detailed description of the model proposed by Baxter et al. [3], in which they investigated the interstitial fluid pressure distribution for the following case:

- Homogeneous tumor (with out necrotic core)
  - case 1: An alymphatic, isolated, uniform tumor.
  - case 2: An alymphatic, uniform tumor, surrounded by normal tissue.
- Heterogeneous tumor (consisting necrotic core) surrounded by normal tissue

In the second part (section (2.2)) we will have a closer look at the model described by Liu et al. [21], where the role of defined interstitial hydraulic conductivity on tumor interstitial fluid pressure distribution was investigated. Liu et al. have analytically found the interstitial fluid pressure distribution for two limiting cases .
In section (2.2.5), for the sake of improvement, we apply our numerical method to investigate the actual tumor interstitial fluid pressure, by considering the introduced continuous variation of the hydraulic conductivity by Liu.
These two models are served as the main backgrounds for the results presented in Chapter 3.

2.1 Based on Baxter-Jain model

Jain et al. (1988) [16] investigated the determining factors on blood flow in the vascular network. Later, Baxter et al. [3] developed a theoretical framework for transvascular exchange and extravascular transport of fluid in tumors. Their numerical models showed that in a uniformly perfused tumor the high interstitial pressure is a major reason for heterogeneous distribution of nonbinding macromolecules. These models were used to predict the interstitial fluid pressure as a function of radial position and the size of tumor; Predictions for their models agreed well with the experimental data and showed that the the tumor interstitial

fluid pressure was lowest at the periphery of the tumor and increased towards the center which concurred the model expectations. Based on their results the heterogeneous distribution of blood supply hindered interstitial transport and rapid extravascular binding of macromolecules; in addition, high interstitial fluid pressures demonstrated a remarkable impact on the infiltration of macromolecules into tumors. Frequently, a tumor is considered in a spherical shape with the following regions:

- Necrotic Region
- Semi-Necrotic Region
- Well-Vascularized Region

The biological parameters such as the micro-vessel permeability, interstitial fluid pressure, interstitial fluid velocity and tumor shape and size affect the drug delivery process. A model shows the transportation of fluid and the distribution of tumor interstitial fluid pressure according to Starling's law , which is extracted to explain the effect of capillary-capillary interaction, and Darcy's law [3], which reflects the condition of the porous tissue [20].

A solid tumor is spatially heterogeneous with large differences in the vasculature and in the cells between different regions. The center of the tumor contains a necrotic core. The cancerous cells divide most actively in the outer region, where there is a good supply of oxygen and nutrients because of existence of a large blood supply in addition to an abundance of exchange vessels. Therefore, the physiological parameters, which are incorporated in the models should be spatially dependent in a tumor. In [3], the physiological parameters such as blood vessel surface area per unit volume and the hydraulic conductivity were considered to be independent of time. Another assumption in this work was that the spherical tumor is considered.

2.1.1 Mathematical modeling

Tumor is assumed as a rigid porous media. Since interstitial fluid is a Newtonian fluid, Darcy's law can be used:

$$\boldsymbol{\nabla} p_i = \frac{-\mu}{k}\mathbf{u}_i \tag{2.1.1}$$

In this equitation, the parameters u, p, k, and μ are the interstitial fluid velocity (IFV), the interstitial fluid pressure, permeability, and viscosity, respectively with consistent units. The index i refers to the interstitial fluid. K is defined as the constant hydraulic conductivity of interstitium (cm^2/mmHg.sec) (which describes the ability to move of the interstitial fluid through the interstitium [21]),

$$\frac{k}{\mu} = K$$

Then,

$$\mathbf{u}_i = -K\boldsymbol{\nabla} p_i \tag{2.1.2}$$

and

$$u_i = -K\frac{\partial p_i}{\partial r} \tag{2.1.3}$$

where r is the radial position (cm). On the other hand, the mass-conservation equation for steady-state, in-compressible fluid is given by:

$$\boldsymbol{\nabla}\cdot\mathbf{u}_i = 0$$

It is also possible to use the same equation in porous media without source or sink in the medium. In a tumor as a biological tissue, vascular vessels are considered as the source and lymphatic vessels as sink. Fluid is exchanged between interstitial, blood or lymph vessels. Therefore, the steady state in-compressible form of the continuity equation is:

$$\boldsymbol{\nabla}\cdot\mathbf{u}_i = \begin{cases} \phi_V(r) - \phi_L(r) & r \geq r_n \\ 0 & r < r_n \end{cases} \tag{2.1.4}$$

In Eq.(2.1.4), r_n is the radius of the necrotic core (cm). In biological tissues $\phi_V(r)$ (the rate of fluid flow per unit volume from blood vessels into the interstitium), with unit ($\sec^{-1}$), is the fluid source term , which is given by Starling's Law[1] and $\phi_L(r)$ (the rate of fluid flow per unit volume from interstitium into lymph vessels), with unit ($\sec^{-1}$), is the lymphatic drainage term that is assumed to be proportional to the pressure difference between the interstitial and the lymphatics [39]. Interstitial fluid emanates from permeable tumor vessels and it is described by Starling's Law, which illustrates the role of hydraulic and osmotic[2] forces, (Fig. 2.1), in the movement of fluid across capillary membranes. The classic Starling equation is defined below:

$$\phi_V(r) = \frac{L_P S}{V}(p_V - p_i - \sigma(\pi_V - \pi_i))) \tag{2.1.5}$$

For $r \geq r_n$:

$$\phi_L(r) = \frac{L_{PL} S_L}{V}(p_i - p_L) \tag{2.1.6}$$

and if $r < r_n$:

$$\phi_V(r) = \phi_L(r) = 0 \tag{2.1.7}$$

In Eq.(2.1.6), $\frac{J_V}{V}(sec^{-1})$ is the volumetric flow rate out of the vasculature per unit volume of tissue. The volumetric flow rate into the lymphatics is shown as $\frac{J_L}{V}(sec^{-1})$. $\frac{S}{V}(cm^{-1})$ is the surface area per unit volume for transport in the tumor. L_P and L_{PL}(cm/mmHg.sec) are the hydraulic conductivities of the micro-vascular wall and the lymphatic wall, respectively. p_V(mmHg) is the vascular pressure (hydrostatic[1] capillary pressure). Moreover, p_i, p_L, π_V, and π_i (all with unit mmHg) are the interstitial pressure, the hydrostatic pressure of lymphatics, the oncotic[2] pressure of the plasma (in the plasma of blood vessels that tend to pull water into circularly system), and the oncotic pressure of the interstitial fluid, respectively. The average osmotic reflection coefficient for plasma proteins is defined by σ. As a general elucidation of osmotic pressure, according to Fig.(2.1a), assuming that the right hand side of the tube is a solution of water and sugar. While the left side is filled by pure water and it comes up to the same height of the solution. Consider the existence of a border of semipermeable membrane between pure water and sugar solution. Since the flow of pure water through the semipermeable membrane is greater than the solution, some pure water passes the membrane. So, the amount of the liquid inside the right side of the tube comes up. The equilibrium situation is shown in Fig.(2.1b) in which the pressure differential represents the osmotic pressure of the solution and it equalizes the flow rate of fluid in the two sides of the tube. The original situation of Fig.(2.1a) occurs, by exerting an osmotic pressure of the water and sugar solution to the liquid in the right side of the tube (see Fig.(2.1c)). As in this work we are talking about different types of pressure for a vein and interstitial, osmotic and hydrostatic pressures are clarified in Fig.(2.2). The baseline values of parameters are presented in Table (2.1).

[1]Starling's Law illustrates the role of hydraulic and osmotic forces in the movement of fluid across capillary membranes.

[2]Osmotic pressure is the minimum pressure which needs to be applied to a solution to prevent the inward flow of water across a semipermeable membrane. It is also defined as the measure of the tendency of a solution to take in water by osmosis[29].

[1]Capillary hydrostatic pressure is the force that is applied by a fluid against the capillary wall. It helps the fluid to move between capillaries and the interstitial fluid. At the arterial end of the capillary the maximum capillary hydrostatic pressure occurs. While, the lowest pressure is seen at the venular end. The pumping action of heart produces the capillary hydrostatic pressure [41].

[2]Oncotic pressure, or colloid osmotic pressure, is a form of osmotic pressure is applied in a blood vessel's plasma that usually tends to pull water into the circulatory system. It is the opposing force to hydrostatic pressure[27].

Parameter	Baseline value in Normal Tissue	Baseline Value in Tumor Tissue
$L_p[cm/mmHgsec]$	0.36×10^{-7}	2.8×10^{-7}
$K[cm^2/mmHgsec]$	8.53×10^{-9}	4.13×10^{-8}
$S/V[cm^{-1}]$	70	200
$p_v[mmHg]$	15.6	15.6
$\pi_v[mmHg]$	20	20
$\pi_i[mmHg]$	10	15
σ	0.91	0.82

Table 2.1: Baseline parameters used in the work by Baxter et al.

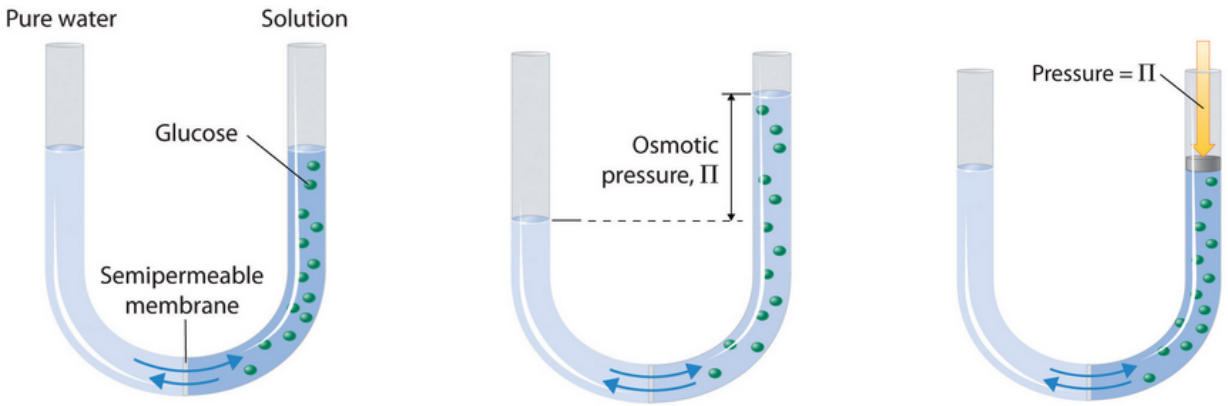

Figure 2.1: The application of the osmotic pressure [6]. (a) initial state, (b) equilibrium, (c) applied osmotic pressure

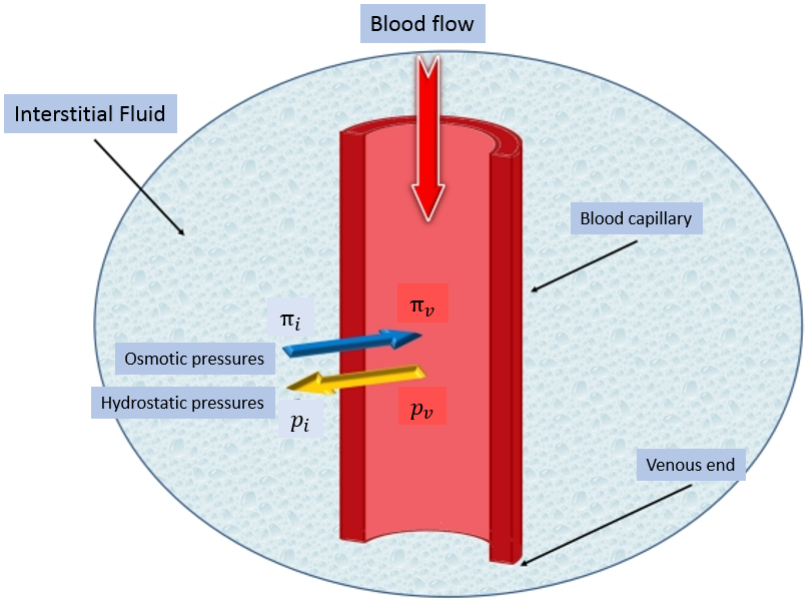

Figure 2.2: Schematic of a typical vein and different types of pressure [36].

Refer to Eqs.(2.1.2) and (2.1.4) (combination of Darcy's Law and Continuity equation), we have:

$$-\boldsymbol{\nabla}\cdot K\boldsymbol{\nabla}p_i = \phi_V(r) - \phi_L(r) \tag{2.1.8}$$

For a special case, where the hydraulic conductivity of the interstitium is constant and there are no source and sink terms, the interstitial pressure is defined with the below Laplace equation:

$$\boldsymbol{\nabla}^2 p_i = 0$$

By considering constant values for all parameters except for p_i and r, we will have the following equation:

$$-\boldsymbol{\nabla}\cdot K\boldsymbol{\nabla}p_i = \frac{L_P S}{V}(p_V - p_i - \sigma_T(\pi_V - \pi_i)) - \frac{L_{PL}S_L}{V}(p_i - p_L) \tag{2.1.9}$$

$\Longrightarrow$

$$\begin{aligned}
\boldsymbol{\nabla}^2 p_i &= -\frac{L_p S}{KV}p_V + \frac{L_P S}{KV}p_i + \frac{L_P S}{KV}\sigma_T\pi_v - \frac{L_P S}{KV}\sigma_T\pi_i + \frac{L_{PL}S_L}{KV}p_i - \frac{L_{PL}S_L}{KV}p_L \\
&= \frac{L_P S}{KV}p_i + \frac{L_{PL}S_L}{KV}p_i - \frac{L_P S}{KV}(p_V - \sigma_T(\pi_v - \pi_i)) - \frac{L_{PL}S_L}{KV}p_L \\
&= \frac{L_P S + L_{PL}S_L}{KV}(p_i - \frac{L_P S(p_V - \sigma_T(\pi_v - \pi_i)) + L_{PL}S_L p_L}{L_P S + L_{PL}S}) \\
&= \frac{R^2}{R^2}\frac{L_P S + L_{PL}S_L}{KV}(p_i - \frac{L_P S(p_V - \sigma_T(\pi_v - \pi_i)) + L_{PL}S_L p_L}{L_P S + L_{PL}S})
\end{aligned}$$

$\Longrightarrow$

$$\boldsymbol{\nabla}^2 p_i = \frac{\alpha^2}{R^2}(p_i - p_{ss}) \tag{2.1.10}$$

The dimensionless parameter, α, is *a size of the proportion of interstitial to vascular resistances to fluid flow* [3], which is introduced by the following equation:

$$\alpha = R\sqrt[2]{(L_p S + L_{pL}S_L)/KV} \tag{2.1.11}$$

The steady-state pressure, p_{ss}, is *the interstitial pressure at which the flux from the vascular equals influx into the lymphatics* [3]; p_{ss} is introduced by the following equation:

$$p_{ss} = (L_p S p_e + L_{pL} S_L p_L)/(L_p S + L_{pL} S_L) \tag{2.1.12}$$

The interstitial pressure in the center of the tumor has its maximum value which is equal to the effective pressure, p_e:

$$p_e = [p_V - \sigma_T(\pi_V - \pi_i)] \tag{2.1.13}$$

Referring to Appendix 1,

$$\nabla^2 = \frac{1}{r^2}\frac{\partial}{\partial r}(r^2\frac{\partial}{\partial r}) + \frac{1}{r^2\sin\theta}\frac{\partial}{\partial\theta}(\sin\theta\frac{\partial}{\partial\theta}) + \frac{1}{r^2\sin^2\theta}\frac{\partial^2}{\partial\phi^2}$$

Therefore, if we assume spherically symmetry, the Laplace equation (2.1.10) is described as following,

$$\frac{1}{r^2}\frac{\partial}{\partial r}(r^2\frac{\partial p_i}{\partial r}) = \frac{\alpha^2}{R^2}(p_i - p_{ss}) \tag{2.1.14}$$

2.1.2 Homogeneous tumor

Here, a homogeneous tumor is defined as existing alive cancerous cells all through a tumor with equal scattering of blood vessels. Baxter et al. [3] categorized the investigation of the homogeneous tumor interstitial fluid pressure from the two below aspects:

- Case 1 : An alymphatic, isolated, homogeneous tumor.
- Case 2 : An alymphatic, homogeneous tumor surrounded by normal tissue.

Boundary conditions

There is no-flux boundary condition at the center of the tumor due to symmetry:

$$\boldsymbol{\nabla} p_i|_{r=0} = 0 \tag{2.1.15}$$

At the outer edge of the solid tumor, the two following boundary conditions are possible.
First, where the pressure in the surrounding tissue or space is fixed, the tumor pressure is the same as the surrounding pressure, p_∞:

$$p_i|_{r=R} = p_\infty \tag{2.1.16}$$

Second, where the solid tumor is surrounded by normal tissues, the continuity of pressure and velocity gives the following boundary condition:

$$-K_T\frac{dp_i}{dr}|_{r=R^-} = -K_N\frac{dp_i}{d_r}|_{r=R^+} \tag{2.1.17}$$

$$p_i|_{r=R^-} = p_i|_{r=R^+} \tag{2.1.18}$$

where R^- and R^+ represent the tumor and normal tissue radius at the outer edge of the solid tumor; K_T and K_N are the hydraulic conductivities of the interstitium in tumor and normal tissues, respectively.
It should be noted that, in the second type, all the equations mentioned for the tumor tissue have to be solved for the normal tissue, as well. It is clear that for the normal tissue, far from the solid tumor that the pressure is constant, the first type of boundary condition, Eq. (2.1.16), must be applied. The solution now can be obtained analytically or numerically to find the interstitial fluid pressure and interstitial fluid velocity profiles for each of the two boundary conditions [3].

Now, finding a general solution of Eq.(2.1.14) is aimed. Consider Eq.(2.1.14),

$$\frac{1}{r^2}\frac{\partial}{\partial r}(r^2\frac{\partial p_i}{\partial r}) = \frac{\alpha^2}{R^2}p_i - \frac{\alpha^2}{R^2}p_{ss}$$

As p_{ss} is constant, first we ignore the part of the equation consisting p_{ss} and consider the following equation:

$$\frac{1}{r^2}\frac{\partial}{\partial r}(r^2\frac{\partial p}{\partial r}) = \frac{\alpha^2}{R^2}p \tag{2.1.19}$$

$\Longrightarrow$

$$\frac{\partial}{\partial r}(r^2\frac{\partial p}{\partial r}) = r^2\frac{\alpha^2}{R^2}p$$

$\Longrightarrow$

$$2r\frac{\partial p}{\partial r} + r^2\frac{\partial^2 p}{\partial r^2} = r^2\frac{\alpha^2}{R^2}p$$

$\Rightarrow$

$$r^2p'' + 2rp' - r^2\frac{\alpha^2}{R^2}p = 0 \tag{2.1.20}$$

The standard form of Eq.(2.1.20) with the constant $\delta = \frac{\alpha^2}{R^2}$ is:

$$p'' + \frac{2}{r}p' - \delta p = 0 \tag{2.1.21}$$

Based on the definition of the Ricatti equation given in [15], the solution of Eq. (2.1.21) can be written as following,

$$p = \frac{1}{r}e^{\frac{\alpha}{R}(2c_2+r)} - \frac{1}{r}e^{\frac{\alpha}{R}(2c_1+2c_2-r)} \tag{2.1.22}$$

where c_1 and c_2 are constants of integration. We refer to Appendix 2 for details. Moreover, define,

$$P_1 = \frac{1}{r}e^{\frac{\alpha}{R}(2c_2+r)}$$

and

$$P_2 = -\frac{1}{r}e^{\frac{\alpha}{R}(2c_1+2c_2-r)}$$

It must be pointed out that based on direct computations it can be shown that both P_1 and P_2, can individually solve Eq.(2.1.19). As we have a constant part of $(-\frac{\alpha^2}{R^2}p_{ss})$ in Eq.(2.1.14), we add constant W to Eq.(2.1.22) to get the solution of Eq.(2.1.14). As a result, the solution of Eq.(2.1.14) is written as:

$$p = P_1 + P_2 + W = \frac{1}{r}e^{\frac{\alpha}{R}(2c_2+r)} - \frac{1}{r}e^{\frac{\alpha}{R}(2c_1+2c_2-r)} + W \tag{2.1.23}$$

where W is constant and added to the solution because of the constant value of p_{ss} in the right hand side of Eq. (2.1.14). Values for c_1, c_2 and W will be determined from boundary conditions as well as the main Eq.(2.1.14) in the various cases that follows.

2.1.2.1 Analytical solution for isolated tumor

Baxter et al. [3] examined a uniform tumor in spherical shape, without any necrotic core, which is homogeneously vascularized (see Fig.2.3). Moreover, they ignored the existence of lymphatic drainage system and binding of the solute (the case describes the transport of non-reacting macromolecule in a tumor without a lymphatic system). According to these assumptions, we set the lymphatic drainage term, J_L (in Eq.(2.1.15)) and the radius of necrotic core, r_n (in Eq.(2.1.14)) equal to zero.

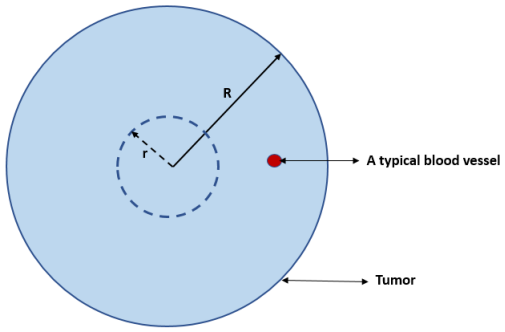

Figure 2.3: Schematic of a uniform spherical tumor without necrotic core in the center and shown typical vascular in the periphery region, R is the tumor radius and r is the radial position.

Consider Eq.(2.1.14) and its solution stated in Eq.(2.1.23) and relevant boundary conditions for this case which are defined in Eqs. (2.1.15) and (2.1.16). According to the first boundary condition (Eq.(2.1.15)), $\frac{\partial p_i}{\partial r}|_{r=0} = 0$. Therefore,

$$-\frac{1}{r^2}e^{\frac{\alpha}{R}(2c_2+r)} + \frac{\alpha}{rR}e^{\frac{\alpha}{R}(2c_2+r)} + \frac{1}{r^2}e^{\frac{\alpha}{R}(2c_1+2c_2-r)} + \frac{\alpha}{rR}e^{\frac{\alpha}{R}(2c_1+2c_2-r)} = 0$$

To figure out how the above equation is behaving as r goes to zero, we split it into four items as in the following.

$$L_1 = -\frac{1}{r^2}e^{\frac{\alpha 2c_2}{R}}e^{\frac{\alpha r}{R}} = -\frac{e^{\frac{2\alpha c_2}{R}}}{r^2}(1 + \frac{\alpha}{R}r + \frac{1}{2}\frac{\alpha^2}{R^2}r^2 + ...)$$

$\Longrightarrow$

$$L_1 = -\frac{e^{\frac{2\alpha c_2}{R}}}{r^2} - \frac{\alpha}{R}\frac{e^{\frac{2\alpha c_2}{R}}}{r} - \frac{\alpha^2}{R^2}\frac{e^{\frac{2\alpha c_2}{R}}}{2}$$

$$L_2 = \frac{1}{r}\frac{\alpha}{R}e^{\frac{2\alpha c_2}{R}}e^{\frac{\alpha r}{R}} = \frac{1}{r}\frac{\alpha}{R}e^{\frac{2\alpha c_2}{R}}(1 + \frac{\alpha}{R}r + \frac{1}{2}\frac{\alpha^2}{R^2}r^2 + ...)$$

$\Longrightarrow$

$$L_2 = \frac{1}{r}\frac{\alpha}{R}e^{\frac{\alpha 2c_2}{R}} + \frac{\alpha^2}{R^2}e^{\frac{\alpha 2c_2}{R}}$$

$$L_3 = \frac{1}{r^2}e^{\frac{\alpha(2c_1+2c_2)}{R}}e^{\frac{\alpha r}{R}} = \frac{1}{r^2}e^{\frac{\alpha(2c_1+2c_2)}{R}}(1 - \frac{\alpha}{R}r + \frac{1}{2}\frac{\alpha^2}{R^2}r^2 - ...)$$

$\Longrightarrow$

$$L_3 = \frac{1}{r^2}e^{\frac{\alpha(2c_1+2c_2)}{R}} - \frac{1}{r}\frac{\alpha}{R}e^{\frac{\alpha(2c_1+2c_2)}{R}} + \frac{1}{2}\frac{\alpha^2}{R^2}e^{\frac{\alpha(2c_1+2c_2)}{R}}$$

$$L_4 = \frac{1}{r}\frac{\alpha}{R}e^{\frac{\alpha(2c_1+2c_2)}{R}}e^{\frac{-\alpha r}{R}} = \frac{1}{r}\frac{\alpha}{R}e^{\frac{\alpha(2c_1+2c_2)}{R}}(1 - \frac{\alpha}{R}r + \frac{1}{2}\frac{\alpha^2}{R^2} - ...)$$

$\Longrightarrow$

$$L_4 = \frac{1}{r}\frac{\alpha}{R}e^{\frac{\alpha(2c_1+2c_2)}{R}} - \frac{\alpha^2}{R^2}e^{\frac{\alpha(2c_1+2c_2)}{R}}$$

$\Longrightarrow$

$$L_1 + L_2 + L_3 + L_4 = -\frac{1}{r^2}e^{\frac{2\alpha c_2}{R}} - \frac{1}{r}\frac{\alpha}{R}e^{\frac{2\alpha c_2}{R}} - \frac{1}{2}\frac{\alpha^2}{R^2}e^{\frac{2\alpha c_2}{R}} + \frac{1}{r}\frac{\alpha}{R}e^{\frac{\alpha 2c_2}{R}} + \frac{\alpha^2}{R^2}e^{\frac{\alpha 2c_2}{R}} + \frac{1}{r^2}e^{\frac{\alpha(2c_1+2c_2)}{R}}$$

$$-\frac{1}{r}\frac{\alpha}{R}e^{\frac{\alpha(2c_1+2c_2)}{R}} + \frac{1}{2}\frac{\alpha^2}{R^2}e^{\frac{\alpha(2c_1+2c_2)}{R}} + \frac{1}{r}\frac{\alpha}{R}e^{\frac{\alpha(2c_1+2c_2)}{R}} - \frac{\alpha^2}{R^2}e^{\frac{\alpha(2c_1+2c_2)}{R}} = 0$$

So,

$$-\frac{1}{r^2}e^{\frac{2\alpha c_2}{R}} + \frac{1}{r^2}e^{\frac{\alpha(2c_1+2c_2)}{R}} = 0$$

and

$$-\frac{1}{2}\frac{\alpha^2}{R^2}e^{\frac{2\alpha c_2}{R}}+\frac{\alpha^2}{R^2}e^{\frac{\alpha 2c_2}{R}}+\frac{1}{2}\frac{\alpha^2}{R^2}e^{\frac{\alpha(2c_1+2c_2)}{R}}-\frac{\alpha^2}{R^2}e^{\frac{\alpha(2c_1+2c_2)}{R}}=0$$

$$\Longrightarrow$$

$$-e^{\frac{2\alpha c_2}{R}}+2e^{\frac{2\alpha c_2}{R}}+e^{\frac{\alpha(2c_1+2c_2)}{R}}-2e^{\frac{\alpha(2c_1+2c_2)}{R}}=0$$

$$\Longrightarrow$$

$$e^{\frac{2\alpha c_2}{R}}=e^{\frac{\alpha(2c_1+2c_2)}{R}}$$

$$\Longrightarrow e^{\frac{\alpha}{R}(2c_2)}=e^{\frac{\alpha}{R}2c_1}e^{\frac{\alpha}{R}2c_2}\Longrightarrow e^{\frac{\alpha}{R}2c_1}=1\Rightarrow \ln(e^{\frac{\alpha}{R}2c_1})=\ln(1)\Rightarrow e^{\frac{\alpha}{R}2c_1}=0\Rightarrow c_1=0$$

Therefore,

$$p_i=\frac{2}{r}e^{\frac{\alpha}{R}2c_2}\sinh(\frac{\alpha r}{R})+W$$

Now, consider the second boundary condition mentioned in Eq.(2.1.16), $p_i|_{r=R}=p_\infty$. Thus,

$$\frac{2}{R}e^{\frac{\alpha}{R}2c_2}\sinh(\alpha)+W=p_\infty$$

$$\Longrightarrow$$

$$\frac{2}{R}e^{\frac{\alpha}{R}2c_2}\sinh(\alpha)=p_\infty-W$$

$$\Longrightarrow$$

$$e^{\frac{\alpha}{R}2c_2}=(p_\infty-W)\frac{R}{2\sinh\alpha}$$

$$\Longrightarrow$$

$$p_i=\frac{R(p_\infty-W)}{\sinh(\alpha)}\frac{1}{r}\sinh(\frac{\alpha r}{R})+W$$

Therefore,

$$\frac{1}{r^2}\frac{\partial}{\partial r}(r^2\frac{\partial p_i}{\partial r})=\frac{\alpha^2}{R^2}[\frac{R(p_\infty-W)}{\sinh(\alpha)}\frac{1}{r}\sinh(\frac{\alpha r}{R})]$$

Since this solution should satisfy Eq.(2.1.14); therefore,

$$\frac{1}{r^2}\frac{\partial}{\partial r}(r^2\frac{\partial p_i}{\partial r})=\frac{\alpha^2}{R^2}(p_i-p_{ss})=\frac{\alpha^2}{R^2}[\frac{R(p_\infty-W)}{\sinh(\alpha)}\frac{1}{r}\sinh(\frac{\alpha r}{R})]+\frac{\alpha^2}{R^2}W-\frac{\alpha^2}{R^2}p_{ss}$$

$$\Longrightarrow$$

$$W=p_{ss}$$

As a result,

$$p_i=\frac{R(p_\infty-p_{ss})}{\sinh(\alpha)}\frac{1}{r}\sinh(\frac{\alpha r}{R})+p_{ss} \tag{2.1.24}$$

is the particular solution of Eq. (2.1.14). Define $\hat{r}=\frac{r}{R}$ as a dimensionless radial position. Finally, The dimensionless pressure is obtained:

$$\hat{p}=\frac{p_i-p_\infty}{p_{ss}-p_\infty}=\frac{\frac{R(p_\infty-p_{ss})}{\sinh(\alpha)}\frac{1}{r}sinh(\frac{\alpha r}{R})+p_{ss}-p_\infty}{p_{ss}-p_\infty}=1-\frac{\sinh(\alpha\hat{r})}{\hat{r}\sinh(\alpha)} \tag{2.1.25}$$

We have plotted the analytical solution (2.1.25), by implementing Matlab programming code and using parameter values in Table (2.1), and we have investigated the behaviour of tumor interstitial fluid pressure by increasing the size of the radial position (r) from the center of the tumor. The comparison between pressure curvatures for different values of α, defined by Eq.(2.1.11), is shown in Fig.(2.4). By changing the value of interstitial hydraulic conductivity K in Eq.(2.1.11), different values of α are produced; note that in each case (for each α) the interstitial hydraulic conductivity is assumed to be constant throughout the tumor. Increased interstitial hydraulic conductivity, K, results in decreased values for α. According to Fig.(2.4), the maximum pressure happens at the center of the tumor and follows a decreasing trend towards the tumor outer boundary ($\hat{r}=1$). For high values of α the maximum interstitial pressure remains almost unchanged

until a great distance from the center of the tumor after which it experiences a sharp decrease to a minimum value at the outer boundary. As shown in Fig.(2.4), the higher value of α lead to higher interstitial pressure. We would like to mention that, Sefidgar et al. [32] have claimed that α represents the shape of the tumor (see Fig.(2.5)). $\alpha = 1$ gives the spherical shape of the tumor which Baxter et al. [3] have considered in this case.

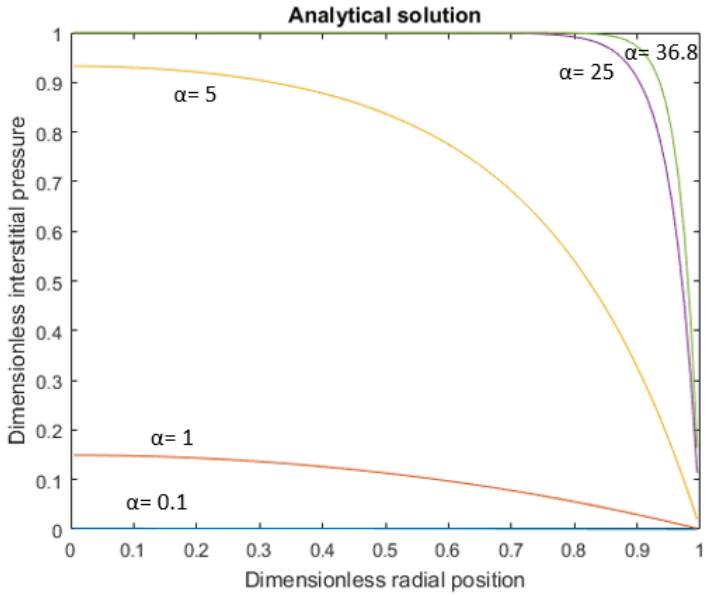

Figure 2.4: Dimensionless interstitial pressure p_i as a function of dimensionless radial position r for different values of α.($\alpha = 0.1, 1, 5, 25, 36.8$)

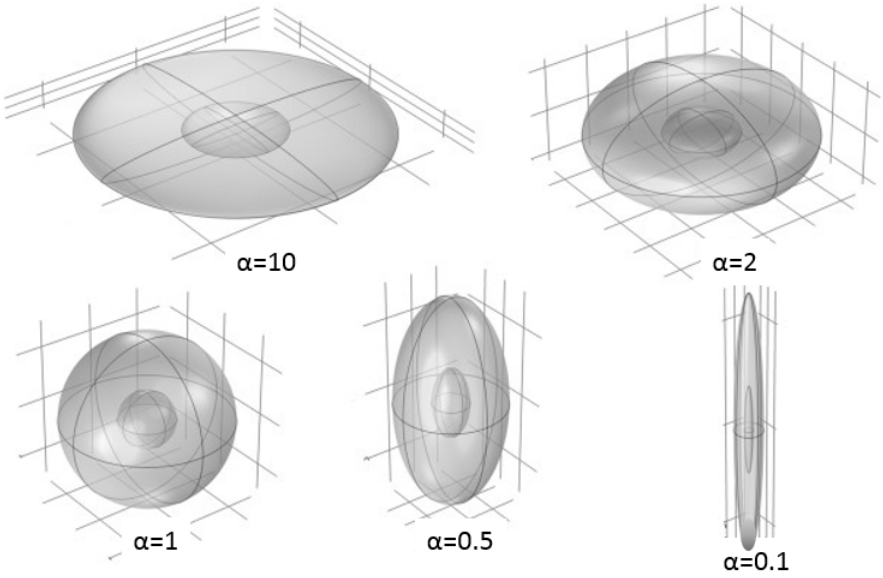

Figure 2.5: Different shapes of tumor corresponding to different values of α [32].

2.1.2.2 Numerical simulation for isolated tumor

Consider Eq.(2.1.14),

$$\frac{1}{r^2}\frac{\partial}{\partial r}(r^2\frac{\partial p_i}{\partial r}) = \frac{\alpha^2}{R^2}(p_i - p_{ss})$$

and two boundary conditions mentioned in Eqs.(2.1.15) and (2.1.16),

$$\boldsymbol{\nabla} p_i|_{r=0} = 0$$

and

$$p_i|_{r=R} = p_\infty$$

In addition to the analytical solution, we have investigated the pressure distribution through the tumor using a following standard numerical approach to approve the behaviour of pressure presented by analytical solution. The baseline parameters presented in Table (2.1) are used.

The spatial domain [0,1] is discritized into M cells. Then we get M points of x_i, $i = 1, 2, .., M$ where x_i is located in the center of $[x_{i-1/2}, x_{i+1/2}]$. The length of each cell is defined by $\delta x = x_{i+1/2} - x_{i-1/2}$. The discretization of p_x at the cell interface $x_{i+1/2}$ is:

$$[p_x]_{i+1/2} = \frac{p_{i+1} - p_i}{\delta x}, i = 1, ..., M-1 \tag{2.1.26}$$

Let x be the radial position. A standard second order discretization can then be written according to the steps below.

$$\frac{1}{x}\frac{\partial}{\partial x}(x^2\frac{\partial p}{\partial x}) = \frac{\alpha^2}{R^2}(p - p_{ss})$$

$\Longrightarrow$

$$\frac{1}{x_i^2\delta x}(x_{i+1/2}^2\frac{\partial p}{\partial x}|_{i+1/2} - x_{i-1/2}^2\frac{\partial p}{\partial x}|_{i-1/2}) = \frac{\alpha^2}{R^2}(p_i - p_{ss})$$

If i=1:

$$\frac{1}{x_1^2\delta x}(x_{3/2}^2\frac{\partial p}{\partial x}|_{3/2} - x_{1/2}^2\frac{\partial p}{\partial x}|_{1/2}) = \frac{\alpha^2}{R^2}(p_1 - p_{ss})$$

According to the first boundary condition (2.1.15) and Eq.(2.1.26), we have:

$$\frac{1}{x_1^2\delta x}(x_{3/2}^2\frac{p_2 - p_1}{\delta x}) = \frac{\alpha^2}{R^2}(p_1 - p_{ss})$$

$\Longrightarrow$

$$x_{3/2}^2(p_2 - p_1) = x_1^2\delta x^2\frac{\alpha^2}{R^2}(p_1 - p_{ss})$$

$\Longrightarrow$

$$x_{3/2}^2 p_2 - (x_{3/2}^2 + x_1^2\delta x^2\frac{\alpha^2}{R^2})p_1 = -\frac{\alpha^2}{R^2}x_1^2\delta x^2 p_{ss} \tag{2.1.27}$$

And, if i=M, then:

$$\frac{1}{x_M^2\delta x}(x_{M+1/2}^2\frac{\partial p}{\partial x}|_{M+1/2} - x_{M-1/2}^2\frac{\partial p}{\partial x}|_{M-1/2}) = \frac{\alpha^2}{R^2}(p_M - p_{ss})$$

As $x_{M+1/2} = 1$ and according to the second boundary condition (2.1.16), we have:

$$\frac{1}{x_M^2\delta x}(\frac{p_\infty - p_M}{\frac{\delta x}{2}} - x_{M-1/2}^2\frac{p_M - p_{M-1}}{\delta x}) = \frac{\alpha^2}{R^2}(p_M - p_{ss})$$

$\Longrightarrow$

$$2(p_\infty - p_M) - x^2_{M-1/2}(p_M - p_{M-1}) = \frac{\alpha^2}{R^2}(p_M - p_{ss})x^2_M \delta x^2$$

$\Longrightarrow$

$$-(2 + x^2_{M-1/2} + \frac{\alpha^2}{R^2}x^2_M \delta x^2)p_M + x^2_{M-1/2}p_{M-1} = -\frac{\alpha^2}{R^2}x^2_M \delta x^2 p_{ss} - 2p_\infty \tag{2.1.28}$$

And for i=2,...,M-1:

$$x^2_{i+1/2}p_{i+1} - (x^2_{i+1/2} + x^2_{i-1/2} + x^2_i \delta x^2 \frac{\alpha^2}{R^2})p_i + x^2_{i-1/2}p_{i-1} = -\frac{\alpha^2}{R^2}x^2_i \delta x^2 p_{ss} \tag{2.1.29}$$

Using Eq.(2.1.29) as well as equations for boundary conditions, Eqs.(2.1.27) and (2.1.28), we obtain a linear equation system for the unknown p_i where $i = 1, ..., M$. Now, let define A as follows. Let define A ($M \times M$ matrix of coefficients of p_i) as in the following,

$$A = \begin{bmatrix} -(x - 3/2^2 + x^2_1 \delta x^2 \frac{\alpha^2}{R^2}) & x^2_{3/2} & 0 & \cdots & 0 \\ x^2_{3/2} & -(x^2_{5/2} + x^2_{3/2} + x^2_2 \delta x^2 \frac{\alpha^2}{r^2}) & x^2_{5/2} & 0 & \cdots \\ 0 & \ddots & & \ddots & \ddots \\ \vdots & \cdots & & & x^2_{M-1/2} \\ 0 & \cdots & 0 & x^2_{M-1/2} & -(2 + x^2_{M-1/2} + \frac{\alpha^2}{R^2}x^2_M \delta x^2) \end{bmatrix}$$

and define B ($M \times 1$):

$$B = \begin{bmatrix} -\frac{\alpha^2}{R^2}x^2_1 \delta x^2 p_{ss} \\ -\frac{\alpha^2}{R^2}x^2_2 \delta x^2 p_{ss} \\ -\frac{\alpha^2}{R^2}x^2_3 \delta x^2 p_{ss} \\ \vdots \\ -\frac{\alpha^2}{R^2}x^2_M \delta x^2 p_{ss} - 2p_\infty \end{bmatrix}$$

Therefore, the linear equation system can be written as $Ap = B$ and p is defined as the vector of unknown pressures. Again, the performance of Matlab programming code by using the baseline values in Table (2.1) helps to see the behaviour of pressure through the tumor. Fig.(2.6) displays the pressure behaviour in tumor using numerical simulation (the markers) superimposed to the results from analytical solution (lines) (Fig.(2.4)); complete agreement between the two approaches is clear in this figure.

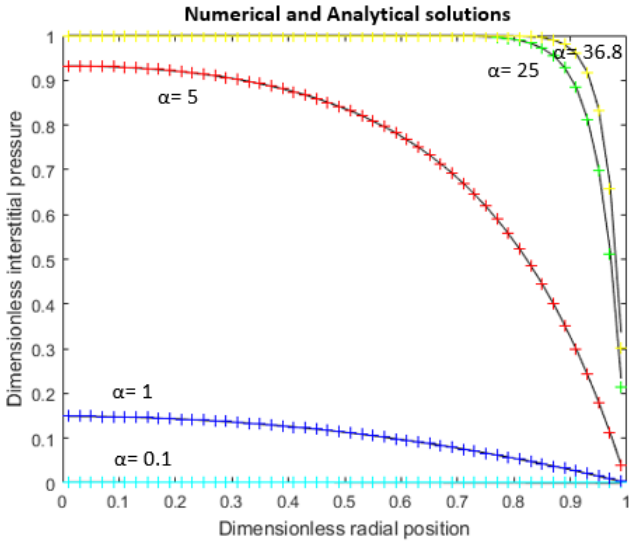

Figure 2.6: Pressure behaviour in tumor using numerical simulation (the markers) and analytical solution (lines), complete agreement between the two approaches is clear.

2.1.2.3 Analytical solution for tumor surrounded by normal tissue

In the case of tumor surrounded by normal tissue, we consider the specified tumor in case 1 (i.e. alymphatic, homogeneous, and without necrotic core) surrounded by a normal tissue (see Fig.(2.7)). In a tumor tissue, the microvessels are longer, larger in diameter, and denser than the microvessels in a normal tissue [20].

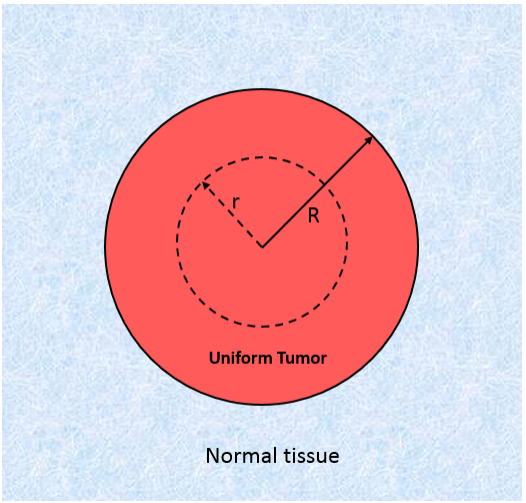

Figure 2.7: Schematic of a homogeneous tumor and its surrounding normal tissue - R: the radius of the tumor, r: the radial position.

According to the solution (2.1.23), now we can write the solution in the two different domains as:

$$p_i^T = \frac{1}{r} e^{\frac{\alpha_T}{R}(2c_2+r)} - \frac{1}{r} e^{\frac{\alpha_T}{R}(2c_1+2c_2-r)} + W \tag{2.1.30}$$

in a tumor tissue; and T represents tumor.
And for a normal tissue, since P_1 (defined in section (2.1.2)) approaches infinity as r goes to infinity, we just

consider P_2 in Eq.(2.1.23); therefore, the solutions can be written as in the following,

$$p_i^N = -\frac{1}{r}e^{\frac{\alpha_N}{R}(2c'_1+2c'_2-r)} + W' \tag{2.1.31}$$

where N represents normal tissue. We must now apply the boundary conditions to compute the unknown constants c_1, c_2, c'_1, c'_1, W and W'. The first boundary condition (2.1.15) can be applied for the pressure solution inside tumor (Eq.(2.1.30)); this results in $c_1 = 0$. Eq.(2.1.30) should satisfy Eq.(2.1.14); therefore, in the tumor $W = p_{ss}$. The second boundary condition (2.1.16) is applied to pressure solution in normal tissue (Eq.(2.1.31)). Therefore,

$$\lim_{r\to\infty} p_i^N = p_\infty$$

$\Longrightarrow$

$$\lim_{r\to\infty} [-\frac{1}{r}e^{\frac{\alpha_N}{R}(2c'_1+2c'_2+r)} + W'] = p_\infty$$

and this is true if $W' = p_\infty$.
So, the solution can be stated as in the following.
If $(r < R)$,

$$p_i^T = \frac{1}{r}e^{\frac{\alpha_T}{R}(2c_2)}(e^{\frac{\alpha_T r}{R}} - e^{-\frac{\alpha_T r}{R}}) + p_{ss} \tag{2.1.32}$$

and if $(r > R)$,

$$p_i^N = -\frac{1}{r}e^{\frac{\alpha_N}{R}(2c'_1+2c'_2)}e^{-\frac{\alpha_N r}{R}} + p_\infty. \tag{2.1.33}$$

According to Eq.(2.1.18):

$$\frac{1}{R}e^{\frac{\alpha_T}{R}(2c_2)}(e^{\alpha_T} - e^{-\alpha_T}) + p_{ss} = -\frac{1}{R}e^{\frac{\alpha_N}{R}(2c'_1+2c'_2)}e^{-\alpha_N} + p_\infty$$

$\Longrightarrow$

$$e^{\frac{\alpha_N}{R}(2c'_1+2c'_2)} = -e^{\alpha_N}e^{\frac{\alpha_T}{R}2c_2}(e^{\alpha_T} - e^{-\alpha_T}) - Re^{\alpha_N}(p_{ss} - p_\infty). \tag{2.1.34}$$

On the other hand,

$$\frac{\partial p_i^T}{\partial r}|_{r=R} = e^{\frac{\alpha_T}{R}2c_2}[\frac{2}{R^2}(-sinh\alpha_T + \alpha_T cosh\alpha_T)]$$

and,

$$\frac{\partial p_i^N}{\partial r}|_{r=R} = \frac{1}{R^2}e^{\frac{\alpha_N}{R}(2c'_1+2c'_2)}(1+\alpha_N)e^{-\alpha_N}.$$

Apply the boundary condition (2.1.17),

$$-K_T[\frac{2}{R^2}e^{\frac{\alpha_T}{R}2c_2}(-sinh\alpha_T + \alpha_T cosh\alpha_T)] = -K_N[\frac{1}{R^2}e^{\frac{\alpha_N}{R}(2c'_1+2c'_2)}(1+\alpha_N)e^{-\alpha_N}]$$

Define $\hat{K}$ as the ratio of hydraulic conductivities of tumor and normal tissue, $\hat{K} = \frac{K_T}{K_N}$, then,

$$\begin{aligned}\frac{2\hat{K}}{R^2}e^{\frac{\alpha_T}{R}2c_2}(-sinh\alpha_T + \alpha_T cosh\alpha_T) &= \frac{(1+\alpha_N)e^{-\alpha_N}}{R^2}e^{\frac{\alpha_N}{R}(2c'_1+2c'_2)} \\ &= \frac{(1+\alpha_N)e^{-\alpha_N}}{R^2}[2e^{\alpha_N}sinh\alpha_T e^{\frac{\alpha_T}{R}2c_2} - Re^{\alpha_N}(p_{ss}-p_\infty)]\end{aligned} \tag{2.1.35}$$

$\Longrightarrow$

$$e^{\frac{\alpha_T}{R}2c_2} = \frac{-R(p_{ss}-p_\infty)(1+\alpha_N)}{2\hat{K}(-sinh\alpha_T + \alpha_T cosh\alpha_T) + 2(1+\alpha_N)sinh\alpha_T} \tag{2.1.36}$$

Inserting $e^{\frac{\alpha_T}{R}2c_2}$ from Eq.(2.1.36) in Eq(2.1.34), results in:

$$e^{\frac{\alpha_N}{R}(2c'_1+2c'_2)} = e^{\alpha_N}\frac{R(p_{ss}-p_\infty)(1+\alpha_N)}{\hat{K}(-sinh\alpha_T + \alpha_T cosh\alpha_T) + (1+\alpha_N)sinh\alpha_T}sinh\alpha_T - Re^{\alpha_N}(p_{ss}-p_\infty)$$

$\Longrightarrow$

$$e^{\frac{\alpha_N}{R}(2c'_1+2c'_2)} = e^{\alpha_N} R(p_{ss}-p_\infty)[\frac{(1+\alpha_N)sinh\alpha_T}{\hat{K}(-sinh\alpha_T+\alpha_T cosh\alpha_T)+(1+\alpha_N)sinh\alpha_T}-1] \tag{2.1.37}$$

As a result, in this case, the particular solution related to the tumor tissue (Eq.(2.1.32)), where $(r<R)$, has been obtained,

$$p_i^T = -\frac{R(p_\infty-p_{ss})}{r}\frac{(1+\alpha_N)}{\hat{K}(-sinh\alpha_T+\alpha_T cosh\alpha_T)+(1+\alpha_N)sinh\alpha_T}sinh\frac{\alpha_T r}{R}+p_{ss} \tag{2.1.38}$$

and for the normal tissue, $(r>R)$, according to Eq.(2.1.33), the particular solution is governed,

$$p_i^N = -\frac{1}{r}e^{\alpha_N} R(p_{ss}-p_\infty)[\frac{(1+\alpha_N)sinh\alpha_T}{\hat{K}(-sinh\alpha_T+\alpha_T cosh\alpha_T)+(1+\alpha_N)sinh\alpha_T}-1]e^{-\frac{\alpha_N r}{R}}+p_\infty$$

$\Longrightarrow$

$$p_i^N = \frac{R(p_{ss}-p_\infty)}{r}\frac{\hat{K}(-sinh\alpha_T+\alpha_T cosh\alpha_T)}{(\hat{K}(-sinh\alpha_T+\alpha_T cosh\alpha_T)+(1+\alpha_N)sinh\alpha_T)e^{-\alpha_N}}e^{-\frac{\alpha_N r}{R}}+p_\infty$$

$\Longrightarrow$

$$p_i^N = \frac{R(p_{ss}-p_\infty)}{r}\frac{\hat{K}(-sinh\alpha_T+\alpha_T cosh\alpha_T)(sinh(\frac{\alpha_N r}{R})-cosh(\frac{\alpha_N r}{R}))}{(\hat{K}(-sinh\alpha_T+\alpha_T cosh\alpha_T)+(1+\alpha_N)sinh\alpha_T)(sinh\alpha_N-cosh\alpha_N)}+p_\infty \tag{2.1.39}$$

The comparison of the pressure behaviour between case 1 (isolated tumor) and case 2 (tumor surrounded by normal tissue) is shown by Baxter et al. [3] in Fig.(2.8). The interstitial pressure, p_i, at the edge of a tumor has the same value as the pressure in the normal tissue. By decreasing the distance towards the center of a tumor, p_i raises quickly (see Fig.(2.8)). According to Eq.(2.1.5) and the definition of the effective pressure, p_e, in Eq.(2.1.13), the driving force for the fluid filtration is the difference between p_e and p_i. Therefore, the pure rate of fluid filtration reaches the highest value at the tumor periphery, while the lowest value is obtained in the center of the tumor. By considering the baseline values for the physiological parameters (Table (2.1)) and Eq.(2.1.13), the calculated p_e is 11.5 mmHg; this value is identical to the highest value of interstitial pressure, p_i, in the tumor. The results from analytical solution agree with the experimental findings [3]. The value of α_N is calculated by considering the related parameters in normal tissue in Table(2.1), which is equal to 17. This applies a steep curvature of pressure and produces a high pressure in the center of the tumor, Fig.(2.8). The presence of functional lymphatics in a normal tissue causes difference between the trend of pressure for isolated tumor and surrounded by normal tissue. Baxter et al. [3] suggested some ways that helps to decrease the interstitial pressure, p_i. The modification of the osmotic pressure of vessels and increasing the interstitial hydraulic conductivity K can be applied to approach the goal of reducing p_i.

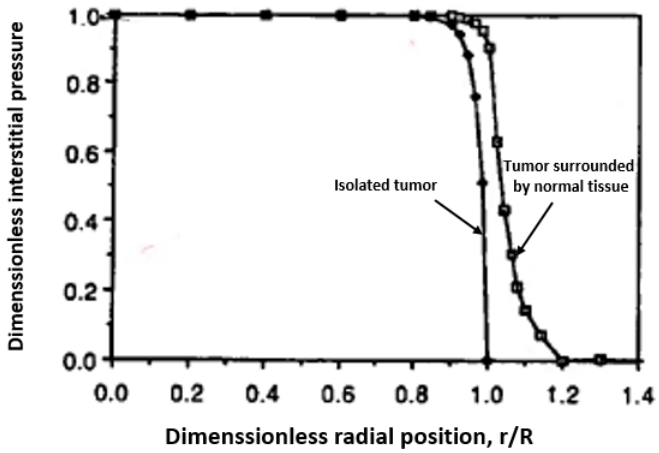

Figure 2.8: Pressure trend difference between two cases of isolated tumor and surrounded by normal tissue with fixed value of $\alpha_T = 36.8$. The unit dimensionless pressure is equivalent to a pressure of 11.5 mmHg.

2.1.3 Heterogeneous tumor

The incorporation of a necrotic core inside the tumor (center of a tumor) causes the heterogeneity of the tumor (see Fig.(2.9)). In this case, the purpose of Baxter et al.[4] was to apply the developed theoretical framework (presented in the previous cases without necrotic core) to the more realistic case of a non-uniformly perfused tumor (nonuniform blood perfusion in the tumor because of existing necrotic core). Here, this specific tumor is considered by a surrounding normal tissue (see Fig.(2.9)). Therefore, it is possible to define three regions of necrotic core, periphery (the region between necrotic core and the edge of the tumor) and normal tissue. Necrotic core region means the area without functional blood or lymph vessels, thus no exchange of fluid or macromolecules with the interstitium [4].

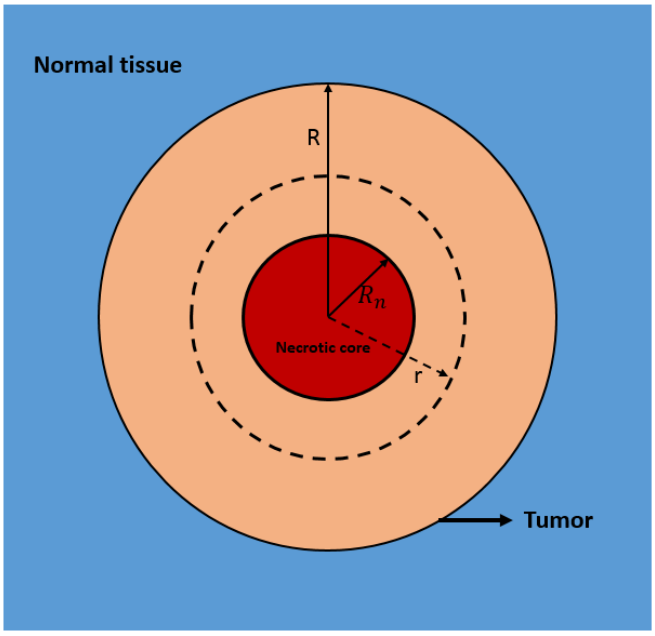

Figure 2.9: Schematic of a heterogeneous tumor surrounded by normal tissue - R: the radius of the tumor, R_n: the radius of the necrotic core, r: the radial position.

Here again the fluid transport equation is defined by the combination of Darcy's Law and continuity equation. Therefore, Eq.(2.1.14) with the solution presented in Eq.(2.1.23) is considered. Contributing relevant boundary conditions leads to find the particular solutions for different regions of necrotic core, periphery and normal tissue.

Boundary conditions

The boundary conditions are defined according to Baxter et al. [4] model. Since there is no source or sink for fluid in the necrotic core, there is no-flux boundary conditions or continuity of pressure at the necrotic core-vialbe tumor interface:

$$\frac{\partial p_i}{\partial r}|_{r=R_n} = 0 \tag{2.1.40}$$

$$p_i|_{r=R_n{}^-} = p_i|_{r=R_n{}^+} \tag{2.1.41}$$

For a tumor surrounded by normal tissue there is continuity of interstitial velocity and pressure between tumor and normal tissue:

$$-K_T \frac{\partial p_i}{\partial r}|_{r=R^-} = -K_N \frac{\partial p_i}{\partial r}|_{r=R^+} \tag{2.1.42}$$

$$p_i|_{r=R^-} = p_i|_{r=R^+} \tag{2.1.43}$$

The superficial velocity is considered here, a macroscopic velocity defined as the flow rate per unit area over an area large compared to any pores, fibers or cells. The actual instantaneous velocity equals the superficial velocity, u_i divided by the interstitial volume fraction. If the volume fractions were equal in normal and tumor tissue, Eq. (2.1.38) would also hold for the instantaneous velocity [4]. The pressure will reach the value of p_∞ deep in the normal tissue:

$$p_i|_{r\to\infty} = p_\infty \tag{2.1.44}$$

2.1.3.1 Analytical solution for tumor surrounded by normal tissue

Consider Eq.(2.1.14) and its solution (2.1.23),

$$\frac{1}{r^2}\frac{\partial}{\partial r}(r^2\frac{\partial}{\partial r}) = \frac{\alpha^2}{R^2}(p_i - p_{ss})$$

$$p_i = \frac{1}{r}e^{\frac{\alpha}{R}(2c_2+r)} - \frac{1}{r}e^{\frac{\alpha}{R}(2c_1+2c_2-r)} + W$$

In Baxter model [4], it is assumed that in the necrotic core, the parameter α , and therefore the right hand side of Eq.(2.1.14) is zero. The solutions should be written separately for three regions where r is the radial position, R_n is the radius of the necrotic core and R is the radius of the tumor.
If $(r < R_n)$, Eq.(2.1.23) will reduce to:

$$p_i^n = W''$$

In the same manner as previous case (section 2.1.2.3), $W = p_{ss}$. Therefore, if $R_n < r < R$, we will have,

$$p_i^T = \frac{1}{r}e^{\frac{\alpha_T}{R}(2c_2+r)} - \frac{1}{r}e^{\frac{\alpha_T}{R}(2c_1+2c_2-r)} + p_{ss} \tag{2.1.45}$$

finally, based on Eq. (2.1.44), $W' = p_\infty$. Therefore, if $r > R$,

$$p_i^N = -\frac{1}{r}e^{\frac{\alpha_N}{R}(2c'_1+2c'_2-r)} + p_\infty \tag{2.1.46}$$

where n, T and N represent necrotic core, tumor (periphery) and normal tissue, respectively. By applying boundary condition (2.1.40) in Eq.(2.1.45), we will have,

$$e^{\frac{\alpha_T}{R}(2c_1+2c_2)} = e^{\frac{\alpha_T}{R}(2c_2)}\frac{e^{\frac{\alpha_T R_n}{R}}(\frac{1}{R_n} - \frac{\alpha_T}{R})}{e^{-\frac{\alpha_T R_n}{R}}(\frac{1}{R_n} + \frac{\alpha_T}{R})}. \tag{2.1.47}$$

By defining A as:

$$A = \frac{e^{\frac{\alpha_T R_n}{R}}(\frac{1}{R_n} - \frac{\alpha_T}{R})}{e^{-\frac{\alpha_T R_n}{R}}(\frac{1}{R_n} + \frac{\alpha_T}{R})} \tag{2.1.48}$$

Eq.(2.1.47) will be,

$$e^{\frac{\alpha_T}{R}(2c_1+2c_2)} = e^{\frac{\alpha_T}{R}(2c_2)}A. \tag{2.1.49}$$

By applying the forth boundary condition (2.1.43) in Eq.(2.1.46),

$$e^{\frac{\alpha_N}{R}(2c'_1+2c'_2)} = -\frac{R}{e^{-\alpha_N}}[\frac{1}{R}e^{\alpha_T}e^{\frac{\alpha_T}{R}2c_2}(1-A) + p_{ss} - p_\infty]$$

Define $\hat{K} = K_T/K_N$. Thus, Eq.(2.1.42) results that,

$$\hat{K}[e^{\alpha_T}e^{\frac{\alpha_T}{R}2c_2}(-1+\alpha_T) + e^{-\alpha_T}e^{\frac{\alpha_T}{R}2c_2}A(1+\alpha_T)] = e^{-\alpha_N}(1+\alpha_N)e^{\frac{\alpha_N}{R}(2c'_1+2c'_2)}. \tag{2.1.50}$$

Put the value of $e^{\frac{\alpha_N}{R}(2c'_1+2c'_2)}$ in Eq.(2.1.50),

$$e^{\frac{\alpha_T}{R}2c_2}[\hat{K}(e^{\alpha_T}(-1+\alpha_T) + e^{-\alpha_T}A(1+\alpha_T)) + (1+\alpha_N)e^{\alpha_T}(1-A)] = -R(1+\alpha_N)(p_{ss}-p_\infty)$$

Define,

$$B = \hat{K}(e^{\alpha_T}(-1+\alpha_T) + e^{-\alpha_T}A(1+\alpha_T)) + (1+\alpha_N)e^{\alpha_T}(1-A) \tag{2.1.51}$$

so,

$$e^{\frac{\alpha_T}{R}2c_2} = \frac{-R(1+\alpha_N)(p_{ss}-p_\infty)}{B} \tag{2.1.52}$$

Refer to Eq.(2.1.41),

$$W'' = \frac{1}{R_n}e^{\frac{\alpha_T}{R}2c_2}e^{\frac{\alpha_T R_n}{R}} - \frac{1}{R_n}e^{\frac{\alpha_T}{R}(2c_1+2c_2)}e^{\frac{-\alpha_T R_n}{R}} + p_{ss}$$

$$= \frac{1}{R_n}\frac{-R(1+\alpha_N)p_{ss}}{B}e^{\frac{\alpha_T R_n}{R}} - \frac{1}{R_n}\frac{-R(1+\alpha_N)p_{ss}}{B}Ae^{\frac{-\alpha_T R_n}{R}} + (p_{ss}-p_\infty)$$

$\Longrightarrow$

$$W'' = (p_{ss}-p_\infty)(1 - \frac{R}{R_n}\frac{(1+\alpha_N)}{B}p_{ss}(e^{\frac{\alpha_T R_n}{R}} - Ae^{-\frac{\alpha_T R_n}{R}})) \tag{2.1.53}$$

Finally, the interstitial fluid pressure distributions in three regions are described as in the following:

$$\begin{cases} p_i^n = (p_{ss}-p_\infty)(1 - \frac{R}{R_n}\frac{(1+\alpha_N)}{B}p_{ss}(e^{\frac{\alpha_T R_n}{R}} - Ae^{-\frac{\alpha_T R_n}{R}})) & (r < R_n)\ , \\ p_i^T = (p_{ss}-p_\infty)[\frac{-R}{r}\frac{(1+\alpha_N)}{B}(e^{\frac{\alpha_T r}{R}} - Ae^{\frac{-\alpha_T r}{R}}) + 1] & (R_n < r < R), \\ p_i^N = -\frac{1}{r}e^{-\frac{\alpha_N r}{R}}(-\frac{R}{e^{-\alpha_N}}[\frac{1}{R}e^{\alpha_T}(\frac{-R(1+\alpha_N)p_{ss}}{B})(1-A) + (p_{ss}-p_\infty)]) & (r > R) \end{cases} \tag{2.1.54}$$

According to Eq.(2.1.6), lymphatics appear by contributing the values of $(\frac{L_{pL}S_L}{V})$ and p_L. In this case, Baxter et al. [4] assumed that $p_L = 0$ because of the fast removal of fluid by distal lymphatics. The combinations by the necrotic core and the effect of its size on the interstitial pressure is illustrated by Baxter et al. [4] in Fig.(2.10). The interstitial pressure profile (in the area between the tumor border and the normal tissue) $(r/R \geq 1)$, Fig.(2.10) is influenced insignificantly by contributing nonuniform perfusion. The percentage of necrotic core presentation is shown by the ratio of R_n to R (R_n/R). In the case of uniform perfused tumor (section (2.1.2)), $R_n/R = 0$. According to Eq.(2.1.54) where $r < R_n$, the value of the interstitial pressure in the necrotic core is constant, as can be seen in Fig.(2.10). First consider a very large necrotic core, $R_n/R = 0.99$. So, an invisible small rim (periphery region) with less functional vessels remains. The interstitial pressure is constant through the necrotic core and then decreases through the normal tissue to the lowest value. Now, consider $R_n/R = 0.90$. A constant and maximum pressure in the necrotic core is clear in Fig.(2.10) and this maximum pressure is higher than that of previous one (very large necrotic core).

In addition, it is decreasing smoothly through the periphery region and finally decreases sharply outside the tumor. Overall, the lowest maximum pressure occurs with the largest necrotic core. While decreasing the size of necrotic core causes an increase in the periphery region, with more functional vessels and consequently an increased maximum value of the interstitial pressure.

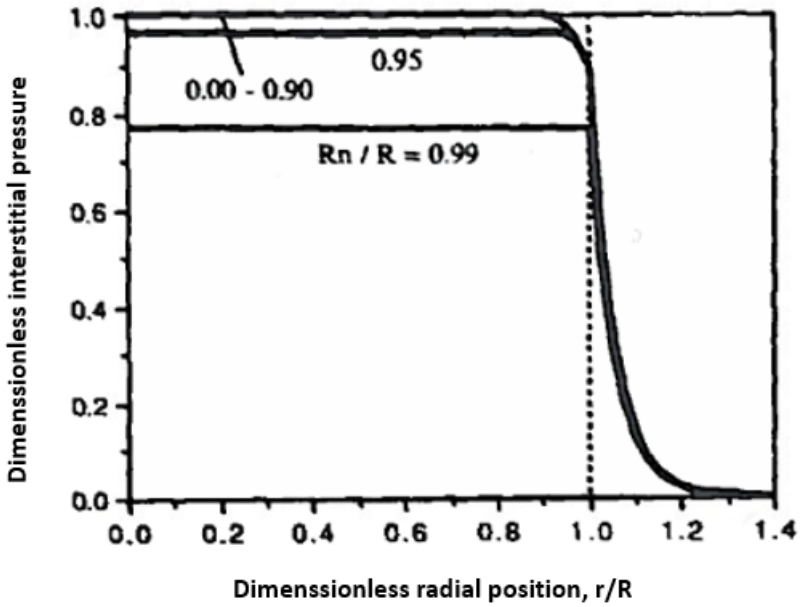

Figure 2.10: The distribution of interstitial pressure in a heterogeneous tumor surrounded by normal tissue for different sizes of necrotic core.

Baxter et al. [3][4] showed that not only the the heterogeneity of blood flow and barriers of interstitial transport, but also elevated interstitial pressure causes nonuniform drug penetration in the tumor matrix. High interstitial pressure influence the transportation system in tumors by acting as a barrier for inflow transport. Later, Soltani et al. [36] illustrated these effects in Fig.(2.11). One of the impacts of high interstitial pressure is that it decreases a moving forces for transcapillary exchange of fluid. High interstitial pressure in the center of a tumor causes low filtration process. While in the periphery region, high filtration happens because of low interstitial pressure. In addition, elevated interstitial pressure helps the fluid to transfer towards the outer layer of a tumor. It creates radially outward convection flux in the interstitium. The concentration gradient of the drug causes an inward diffusion. If the velocity of the diffusion process becomes higher than the velocity of the convection procedure, drugs can penetrate the tumor matrix. The elevated interstitial pressure is distributed equally in the center of a tumor which stops the process of convection. Therefore, the blood in the center of a tumor is perfused heterogeneously. Finally, it leads to a heterogeneous drug distribution. The theoretical frame work of Baxter et al. helped them to understand that the pressure, the status of drug penetration , the hydraulic conductivity of vessels and lymphatics are crucial factors in the actual drug uptake in tumors [36].

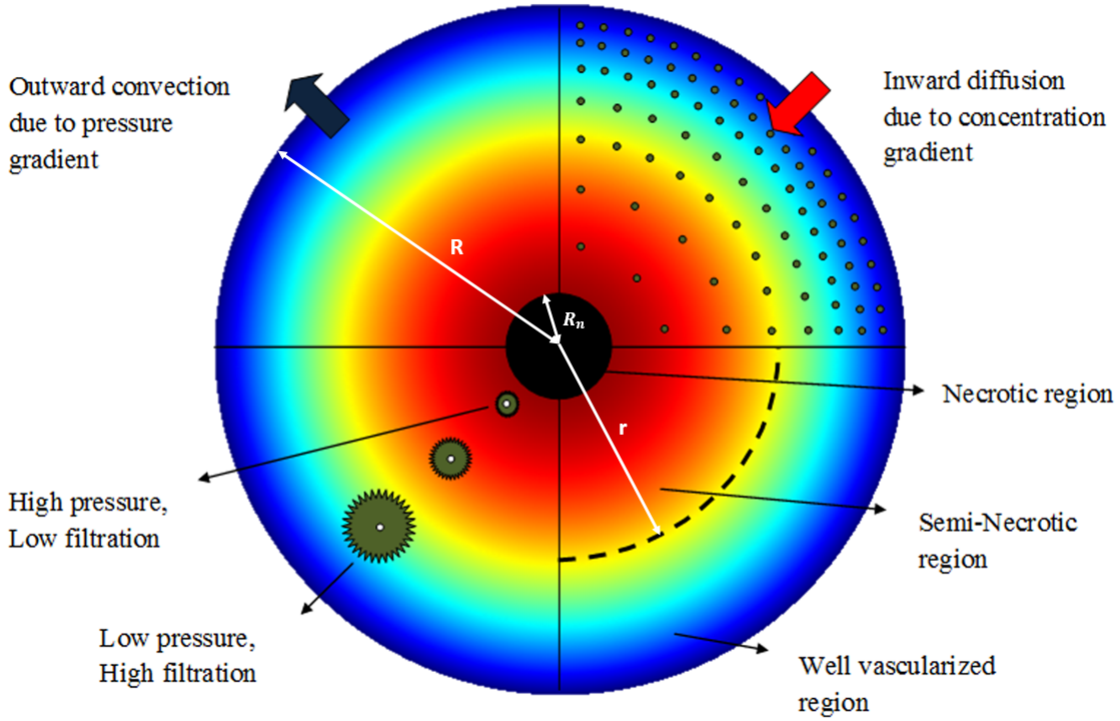

Figure 2.11: Schematic of heterogeneous tumor and the illustrated effect of high interstitial pressure on the drug delivery [36].

The role of lymphatics for macromolecular transport was also studied by using the model defined by Baxter et al. [4]. As lymphatics remove the fluid passed from vessels into interstitium, their presence in the tumor affects reducing the value of maximum pressure. The heterogeneous perfusion and lymphatic drainage have roles on building the structure of the tumor, and the effects of these two factors are considered together to determine the profile of interstitial pressure [4]. Inside our body, lymphatic vessels are widely distributed and they are more permeable to fluid and solutes than the blood capillaries [18]. The main task of the lymphatic system is to return the interstitial fluid to the blood circulation. Large particles such as tumor cells, which are detached from a primary tumor, can enter the lymph by passing between the cells of the lymphatic network [40]. One of the characteristics of solid tumors is related to a poor or non-functional lymphatic system [18]. The lack of lymphatic drainage in solid tumors affects on the drug delivery process to the tumor matrix. In addition to investigating the role of necrotic core on determining the interstitial pressure, Baxter at al. [4], in Fig(2.12), showed the effect of having functional lymphatics, on the interstitial pressure throughout the tumor, surrounded by normal tissue without a necrotic core. Similar to the results of the necrotic core efficiency, the outcomes show that lymphatics have a negligible influence on the shape of the interstitial pressure profile. However, lymphatics have significant effect on the value of steady state pressure, p_{ss}, defined in Eq.(2.1.12). As it is mentioned before, the presence of lymphatics correlates with the value of $\frac{L_{pL}S_L}{V}$. Since it is obvious in Fig(2.12), for the alymphatic tumor, where $\frac{L_{pL}S_L}{V} = 0.00$, the highest maximum interstitial pressure happens with the value of 11.5 (mmHg). While the value of maximum interstitial pressure is decreasing by raising the values of $\frac{L_{pL}S_L}{V}$. It illustrates that the presence of lymphatic in the tumor decreases the elevated interstitial pressure and consequently facilitates the drug delivery process.

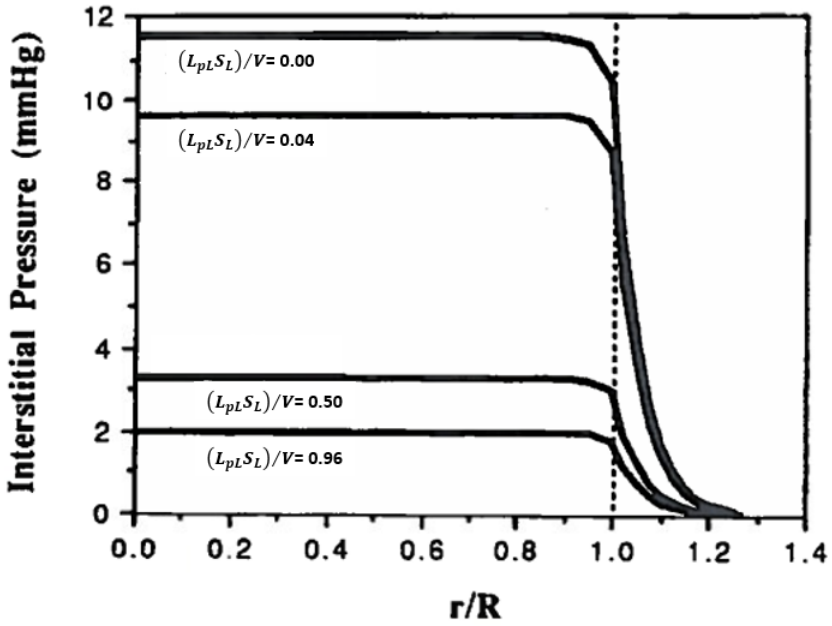

Figure 2.12: The efficiency of lymphatics on the distribution of the interstitial pressure in the homogeneous tumor surrounded by normal tissue - $\frac{r}{R}$: dimensionless radial position.

2.2 Based on Liu-Schlesinger model

Traditionally, the hydraulic conductivity K has been considered as a constant both in the tumor and normal tissue to determine the TIFP distribution (as it was in Baxter et al. model [3][4]). However, investigations demonstrate that the hydraulic conductivity is not a constant in most tissues and it should be a spatially dependent variable. Many factors correlates with the hydraulic conductivity, K, (see Fig.(2.13)). Beside those, K depends on the intrinsic permeability of the material and the degree of saturation, as well as the density and viscosity of the fluid. In this section we are focusing on the model and assumptions used by L.J Liu and M. Schlesinger [21]. Their main concern was to express a proper and valid hydraulic conductivity to determine the real tumor interstitial fluid pressure distribution. They have assumed avascular or poorly vascularized heterogeneous tumor. In addition, they introduced a continuous change of the interstitial hydraulic conductivity in order to correspond to the actual TIFP distribution [21]. Similar to Baxter et al. model [3][4], fluid transport is described by Darcy's law be cause of the fact that the surroundings of the interstitial fluid is considered as a porous medium[21].

$$\mathbf{u} = -K\boldsymbol{\nabla} p \tag{2.2.1}$$

Eq.(2.2.1) illustrates that interstitial fluid flow corresponds with the hydraulic conductivity K, and the gradient of fluid pressure which is the driving force also straightly relates to the hydraulic conductivity.

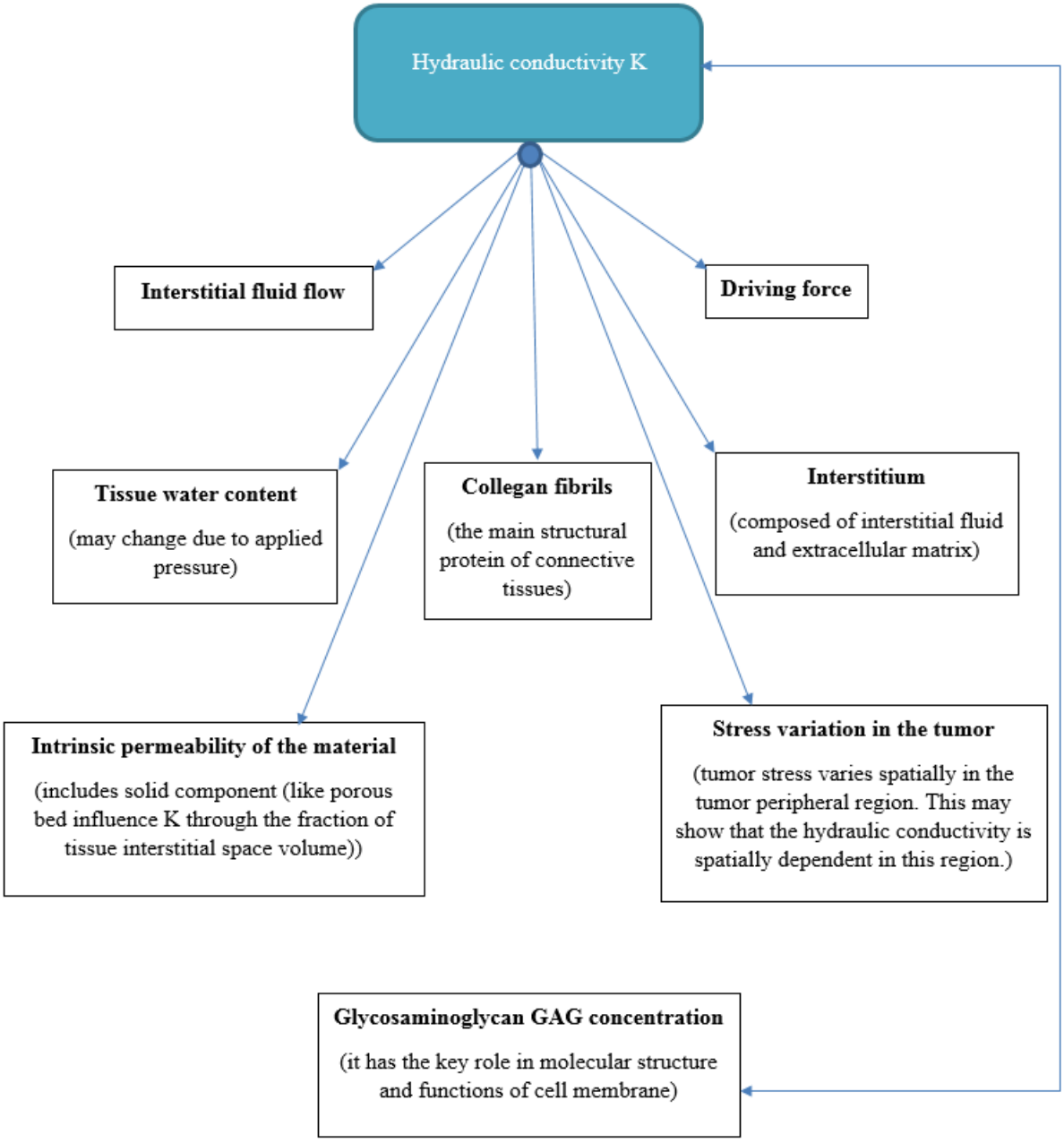

Figure 2.13: Factors which correlate with hydraulic conductivity (K) as described in [21] .

2.2.1 Mathematical modeling

Liu et al. [21], divided a typical tumor and its surroundings into three different regions as illustrated in Fig.(2.14). They suggested an intermediary region between the surface of the tumor and its surrounding normal tissue, through which the interstitial fluid moves from tumor to normal tissue. Because of the difference in density of vascular networks in the center of the tumor compared to the periphery region, the impact of the hydraulic conductivity may be different in the various regions [20]. The hydraulic conductivity is introduced as a continuous changing parameter by Liu et al. [21] which allows for a different, perhaps more realistic, TIFP behaviour in the different regions. For the sake of simplicity, Liu et al. imagine the tumor with a spherical structure. By attending to the difference of vascular network distribution and cell activity in various regions, especially the change of tumor interstitial fluid pressure, tumor is divided into three following regions [20]:

1. a necrotic central core where most cells are dead and there are no small functional vessels and where the tumor interstitial fluid pressure, p_0, is uniform. Interstitial hydraulic conductivity can be taken as constant K'.

2. a vascularized periphery region. Here, tumor blood vessels are plenty. This region is the main source of tumor interstitial fluid.

3. an intermediary region. In this area, there is almost no tumor fluid source and only lymphatics exists for tumor fluid to be absorbed.

The outer area, is the normal tissue region, where interstitial fluid pressure and interstitial hydraulic conductivity can be chosen as constants p_∞ and K, respectively. It is assumed that there are no functional lymphatics within the tumor but some enlarged lymphatics exist near the periphery. In the necrotic core, there is no living tissue and no functional exchange vessels. There is no source or drain in the necrotic core region. In the blood vessel area, there is fluid source and negligible drainage system. It is assumed that the drain exists near the edge of the tumor. Outside the tumor (in the intermediary region), there are drains due to the functional lymphatics in the normal tissue. In the well vascularized area, the abundance of blood vessel capillaries are significant [20]. Generally, the necrotic core is in the central region of the tumor and R_0 represents the radius of the necrotic core. The functional blood vessels are distributed in the periphery with the limited area of $R_0 < r < R_s$, where R_s represents tumor surface. Moreover, R_m is the maximum distance size that the tumor fluid can move before being normalized (see Fig.(2.14)).

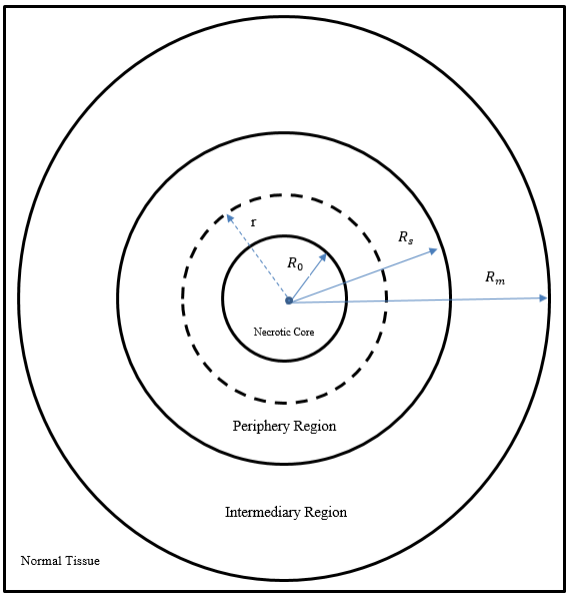

Figure 2.14: Schematic of a heterogeneous tumor surrounded by normal tissue with defined regions- r: radial position

Here again, the same as the definition in Eq.(2.1.4) in section (2.1.1), the continuity equation for steady-state incompressible flow is defined as in the following:

$$\nabla \cdot \vec{u}(\vec{r}) = \frac{J_V}{V} - \frac{J_L}{V} \tag{2.2.2}$$

Where $\frac{J_V}{V}$ ($\sec^{-1}$) is the volumetric net flow rate for fluid coming out of blood vessels i.e. the fluid source term which is given by Starling's Law, and $\frac{J_L}{V}$ ($\sec^{-1}$) is the volumetric flow rate for fluid being absorbed into the lymphatics i.e. the lymphatic drainage term assumed to be proportional to the pressure difference between the interstitium and lymphatics. The Interstitial fluid emanates from permeable tumor vessels and is described by Starling's Law, which illustrates the role of hydrostatic and osmotic forces in the movement of fluid across capillary membranes. Below the classic Starling equation is shown,

$$J_V = L_V S[(p_V - p_i) - \sigma(\pi_V - \pi_i)] \tag{2.2.3}$$

where, L_V (cm/mmHg sec) is the hydraulic conductivity of the vessel membrane, S (cm^2) is the surface area for filtration. In addition, as we have incompressible fluids, p_V (mmHg) is the hydrostatic capillary pressure, p_i (mmHg) is the interstitial pressure, σ is the reflection coefficient, π_p (mmHg) is the plasma oncotic pressure and π_i (mmHg) is the interstitial osmotic pressure. In the model described by Baxter et al. [3][4], only arterioles were considered, while Liu et al. [21] considered the whole structure of the blood capillaries (arterial and venous capillaries). As shown in Fig.(2.15), in our body the blood flows through the large arterioles and into the microvasculatures, where it delivers nutrition and oxygen through arterial capillaries in different organs and tissues. Meanwhile, through blood vessel capillary, excess fluid is absorbed by the capillaries and to the venules and transported back to the pulmonary system and the heart. Normally, lymphatic capillaries are distributed next to the blood capillaries. Through lymphatics, fluid flows only in one direction to the heart and remove the excess fluid from the interstitium.

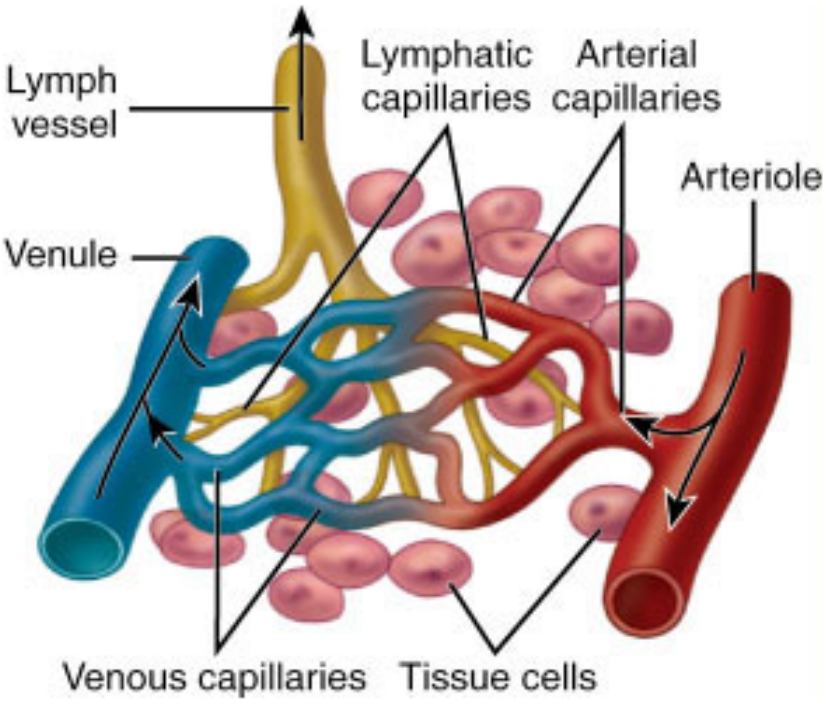

Figure 2.15: Capillary bed. The blood transfer occurs in between arterial and venous capillaries [7].

The flow rate is described as in the following (A represents arterioles):

$$J_S = S_A L_A[p_A - p(\vec{r}) - \sigma_A(\pi_A - \pi_{Ai})] \tag{2.2.4}$$

As an improvement of the model presented by Baxter et al [3], Liu et al. [21] expressed the net flow rate by considering both arterioles and venules,

$$J_S = \frac{S_A}{V} L_A[p_A - p(\vec{r}) - \sigma_A(\pi_A - \pi_{Ai})] + \frac{S_V}{V} L_V[p_V - p(\vec{r}) - \sigma_V(\pi_V - \pi_{Vi})] \tag{2.2.5}$$

where the indices of A and V represent arterioles and venules, respectively, and the parameters in Eq.(2.2.5) have the same concepts as parameters in Eq.(2.2.3) defined both for arterial and venous capillaries. As it is shown in Fig.(2.16), through arteriole, outward flow of fluid (filtration) is observed by hydrostatic pressure of arterial capillary due to the hydrostatic pressure of arterial capillaries which is higher than the osmotic pressure, $p_A > \pi_A$. Unlike, the venous capillaries, the osmotic pressure here is higher than the hydrostatic pressure, $p_V < \pi_V$. Thus, π_V produces inward flow of fluid (absorption). A typical values of osmotic and hydrostatic pressure both in blood capillaries (consisting arterial and venous) and interstitial and their relationship and consequent functions are illustrated in Fig.(2.17). As shown, the osmotic pressure of the arteriole end and the venule end are the same; while the hydrostatic pressure of the arteriole is higher than the hydrostatic pressure of venule. Note that the direction of the pressures shows the sign of them in the first figure of Fig.(2.17). The filtration pressure is calculated by the summation of the hydrostatic blood capillary pressure and the osmotic interstitium pressure which is not clearly the same for arteriole and venule. The absorption pressure is obtained by summing the osmotic pressure of the interstitium and interstitial hydrostatic pressure.This has the same value for arteriole and venule. The net fluid pressure (NFP) is defined as a difference between the filtration and absorption pressure.

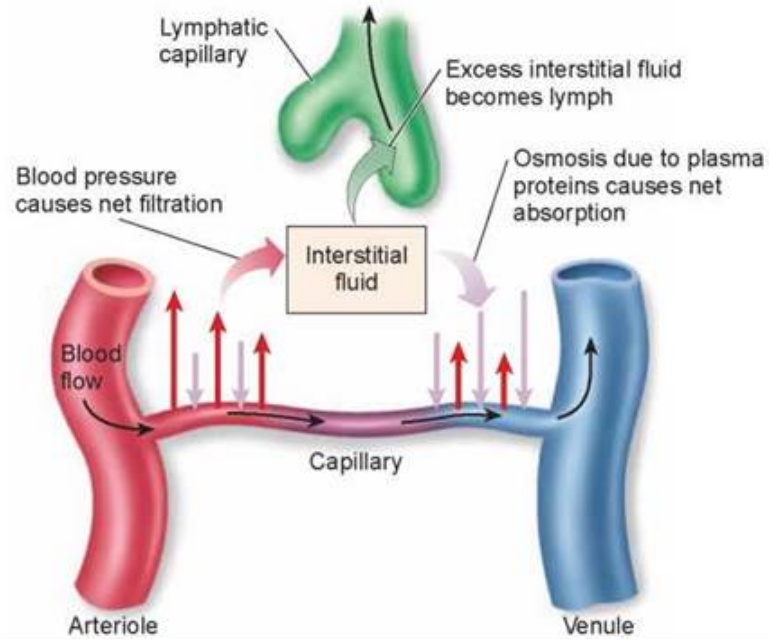

Figure 2.16: Functions of arterial and venous capillaries [44].

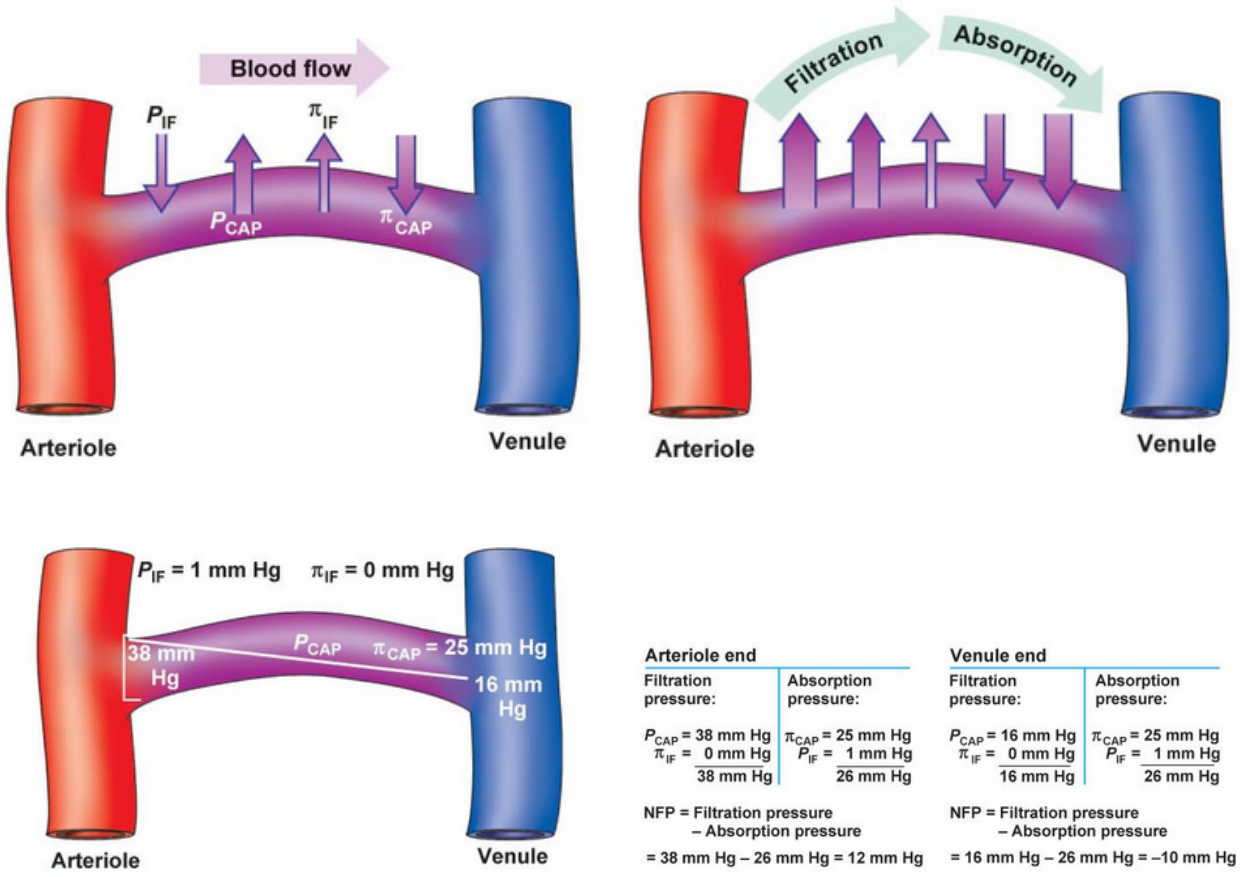

Figure 2.17: Functions of arterial and venous capillaries [9]. P_{IF} and π_{IF} are defined as the hydrostatic and osmotic pressures of the interstitial and P_{CAP} and π_{CAP} are the hydrostatic and osmotic pressure of the blood capillary.

As lymphatic vessels are highly permeable, they have no osmotic pressure, so the pressure difference between the interstitial fluid and the lymph explains the interstitial fluid drainage:

$$\phi_L = \frac{S_L}{V} L_L [p(\vec{r}) - p_L] \tag{2.2.6}$$

where L_L (cm/mmHg sec) is the hydraulic conductivity of lymphatic vessels, and p_L (mmHg) is the pressure in lymphatic vessels. Baluk et al.[2] understood that the basic membrane of blood vessels are not normal in a tumor. As a comparison of the status of blood vessels in a normal tissue and tumor, the entries of tumor blood vessels are more larger and their abundance is higher. Some big proteins can come out from the membrane of blood vessels. The oncotic pressure π in tumors is evaluated. Therefore, the oncotic pressure difference $(\pi_v - \pi)$ is small. Moreover, the hydraulic conductivity and the surface area of blood vessels in a tumor are greater than those in normal tissue. As a result, in a tumor, the net flow of exudates from blood vessels is higher than that in normal tissue [21]. On the other hand, as in the center of the tumor functional lymphatics do not exist, the leaking system is not effective and tumor cells increase the resistance of fluid. In addition, some large proteins which are leaked from the blood vessels may not be drained or absorbed. They sit in the tumor and decrease the facility of transportation of fluid [21]. Some of the interstitial fluid of the tumor enters into the normal tissue. However Starling's law describes the source and sink of interstitial fluid, as the distribution of the vessels and lymphatic in the tumor is not predicted, it is not easy to measure

the amount of fluid flow. The net flow rate across the tumor surface for a volume of V is:

$$\nabla \cdot \vec{u}(\vec{r}) = \frac{J_S(V)}{V} - \frac{J_L(V)}{V} \tag{2.2.7}$$

The distribution of blood vessels and lymphatics describes the transportation of interstitial fluid in addition to defining the distribution of tumor interstitial fluid pressure.

Now, some formulations are presented which will be used to analytically investigate the interstitial fluid pressure for some limiting cases. Liu et al. [21] focused on the two specific types of tumors. A tumor with a very small necrotic core placed in the center which is defined as the spherical case (Fig.(2.18a)). And the case in which the tumor has a very large necrotic core, resulting in a very small rim, which is the planar case (Fig.(2.18b)).

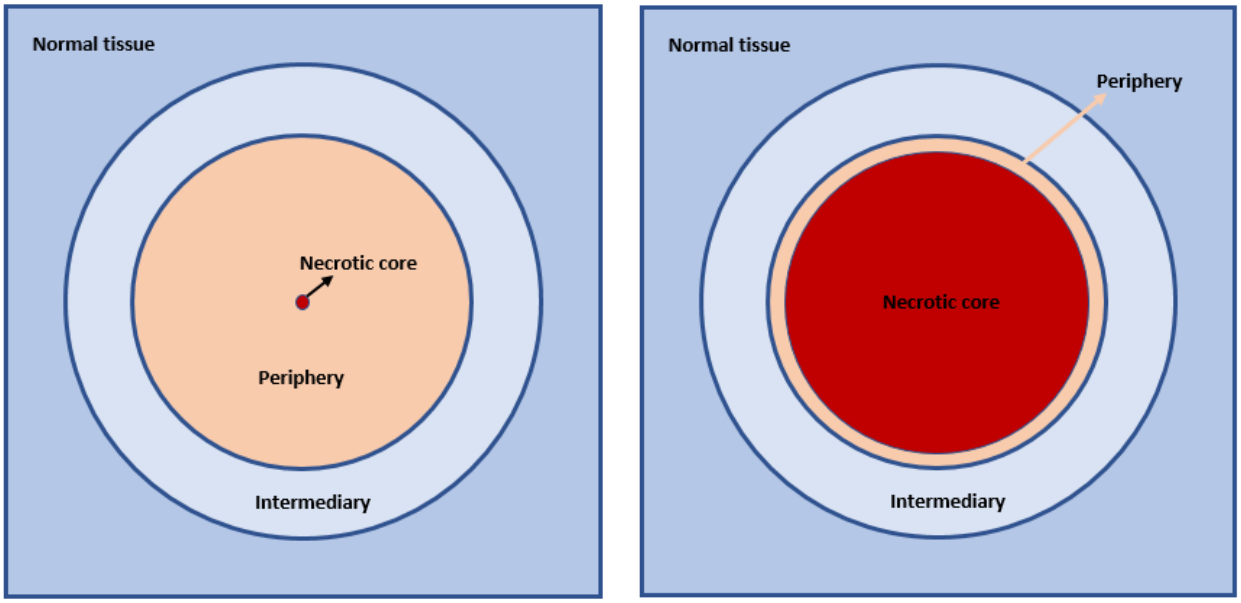

(a) Spherical case (very small necrotic core) (b) Planar case (very large necrotic core)

Figure 2.18: Schematic of tumor for Planar and Spherical cases.

To analytically get the tumor interstitial fluid pressure distribution in these two cases, formulating the related Laplace equation is needed for each case. First, consider the spherical case. Referring to Eqs.(2.2.1), (2.2.5), (2.2.6) and (2.2.7) and referencing Fig.(2.14), if ($R_0 < r < R_s$):

$$\nabla \cdot (-K' \boldsymbol{\nabla} p) = \frac{S_A}{V} L'_A [p_A - \sigma_A(\pi_A - \pi_{Ai})] + \frac{S_V}{V} L'_V [p_V - \sigma_V(\pi_V - \pi_{Vi})] - (\frac{S_A L'_A}{V} + \frac{S_V L'_V}{V}) p(\vec{r}) - \frac{S_L L'_L}{V} [p(\vec{r}) - p_L]$$

$$= \frac{S_A L'_A p_A + S_V L'_V p_V + S_L L'_L p_L - S_A L'_A \sigma_A \Delta\pi_A - S_V L'_V \sigma_V \Delta\pi_V}{S_A L'_A + S_V L'_V + S_L L'_L} (\frac{S_A L'_A + S_V L'_V + S_L L'_L}{V}) - \frac{S_A L'_A + S_V L'_V + S_L L'_L}{V} p(\vec{r}).$$

Define α and p_e as in the following,

$$\alpha = \frac{L'_A S_A + L'_V S_V + L'_L S_L}{V}$$

and,

$$p_e = \frac{L'_A S_A p_A + L'_V S_V p_V + L'_L S_L p_L - L'_A S_A \sigma_A \Delta\pi_A - L'_V S_V \sigma_V \Delta\pi_V}{L'_A S_A + L'_V S_V + L'_L S_L}.$$

So,

$$\nabla(K'\boldsymbol{\nabla}p) = \alpha(p - p_e) \tag{2.2.8}$$

Furthermore, if $(R_s < r < R_m)$, as assumptions, there is no source of the tumor interstitial fluid in the periphery region. So,

$$\nabla\cdot(-K\boldsymbol{\nabla}p) = -\frac{S_L L_L}{V}[p - p_L].$$

Define $\beta = \frac{S_L L_L}{V}$, so,

$$\nabla\cdot(K\boldsymbol{\nabla}p) = \beta(p - p_L) \tag{2.2.9}$$

By using ∇^2, calculated in Appendix 1,

$$\nabla^2 = \frac{1}{r^2}\frac{\partial}{\partial r}(r^2\frac{\partial}{\partial r}) + \frac{1}{r^2\sin\theta}\frac{\partial}{\partial\theta}(\sin\theta\frac{\partial}{\partial\theta}) + \frac{1}{r^2\sin^2\theta}\frac{\partial^2}{\partial\phi^2}$$

Consider Eqs.(2.2.8) and (2.2.9) in spherical coordinate and take spherical symmetry in to account. So, the Laplace equation in the spherical case can be written as,

$$\begin{cases} r\frac{d}{dr}(K'\frac{dp(r)}{dr}) + 2K'\frac{dp(r)}{dr} - \alpha r(p - p_e) = 0 \quad \text{(periphery region, } R_0 < r < R_s\text{)} \ , \\ \\ r\frac{d}{dr}(K\frac{dp(r)}{dr}) + 2K\frac{dp(r)}{dr} - \beta r(p - p_L) = 0 \quad \text{(intermediary region, } R_s < r < R_m\text{)}. \end{cases} \tag{2.2.10}$$

In the planar case, we can consider Cartesian coordinates in which Eqs.(2.2.8) and (2.2.9) can be written as,

$$\begin{cases} \frac{d}{dr}[K'\frac{dp(r)}{dr}] - \alpha r(p - p_e) = 0 \quad \text{(periphery region, } R_0 < r < R_s\text{)} \ , \\ \\ \frac{d}{dr}[K\frac{dp(r)}{dr}] - \beta r(p - p_L) = 0 \quad \text{(intermediary region, } R_s < r < R_m\text{)}. \end{cases} \tag{2.2.11}$$

The boundary conditions described by Liu et al. [21] are mentioned below.
In the center of the tumor, the interstitial fluid pressure is monotone at steady state [21]. In this region the fluid velocity is zero because of the fact that the gradient of the pressure is zero. The boundary and continuity conditions are given as follows from [21],

$$p(R_0) = p_0, u(R_0) = -K'\frac{dp(R_0)}{dr} = 0 \tag{2.2.12}$$

$$p(R_m) = p_\infty, u(R_m) = -K\frac{dp(R_m)}{dr} = 0 \tag{2.2.13}$$

$$p(R_s^+) = p(R_s^-) = p(R_s), K\frac{dp(R_s^+)}{dr} = K'\frac{dp(R_s^-)}{dr} = -u(R_s) \tag{2.2.14}$$

2.2.2 Spatially dependency of the interstitial hydraulic conductivity

Here, Liu et al. [21] introduced a continuous change of interstitial hydraulic conductivity and suggested a linearly decreasing interstitial hydraulic conductivity through the periphery region and a linearly increasing interstitial hydraulic conductivity through the intermediary region (They showed the behaviour of interstitial hydraulic conductivity in Fig.(2.19)). In the necrotic core, in addition to the interstitial fluid pressure, p_0, the structure and composition of the interstitium is mostly monotone. Thus, Liu et al. [21] took the interstitial hydraulic conductivity as a constant in the central region, K' . Similarly, the interstitial hydraulic conductivity has been taken as a constant in the normal tissue, K. In the tumor periphery and intermediary region the structure and combination of the interstitium as well as the pressure distribution are changing. So, assume that the hydraulic conductivity in these two regions is dependent to the radial position, r (cm). Based on the relevance between the interstitial hydraulic conductivity and the TIFP distribution, the correct definition of the interstitial hydraulic conductivity is needed to approach the actual tumor interstitial fluid pressure distribution. Thus, the correct definition of the interstitial hydraulic conductivity both in the periphery an intermediary regions is needed.

2.2.2.1 Periphery region

Liu et al. [21] suggested that in the periphery region, where $R_0 < r < R_s$ (see Fig.(2.14), the blood capillary hydraulic conductivity, L_p, increases exponentially with the radial position r. In contrast, the interstitial hydraulic conductivity decreases smoothly by increasing the radial position, r. The abundance of the leaky blood vessels is qiute high in the periphery region and a pressure obstacle occurs [20]. In this region, the structure and composition of the interstitium is not fixed, and the blood vessels may distribute unequally. In the central region the amount of consisting of the water content is more than the existence of vessels and the resistance of the interstitial fluid transport increases in the periphery region. As a result, the interstitial hydraulic conductivity at the central region border is greater than that at the tumor surface. Although it is not easy to define an exact distribution of the interstitial hydraulic conductivity, since the periphery region is narrow, Liu et al. [21] suggested a linear change of interstitial hydraulic conductivity. By defining d_0 as the distance between the periphery and the necrotic region ($d_0 = R_s - R_0$), we have,

$$K'(r) = K' - \frac{K' - K_s}{d_0}(r - R_0) \tag{2.2.15}$$

2.2.2.2 Intermediary region

In the intermediary region (the limited area between the tumor and the normal tissue), where $R_s < r < R_m$, Liu et al. [21] suggested that the interstitial hydraulic conductivity in this region should be treated in such a way that their model produces continuous first derivatives of pressure as a function of r. The interstitial hydraulic conductivity is described by a spatially continuous function $K(r)$, that has a value between the hydraulic conductivity in normal tissue, K, and the hydraulic conductivity at the tumor surface, K_s, because of the fact that the interstitial hydraulic conductivity depends on the intrinsic permeability of the tissue. A smaller interstitial hydraulic conductivity leads to a higher tumor interstitial fluid pressure. By the acceptance of continuous and spatial changes of the interstitial hydraulic conductivity, the assumption of $K > K_s$ is demanded. When defined as $d_m = R_m - R_s$, the variation of $K(r)$ as a linear function of r can be approximated. Thus,

$$K(r) = K_s + \frac{K - K_s}{d_m}(r - R_s) \tag{2.2.16}$$

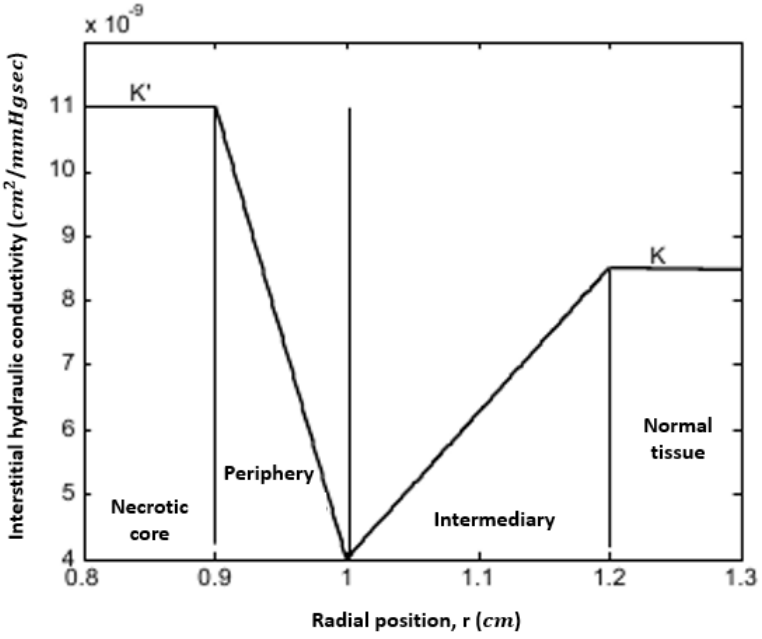

Figure 2.19: The behaviour of interstitial hydraulic conductivity in different regions investigated by Liu et al. [21].

Liu et al. [21] realized that the interstitial hydraulic conductivity has an important role in specifying the distribution of tumor interstitial fluid pressure (TIFP). As it was mentioned, traditionally, the interstitial hydraulic conductivity was considered as a constant.
Liu et al. [21], first, analytically investigate the TIFP distribution for the two cases, shown in Fig.(2.18), by considering constant values of interstitial hydraulic conductivity, K' and K, for tumor and normal tissue, respectively. Then, apply a continuous variation of the interstitial hydraulic conductivities defined in Eqs.(2.2.15) and (2.2.16), to investigate the pressure behaviour only for planar.

We would like to point out that, in this work, the following computations give the full derivation of the two analytical solutions, which were not presented by Liu et al. [21].
In the case of setting constant values of interstitial hydraulic conductivity for a tumor, K', and for normal tissue, K, the analytical solution will be obtained with almost similar analytical method we applied for solving the model presented by Baxter et al. [4]. The difference is that, in Liu et al. model, the parameter $\frac{J_V)}{V}$ in Eq.(2.1.5) changes to Eq.(2.2.5), which includes both arterioles and venules.

2.2.3 Analytical solution for a tumor with very large necrotic core

Consider Eq.(2.2.11).

$$\begin{cases} \frac{d}{dr}[K'\frac{dp(r)}{dr}] - \alpha r(p - p_e) = 0 \quad (R_0 < r < R_s) \ , \\ \\ \frac{d}{dr}[K\frac{dp(r)}{dr}] - \beta r(p - p_L) = 0 \quad (R_s < r < R_m). \end{cases}$$

The solution is obtained as in the following.
If $(R_0 < r < R_s)$:

$$K'\frac{d^2p}{dr^2} - \alpha(p - p_e) = 0$$

then,

$$K'\frac{d^2p}{dr^2} - \alpha p = -\alpha p_e \tag{2.2.17}$$

Consider the homogeneous partial differential equation of Eq.(2.2.17). Then,

$$K'\frac{d^2p}{dr^2} - \alpha p = 0 \tag{2.2.18}$$

define $x = \frac{d^2p}{dr^2}$, so $K'x^2 - \alpha = 0$, then $x = \pm\sqrt{\frac{\alpha}{K'}}$. Accordingly, the solution for Eq.(2.2.18), by defining p_h as the solution for homogeneous case, is obtained,

$$p_h = c_1 e^{\sqrt{\frac{\alpha}{K'}}r} + c_2 e^{-\sqrt{\frac{\alpha}{K'}}r}$$

Define p_{nh} where $p = p_h + p_{nh}$ is the solution of Eq.(2.2.17). Assume that $p_{nh} = A$ solves the Eq.(2.2.17)), so, $K'(0) - \alpha A = -\alpha p_e \Rightarrow A = p_e \Rightarrow p_{nh} = p_e$. Thus, the solution of Eq.(2.2.17) can be written as,

$$p = c_1 e^{\sqrt{\frac{\alpha}{k'}}r} + c_2 e^{-\sqrt{\frac{\alpha}{k'}}r} + p_e \tag{2.2.19}$$

In the similar way, the solution for the region of $(R_s < r < R_m)$ can be obtained. Thus, the general solution of Eq.(2.2.11) is

$$\begin{cases} p = c_1 e^{\sqrt{\frac{\alpha}{k'}}r} + c_2 e^{-\sqrt{\frac{\alpha}{k'}}r} + p_e \quad (R_0 < r < R_s) \ , \\ \\ p = c_3 e^{\sqrt{\frac{\beta}{k}}r} + c_4 e^{-\sqrt{\frac{\beta}{k}}r} + p_L \quad (R_s < r < R_m). \end{cases} \tag{2.2.20}$$

The constants of c_1, c_2, c_3, c_4, p_e and p_L will be calculated by applying the boundary conditions. According to the first boundary condition mentioned in Eq.(2.2.12):

$$c_1 e^{\sqrt{\frac{\alpha}{k'}}R_0} + c_2 e^{-\sqrt{\frac{\alpha}{k'}}R_0} = p_0 - p_e \tag{2.2.21}$$

and,

$$-K'[c_1\sqrt{\frac{\alpha}{K'}}e^{\sqrt{\frac{\alpha}{K'}}R_0} - c_2\sqrt{\frac{\alpha}{K'}}e^{-\sqrt{\frac{\alpha}{K'}}R_0}] = 0$$

$\Longrightarrow$

$$c_1e^{\sqrt{\frac{\alpha}{K'}}R_0} - c_2e^{-\sqrt{\frac{\alpha}{K'}}R_0} = 0. \tag{2.2.22}$$

By combining the two Eqs.(2.2.21) and (2.2.22) we get:

$$c_1e^{\sqrt{\frac{\alpha}{K'}}R_0} = \frac{p_0 - p_e}{2} \tag{2.2.23}$$

The value of c_2 can be obtained by putting the value of c_1 in Eq.(2.2.22),

$$c_2 = \frac{p_0 - p_e}{2}e^{\sqrt{\frac{\alpha}{K'}}R_0} \tag{2.2.24}$$

Relying on the second boundary condition, Eq.(2.2.13):

$$c_3e^{\sqrt{\frac{\beta}{k}}R_m} + c_4e^{-\sqrt{\frac{\beta}{k}}R_m} = p_\infty - p_L \tag{2.2.25}$$

and,

$$-K[c_3\frac{\beta}{k}e^{\sqrt{\frac{\beta}{k}}R_m} - c_4\frac{\beta}{k}e^{-\sqrt{\frac{\beta}{k}}R_m}] = 0$$

then,

$$c_3e^{\sqrt{\frac{\beta}{k}}R_m} - c_4e^{-\sqrt{\frac{\beta}{k}}R_m} = 0 \tag{2.2.26}$$

The summation of Eqs. (2.2.25) and (2.2.26) gives the value of c_3

$$c_3e^{\sqrt{\frac{\beta}{k}}R_m} = \frac{p_\infty - p_L}{2}$$

Place c_3 in Eq.(2.2.26). Then,

$$c_4 = \frac{p_\infty - p_L}{2}e^{\sqrt{\frac{\beta}{k}}R_m} \tag{2.2.27}$$

According to the third boundary condition mentioned in Eq.(2.2.14):

$$c_3e^{\sqrt{\frac{\beta}{k}}R_s} + c_4e^{-\sqrt{\frac{\beta}{k}}R_s} + p_L = c_1e^{\sqrt{\frac{\alpha}{k'}}R_s} + c_2e^{-\sqrt{\frac{\alpha}{k'}}R_s} + p_e$$

$\Longrightarrow$

$$(p_\infty - p_L)[e^{\sqrt{\frac{\beta}{K}}(R_s-R_m)} + e^{-\sqrt{\frac{\beta}{K}}(R_s-R_m)}] + 2p_L = (p_0 - p_e)[e^{\sqrt{\frac{\alpha}{K'}}(R_s-R_0)} + e^{-\sqrt{\frac{\alpha}{K'}}(R_s-R_0)}] + 2p_e \tag{2.2.28}$$

Define $A = e^{\sqrt{\frac{\beta}{K}}(R_s-R_m)} + e^{-\sqrt{\frac{\beta}{K}}(R_s-R_m)}$ and $B = e^{\sqrt{\frac{\alpha}{K'}}(R_s-R_0)} + e^{-\sqrt{\frac{\alpha}{K'}}(R_s-R_0)}$. Then, Eq.(2.2.28) can be written as in the following,

$$p_\infty A - p_L A + 2p_L = p_0 B - p_e B + 2p_e$$

$\Longrightarrow$

$$-(A-2)p_L + (B-2)p_e = Bp_0 - Ap_\infty \tag{2.2.29}$$

In addition, from the third boundary condition mentioned in Eq.(2.2.14),

$$K[c_3\sqrt{\frac{\beta}{k}}e^{\sqrt{\frac{\beta}{k}}R_s} - c_4\sqrt{\frac{\beta}{k}}e^{-\sqrt{\frac{\beta}{k}}R_s}] = K'[c_1\sqrt{\frac{\alpha}{K'}}e^{\sqrt{\frac{\alpha}{K'}}R_s} - c_2\sqrt{\frac{\alpha}{K'}}e^{-\sqrt{\frac{\alpha}{K'}}R_s}] = -u(R_s) \tag{2.2.30}$$

$\Longrightarrow$

$$K\sqrt{\frac{\beta}{K}}[\frac{p_\infty - p_L}{2}][e^{\sqrt{\frac{\beta}{K}}(R_s-R_m)} - e^{-\sqrt{\frac{\beta}{K}}(R_s-R_m)}] = K'\sqrt{\frac{\alpha}{K'}}[\frac{p_0 - p_e}{2}][e^{\sqrt{\frac{\alpha}{K'}}(R_s-R_0)} - e^{-\sqrt{\frac{\alpha}{K'}}(R_s-R_0)}]$$

by defining $C = e^{\sqrt{\frac{\beta}{K}}(R_s-R_m)} - e^{-\sqrt{\frac{\beta}{K}}(R_s-R_m)}$, $D = e^{\sqrt{\frac{\alpha}{K'}}(R_s-R_0)} - e^{-\sqrt{\frac{\alpha}{K'}}(R_s-R_0)}$ and $\hat{K} = \frac{K'\sqrt{\frac{\alpha}{K'}}}{K\sqrt{\frac{\beta}{K}}}$, we have,

$$p_\infty C - p_L C = \hat{K}[p_0 D - p_e D]$$

$\Longrightarrow$

$$-Cp_L + \hat{K}Dp_e = -Cp_\infty + \hat{K}Dp_0 \tag{2.2.31}$$

As a result, p_L is obtained from Eq.(2.2.31):

$$p_L = p_\infty - \frac{\hat{K}D}{C}p_0 + \frac{\hat{K}D}{C}p_e \tag{2.2.32}$$

By substituting p_L in Eq.(2.2.29), p_e will be obtained:

$$-(A-2)[p_\infty - \frac{\hat{K}D}{C}p_0 + \frac{\hat{K}D}{C}p_e] + (B-2)p_e = Bp_0 - Ap_\infty$$

$\Longrightarrow$

$$p_e[-\frac{A\hat{K}D}{C} + \frac{2\hat{K}D}{C} + (B-2)] = [-\frac{A\hat{K}D}{C} + \frac{2\hat{K}D}{C} + B]p_0 - 2p_\infty$$

Define $E = -\frac{A\hat{K}D}{C} + \frac{2\hat{K}D}{C} + (B-2)$ and $F = -\frac{A\hat{K}D}{C} + \frac{2\hat{K}D}{C} + B$ then,

$$p_e = \frac{Fp_0 - 2p_\infty}{E} \tag{2.2.33}$$

Consequently, the interstitial fluid pressure can be obtained for two regions of periphery and intermediary.

For the region of $R_0 < r < R_s$ (periphery), the tumor interstitial fluid pressure is obtained as follows:

$$\begin{aligned} p &= c_1 e^{\sqrt{\frac{\alpha}{k'}}r} + c_2 e^{-\sqrt{\frac{\alpha}{k'}}r} + p_e \\ &= \frac{p_0 - p_e}{2} e^{-\sqrt{\frac{\alpha}{k'}}R_0} e^{\sqrt{\frac{\alpha}{k'}}r} + \frac{p_0 - p_e}{2} e^{\sqrt{\frac{\alpha}{k'}}R_0} e^{-\sqrt{\frac{\alpha}{k'}}r} + p_e \\ &= (\frac{p_0 - p_e}{2})[e^{\sqrt{\frac{\alpha}{k'}}(r-R_0)} + e^{-\sqrt{\frac{\alpha}{k'}}(r-R_0)}] + p_e \end{aligned} \tag{2.2.34}$$

For the sake of simplicity, define $M = e^{\sqrt{\frac{\alpha}{k'}}(r-R_0)} + e^{-\sqrt{\frac{\alpha}{k'}}(r-R_0)}$. Then,

$$\begin{aligned} p &= \frac{p_0}{2}M - \frac{p_e}{2}M + p_e \\ &= \frac{p_0}{2}M - (\frac{M-2}{2})p_e \end{aligned} \tag{2.2.35}$$

By referring to Eq.(2.2.30), p_e is calculable,

$$K'[c_1\sqrt{\frac{\alpha}{K'}}e^{\sqrt{\frac{\alpha}{K'}}R_s} - c_2\sqrt{\frac{\alpha}{K'}}e^{-\sqrt{\frac{\alpha}{K'}}R_s}] = -u(R_s)$$

so,

$$K'\sqrt{\frac{\alpha}{K'}}\frac{p_0 - p_e}{2}[e^{\sqrt{\frac{\alpha}{K'}}(R_s-R_0)} - e^{-\sqrt{\frac{\alpha}{K'}}(R_s-R_0)}] = -u(R_s)$$

so,

$$p_e = \frac{2u(R_s)}{K'\sqrt{\frac{\alpha}{K'}}[e^{\sqrt{\frac{\alpha}{K'}}(R_s-R_0)} - e^{-\sqrt{\frac{\alpha}{K'}}(R_s-R_0)}]} + p_0$$

Place p_e in Eq.(2.2.35),

$$p = \frac{p_0}{2}M - (\frac{M-2}{2})\frac{2u(R_s)}{K'\sqrt{\frac{\alpha}{K'}}[e^{\sqrt{\frac{\alpha}{K'}}(R_s-R_0)} - e^{-\sqrt{\frac{\alpha}{K'}}(R_s-R_0)}]} - \frac{M}{2}p_0 + p_0 \tag{2.2.36}$$

Consequently, if $(R_0 < r < R_s)$, the solution of Eq.(2.2.11) is obtained, by placing the value of M in Eq.(2.2.36),

$$p(r) = -\frac{u(R_s)(e^{\sqrt{\frac{\alpha}{k'}}(r-R_0)} + e^{-\sqrt{\frac{\alpha}{k'}}(r-R_0)} - 2)}{K'\sqrt{\frac{\alpha}{K'}}[e^{\sqrt{\frac{\alpha}{K'}}(R_s-R_0)} - e^{-\sqrt{\frac{\alpha}{K'}}(R_s-R_0)}]} + p_0 = -\frac{u(R_s)(e^{\sqrt{\frac{\alpha}{k'}}\frac{(r-R_0)}{2}} - e^{-\sqrt{\frac{\alpha}{k'}}\frac{(r-R_0)}{2}})^2}{K'\sqrt{\frac{\alpha}{K'}}[e^{\sqrt{\frac{\alpha}{K'}}(R_s-R_0)} - e^{-\sqrt{\frac{\alpha}{K'}}(R_s-R_0)}]} + p_0 \tag{2.2.37}$$

Moreover, for the region of $R_s < r < R_m$ (intermediary),

$$p = c_3 e^{\sqrt{\frac{\beta}{k}}r} + c_4 e^{-\sqrt{\frac{\beta}{k}}r} + p_L = \frac{p_\infty - p_L}{2}[e^{\sqrt{\frac{\beta}{k}}(r-R_m)} + e^{-\sqrt{\frac{\beta}{k}}(r-R_m)}]$$

Define $N = e^{\sqrt{\frac{\beta}{k}}(r-R_m)} + e^{-\sqrt{\frac{\beta}{k}}(r-R_m)}$, then,

$$p = \frac{N}{2}(p_\infty - p_L) + p_L \tag{2.2.38}$$

Eq.(2.2.32) shows that $p_\infty - p_L = \frac{\hat{K}D}{C}(p_0 - p_e)$ and from Eq.(2.2.30) p_L is obtained as in the following,

$$K[c_3\sqrt{\frac{\beta}{k}}e^{\sqrt{\frac{\beta}{k}}R_s} - c_4\sqrt{\frac{\beta}{k}}e^{-\sqrt{\frac{\beta}{k}}R_s}] = -u(R_s)$$

$\Longrightarrow$

$$K\sqrt{\frac{\beta}{K}}\frac{(p_\infty - p_L)}{2}[e^{\sqrt{\frac{\beta}{K}}(R_s-R_m)} - e^{-\sqrt{\frac{\beta}{K}}(R_s-R_m)}] = -u(R_s)$$

$$p_L = \frac{2u(R_s)}{K\sqrt{\frac{\beta}{K}}[e^{\sqrt{\frac{\beta}{K}}(R_s-R_m)} - e^{-\sqrt{\frac{\beta}{K}}(R_s-R_m)}]} + p_\infty$$

So, we can rewrite Eq.(2.2.38) as the following equation,

$$p = \frac{N}{2}(\frac{\hat{K}D}{C}(p_0 - p_e)) + \frac{2u(R_s)}{K\sqrt{\frac{\beta}{K}}[e^{\sqrt{\frac{\beta}{K}}(R_s-R_m)} - e^{-\sqrt{\frac{\beta}{K}}(R_s-R_m)}]} + p_\infty$$

Place p_e from Eq.(2.2.33). Then,

$$\begin{aligned} p &= \frac{N}{2}\frac{\hat{K}D}{C}(p_0 - [\frac{Fp_0 - 2p_\infty}{E}]) + \frac{2u(R_s)}{K\sqrt{\frac{\beta}{K}}[e^{\sqrt{\frac{\beta}{K}}(R_s-R_m)} - e^{-\sqrt{\frac{\beta}{K}}(R_s-R_m)}]} + p_\infty \\ &= \frac{N\hat{K}D}{2C}(\frac{Ep_0 - Fp_0 - 2p_\infty}{E}) + \frac{2u(R_s)}{K\sqrt{\frac{\beta}{K}}[e^{\sqrt{\frac{\beta}{K}}(R_s-R_m)} - e^{-\sqrt{\frac{\beta}{K}}(R_s-R_m)}]} + p_\infty \end{aligned} \tag{2.2.39}$$

Put the values of E and F in Eq.(2.2.39), then,

$$p = \frac{N\hat{K}D}{2C}(\frac{-2p_0 + 2p_\infty}{E}) + \frac{2u(R_s)}{K\sqrt{\frac{\beta}{K}}[e^{\sqrt{\frac{\beta}{K}}(R_s-R_m)} - e^{-\sqrt{\frac{\beta}{K}}(R_s-R_m)}]} + p_\infty$$

As a result, for the region of $(R_s < r < R_m)$, the tumor interstitial fluid pressure is written in the following,

$$p(r) = \frac{\hat{K}D[e^{\sqrt{\frac{\beta}{k}}(r-R_m)} + e^{-\sqrt{\frac{\beta}{k}}(r-R_m)}]}{C}(\frac{p_\infty - 2p_0}{E}) + \frac{2u(R_s)}{K\sqrt{\frac{\beta}{K}}[e^{\sqrt{\frac{\beta}{K}}(R_s-R_m)} - e^{-\sqrt{\frac{\beta}{K}}(R_s-R_m)}]} + p_\infty$$

with defined constant values of $\hat{K}$, C, D, E.

2.2.4 Analytical solution for a tumor with small necrotic core

Consider Eq.(2.2.10),

$$\begin{cases} r\frac{d}{dr}(K'\frac{dp(r)}{dr}) + 2K'\frac{dp(r)}{dr} - \alpha r(p - p_e) = 0 \quad \text{(periphery region, } R_0 < r < R_s\text{)} \ , \\ \\ r\frac{d}{dr}(K\frac{dp(r)}{dr}) + 2K\frac{dp(r)}{dr} - \beta r(p - p_L) = 0 \quad \text{(intermediary region, } R_s < r < R_m\text{)}. \end{cases}$$

Here, by obeying the same steps as we had in section (2.1.2), the solution can be written as in the following,

$$\begin{cases} p = \frac{1}{r}e^{\sqrt{\alpha}(2c_2+r)} - \frac{1}{r}e^{\sqrt{\alpha}(2c_1+2c_2-r)} + p_e \quad (R_0 < r < R_s) \ , \\ \\ p = \frac{1}{r}e^{\sqrt{\beta}(2c_4+r)} - \frac{1}{r}e^{\sqrt{\beta}(2c_3+2c_4-r)} + p_L \quad (R_s < r < R_m). \end{cases}$$

And, according to the boundary conditions mentioned in Eqs.(2.2.12), (2.2.13) and (2.2.14), the constants of c_1, c_2, c_3 and c_4 can be calculated. The full computations to obtain the analytical solution for this case are provided in Appendix 3.

By considering the continuous variation of the interstitial hydraulic conductivity (different constant values of interstitial hydraulic conductivity in the tumor and normal tissue, in addition to defined interstitial hydraulic conductivities in Eqs.(2.2.15) and (2.2.16) for periphery and intermediary, respectively), typically, it is not possible to obtain an analytical solution of Eq.(2.2.2). Therefore, instead of analytic analysis, we will focus on solving the problem (Eq.(2.2.2)) based on a following numerical method.

2.2.5 Two-dimensional formulation and numerical approach

Now let us look at the general two-dimensional mathematical formulation of our TIFP problem. Similar to liu et al. [21] model, we also obey the categorization of the tumor, surrounded by normal tissue, to three regions of the necrotic core $(r < R_0)$, periphery region $(R_0 < r < R_s)$ and intermediary region $(R_s < r < R_m)$ (see Fig.(2.14)) and use the linear interstitial hydraulic conductivity in periphery and intermediary regions defined in Eqs.(2.2.15) and (2.2.16), respectively. Consider the combination of the two equations of (2.2.1) and (2.2.2),

$$-\boldsymbol{\nabla}\cdot(K\boldsymbol{\nabla}p) = \frac{J_S}{V} - \frac{J_L}{V}$$

Previously, J_S and J_L were defined in section (2.2.1) as follows:

$$J_S = S_A L_A[p_A - p(\vec{r}) - \sigma_A(\pi_A - \pi_{Ai})] + S_V L_V[p_V - p(\vec{r}) - \sigma_V(\pi_V - \pi_{Vi})]$$

and,

$$J_L = S_L L_L[p(\vec{r}) - p_L]$$

as explained in section 2.2.1, L_A, L_V and L_L are the arterial, venous and lymphatic hydraulic conductivity, respectively. In addition, p_A, p_V and p_L are arterial, venous and lymphatic capillary hydrostatic pressure, respectively. π_i is osmotic pressure for $i = A, Ai, V, Vi$.
So,

$$-\boldsymbol{\nabla}\cdot(K\boldsymbol{\nabla}p) = C_1 p + C_2 \tag{2.2.40}$$

and,

$$-(\boldsymbol{\nabla}\cdot(K\boldsymbol{\nabla}p)+C_1p)=C_2$$

where,

$$C_1=-\frac{(S_AL_A+S_VL_V+S_LL_L)}{V}$$

and

$$C_2=\frac{S_AL_A}{V}p_A-\frac{S_AL_A}{V}\sigma_A(\pi_A-\pi_{Ai})+\frac{S_VL_V}{V}p_V-\frac{S_VL_V}{V}\sigma_V(\pi_V-\pi_{Vi})+\frac{S_LL_L}{V}p_L$$

The following procedure is applicable to create dimensionless parameters.
Define $(\hat{x},\hat{y})$ (dimensionless parameters) such that $\hat{x}=\frac{x}{L}$, $\hat{y}=\frac{y}{L}$, where L is the characteristic length of position. In addition, introduce characteristic parameters of p^*, K^* as characteristic pressure and characteristic interstitial hydraulic conductivity, respectively. Thus, $\hat{p}=\frac{p}{p^*}$ and $\hat{K}=\frac{K}{K^*}$ are dimensionless. Consequences are presented in the following,

$$\boldsymbol{\nabla}p=p^*\boldsymbol{\nabla}(\hat{p})=p^*(\frac{\partial}{\partial x}\hat{p},\frac{\partial}{\partial y}\hat{p})$$

As, $(\frac{\partial}{\partial x}=\frac{\partial}{\partial\hat{x}}\cdot\frac{\partial\hat{x}}{\partial x})$, then,

$$\begin{aligned}\boldsymbol{\nabla}p&=p^*(\frac{\partial\hat{p}}{\partial\hat{x}}\cdot\frac{\partial\hat{x}}{\partial x},\frac{\partial\hat{p}}{\partial\hat{y}}\cdot\frac{\partial\hat{y}}{\partial y})\\&=\frac{p^*}{L}(\hat{\boldsymbol{\nabla}}\hat{p})\end{aligned}$$

Therefore,

$$\boldsymbol{\nabla}\cdot(K\boldsymbol{\nabla}p)=\boldsymbol{\nabla}\cdot(K^*\hat{K}\frac{p^*}{L}\hat{\boldsymbol{\nabla}}\hat{p})=\frac{K^*p^*}{L^2}\hat{\boldsymbol{\nabla}}.(\hat{K}\hat{\boldsymbol{\nabla}}\hat{p})$$

$$-\boldsymbol{\nabla}\cdot(K\boldsymbol{\nabla}p)=C_1p+C_2$$

$\Longrightarrow$

$$\frac{K^*p^*}{L^2}\hat{\boldsymbol{\nabla}}.(\hat{K}\hat{\boldsymbol{\nabla}}\hat{p})=C_1p^*\hat{p}+C_2$$

Define $\hat{L}_i=\frac{L_i}{\frac{K^*}{L}}=\frac{L}{K^*}L_i$, where i represents A (arterioles), V (venules) and L (lymphatics). So, relying on the definition of C_1,

$$\begin{aligned}C_1&=-\frac{(S_AL_A+S_VL_V+S_LL_L)}{V}\\&=-\frac{(L^2\hat{S}_AL_A+L^2\hat{S}_VL_V+L^2\hat{S}_LL_L)}{L^3\hat{V}}\\&=-\frac{1}{L}\frac{(\hat{S}_AL_A+\hat{S}_VL_V+\hat{S}_LL_L)}{\hat{V}}\\&=-\frac{1}{L}\frac{K^*}{L}(\frac{\hat{S}_A\hat{L}_A+\hat{S}_V\hat{L}_V+\hat{S}_L\hat{L}_L}{\hat{V}})\\&=-\frac{K^*}{L^2}(\frac{\hat{S}_A\hat{L}_A+\hat{S}_V\hat{L}_V+\hat{S}_L\hat{L}_L}{\hat{V}})\end{aligned}\tag{2.2.41}$$

In addition, define $\hat{p}_A = \frac{p_A}{p^*}$, $\hat{p}_V = \frac{p_V}{p^*}$, $\hat{p}_L = \frac{p_L}{p^*}$ and $\hat{\pi}_i = \frac{\pi_i}{p^*}$ where $i = A, V$. Therefore, according to the definition of C_2,

$$\begin{aligned}
C_2 &= \frac{S_A L_A}{V} p_A - \frac{S_A L_A}{V} \sigma_A (\pi_A - \pi_{Ai}) + \frac{S_V L_V}{V} p_V - \frac{S_V L_V}{V} \sigma_V (\pi_V - \pi_{Vi}) + \frac{S_L L_L}{V} p_L \\
&= \frac{L^2 \hat{S}_A L_A}{L^3 \hat{V}} \hat{p}_A p^* - \frac{L^2 \hat{S}_A L_A}{L^3 \hat{V}} \sigma_A (\hat{\pi}_A p^* - \hat{\pi}_{Ai} p^*) + \frac{L^2 \hat{S}_V L_V}{L^3 \hat{V}} \hat{p}_V p^* - \frac{L^2 \hat{S}_V L_V}{L^3 \hat{V}} \sigma_V (\hat{\pi}_V p^* - \hat{\pi}_{Vi} p^*) + \frac{L^2 \hat{S}_L L_L}{L^3 \hat{V}} \hat{p}_L p^* \\
&= \frac{p^*}{L} \left(\frac{\hat{S}_A L_A}{\hat{V}} \hat{p}_A - \frac{\hat{S}_A L_A}{\hat{V}} \sigma_A (\hat{\pi}_A - \hat{\pi}_{Ai}) + \frac{\hat{S}_V L_V}{\hat{V}} \hat{p}_V - \frac{\hat{S}_V L_V}{\hat{V}} \sigma_V (\hat{\pi}_V - \hat{\pi}_{Vi}) + \frac{\hat{S}_L L_L}{\hat{V}} \hat{p}_L \right) \\
&= p^* \frac{K^*}{L^2} \left(\frac{\hat{S}_A \hat{L}_A}{\hat{V}} \hat{p}_A - \frac{\hat{S}_A \hat{L}_A}{\hat{V}} \sigma_A (\hat{\pi}_A - \hat{\pi}_{Ai}) + \frac{\hat{S}_V \hat{L}_V}{\hat{V}} \hat{p}_V - \frac{\hat{S}_V \hat{L}_V}{\hat{V}} \sigma_V (\hat{\pi}_V - \hat{\pi}_{Vi}) + \frac{\hat{S}_L \hat{L}_L}{\hat{V}} \hat{p}_L \right)
\end{aligned} \tag{2.2.42}$$

Then we get:

$$\hat{\boldsymbol{\nabla}} . (\hat{K} \hat{\boldsymbol{\nabla}} \hat{p}) = \hat{C}_1 \hat{p} + \hat{C}_2$$

where,

$$\hat{C}_1 = \frac{\hat{S}_A \hat{L}_A + \hat{S}_V \hat{L}_V + \hat{S}_L \hat{L}_L}{\hat{V}}$$

and correspondingly for $\hat{C}_2$,

$$\hat{C}_2 = \frac{\hat{S}_A \hat{L}_A}{\hat{V}} \hat{p}_A - \frac{\hat{S}_A \hat{L}_A}{\hat{V}} \sigma_A (\hat{\pi}_A - \hat{\pi}_{Ai}) + \frac{\hat{S}_V \hat{L}_V}{\hat{V}} \hat{p}_V - \frac{\hat{S}_V \hat{L}_V}{\hat{V}} \sigma_V (\hat{\pi}_V - \hat{\pi}_{Vi}) + \frac{\hat{S}_L \hat{L}_L}{\hat{V}} \hat{p}_L$$

For a general heterogeneous interstitial hydraulic conductivity K it is typically not possible to obtain an analytical solution of Eq.(2.2.40). Thus, instead of analytic analysis, we will focus on solving the problem (Eq.(2.2.40)) by using a numerical method. In order to perform a relatively systematic investigation with some degree of realism it is useful to employ unstructured grids that can easily adapt to the geometry. We thus used the numerical method from [12] in combination with triangular grids. The numerical method from [12] is a so called multi-point flux approximation (MPFA) method, which delivers accurate results with unstructured triangulations (see Fig.(3.1)).

Previously, the required technical work flow has been implemented at International Research Institute of Stavanger (IRIS). It involves using the unstructured grid generator triangle [34] for generating the necessary triangulation. The pressure equation solver which implements the concrete MPFA method is written in C++. During our work, this C++ implementation was extended such that Eq.(2.2.40) could be solved. In practice that meant that the right hand side of Eq.(2.2.40) (which can be seen to be a function of the unknown pressure p) had to be added within the existing C++ framework. At the end, the ParaView software is used to visualize the tumor interstitial fluid pressure distribution for different cases.

Chapter 3

Results and Discussion

Tumor interstitial fluid pressure can be challenging to simulate by numerical methods, since the parameter values are critical to get realistic results. It is challenging to get true experimentally measured values and parameters, such as arterial, venous and lymphatic hydraulic conductivities, and many of the values that are used for numerical models come from rather old works (for example, Table 2.1 used by Baxter et al. is one of the main references for the parameter values).
In this numerical model, the used baseline parameter values are presented in the Table (3.1), which is based on Table (2.1).
In this chapter, we are using our numerical method to investigate the influence of different factors on determining TIFP distribution. The influence of the size of necrotic core simultaneously with the application of non-constant interstitial hydraulic conductivity (explained by Liu et al. [21]) or constant interstitial hydraulic conductivity (explained by Baxter et al. [4]) and their comparison are investigated. In addition, the size of necrotic, periphery and intermediary regions may affect the TIFP distribution. In the periphery region, the effect of the abundance of blood vessel capillaries (arterial and venous capillary hydraulic conductivities) is inquired. Finally, to discover the role of the non-uniform distribution of blood vessels on the TIFP distribution, the more real case of tumor is produced by including some region as blood vessel source in the periphery region which leads to have an asymmetry distribution of TIFP.
In our idealized model, as shown in Fig.(2.14), circles illustrate different regions (necrotic core, periphery and intermediary). We have adjusted $(0.5, 0.5)$ as the center coordinates of the circles and the normal tissue is restricted by a square with the dimensionless length and width of 1.00 and we adjust zero pressure at the outer boundary condition. Moreover, for every case, we use dimensionless parameters obtained in section (2.2.5).
A typical schematic of our model combined with triangular grids is shown in Fig.(3.1). The triangular grids are generated by using the grid generator Triangle. It is clearly seen that the triangular grids adapt well to the computational tumor geometry defined by three circles representing the necrotic core, periphery and intermediary region, respectively.

Parameter	Baseline value in Normal Tissue	Baseline Value in Tumor Tissue
$L_A, L_V, L_L[cm/mmHgsec]$	0.36×10^{-7}	2.8×10^{-7}
$K[cm^2/mmHgsec]$	8.53×10^{-9}	4.13×10^{-8}
$S/V[cm^{-1}]$	70	200
$p_A[mmHg]$	78	78
$\pi_A[mmHg]$	20	20
$\pi_{Ai}[mmHg]$	10	15
$p_V[mmHg]$	15.6	15.6
$\pi_V[mmHg]$	20	20
$\pi_{Vi}[mmHg]$	10	15
$p_L[mmHg]$	15.6	15.6
σ	0.91	0.82

Table 3.1: Baseline parameters used in our work.

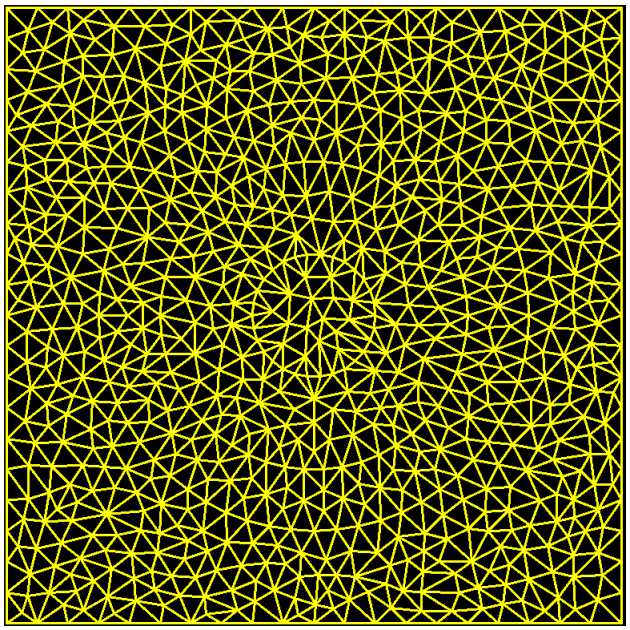

Figure 3.1: Triangular Grids with three regions.

Moreover, for the sake of illustration, a corresponding typical TIFP distribution for the same problem but with a significantly higher number of with triangular grids is visualized in Fig.(3.2).

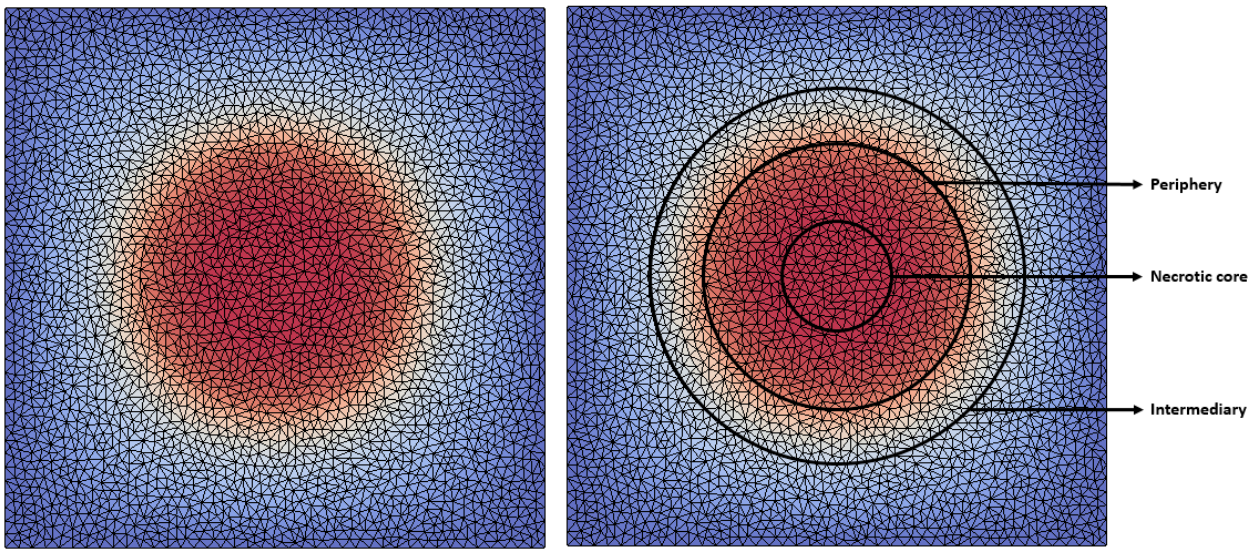

Figure 3.2: A typical distribution of TIFP for 6256 grids.

3.1 Grid resolution

The numerical scheme utilized in this thesis has previously been shown to exhibit convergence [12]. Here, we want to find a sufficient grid resolution for the problem in this study. To show the convergence of TIFP between different number of grids, we present two examples and investigate TIFP distributions with two different number of grids for each one. First, lets set the dimensionless radii of necrotic core, periphery and intermediary as 0.10, 0.25, 0.35, respectively. The TIFP distributions for two different number of grids are shown in Fig.(3.3). The maximum value of dimensionless TIFP with 12910 grids is 1.484; which is almost the same as the maximum value of dimensionless TIFP with 6256 grids, 1.481.

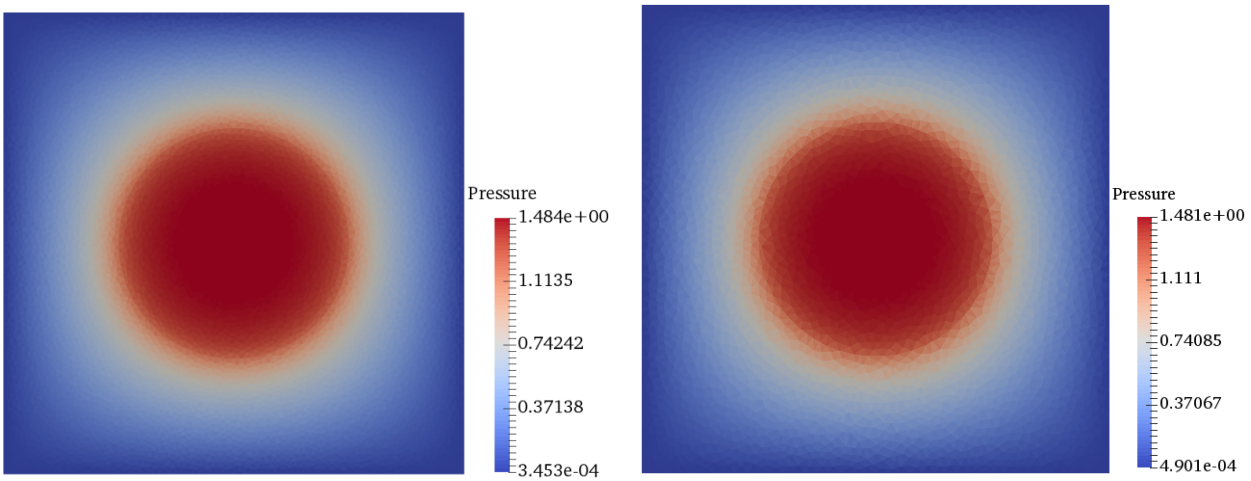

(a) 12910 grids (b) 6256 grids

Figure 3.3: The same maximum values of TIFP for two different number of grids. The dimensionless radii of necrotic, periphery and intermediary are 0.10, 0.25, 0.35, respectively.

Lets take the second example for a tumor with dimensionless radii of 0.05, 0.25, 0.35 for necrotic core, periphery and intermediary, respectively. The maximum values of TIFP for two different number of grids are shown in Fig.(3.4). With 12984 grids, the maximum TIFP is 2.034 which is almost the same value as 2.032 with 6217 grids.

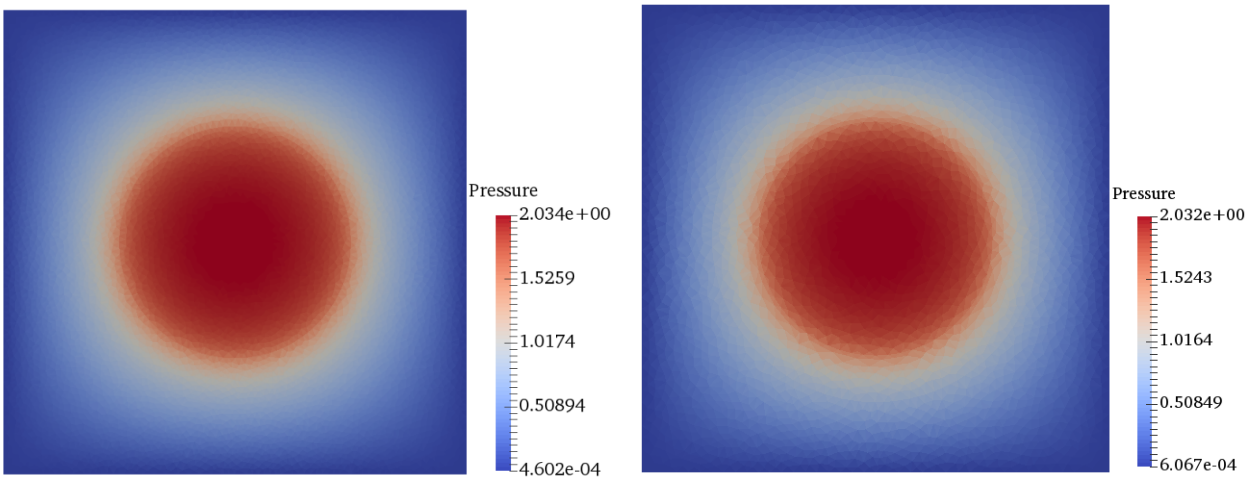

(a) 12984 grids (b) 6217 grids

Figure 3.4: The same maximum values of TIFP for two different number of grids. The dimensionless radii of necrotic, periphery and intermediary are 0.05, 0.25, 0.35, respectively.

Consequently, from the numerical test it is concluded that using around 6000 grid cells is sufficient to study the following problems.

3.2 Systematic change of the necrotic core radius

Here we are focusing on recognizing the effect of the size of necrotic core on the TIFP distribution. So, consider the fixed dimensionless radii of 0.25 and 0.35 for the periphery and intermediary circles, respectively, with the center coordinates of $(0.5, 0.5)$ (the basic schematic of a tumor surrounded by normal tissue consists of necrotic core, periphery and intermediary regions is shown in Fig.(2.14)). The question is that does the increased radius of the necrotic core changes the behaviour of the dimensionless interstitial fluid pressure?

Simultaneously, the effect of non-constant interstitial hydraulic conductivity (Liu et al.) and constant interstitial hydraulic conductivity (Baxter et al.) in addition to the size of necrotic core is inquired in this section. As it is mentioned in Chapter 2, a non-constant interstitial hydraulic conductivity was explained by Liu et al. [21]; which gets different constant values for necrotic core and normal tissue and gets different radially dependent variables through the periphery and intermediary regions (see Fig.(2.14) and section (2.2.1)). By considering this kind of interstitial hydraulic conductivity, Liu et al. reveals a more real tumor compare to the model described by Baxter et al. [4] in which the tumor surrounding by normal tissue is categorized to necrotic core and periphery regions and the interstitial hydraulic conductivities for these two regions are constants with different values (the intermediary region is not included).

Consider the spherical case, including a very small necrotic core, Fig.(2.18a), and the planar case, containing a very big necrotic core, Fig.(2.18b); so that 0.005 and 0.22 are adjusted as dimensionless radii of necrotic core for spherical and planar, respectively.
The comparisons between applying constant and non-constant interstitial hydraulic conductivity are illustrated in Fig.(3.5), for spherical case, and Fig.(3.6), for planar case. As shown in Fig.(3.5), for the spherical case, the maximum interstitial fluid pressure for non-constant interstitial hydraulic conductivity is higher than that of constant interstitial hydraulic conductivity. The same results happen for the planar case in Fig.(3.6). In addition, the comparison of Figs.(3.5) and (3.6) shows that the interstitial fluid pressure in the spherical case is higher than that of the planar case. It means that the largest size of necrotic core results very low value of maximum interstitial fluid pressure.
Very small necrotic core inside the tumor leads to the existence of more vessels and consequently existence of hydrostatic and osmotic pressures of vessel capillaries in the periphery. Thus, the excess fluid remains in the periphery region and then the interstitial will be less permeable. As the interstitial hydraulic conductivity correlates with the permeability, it decreases and the fluid hardly flows so very high interstitial fluid pressure occurs (Fig.(3.5)).
The case with the highest interstitial fluid pressure happens in the well-vascularized tumor without necrotic core. In contrast, very large necrotic core will give a very small vascular region (periphery). Consequently, lower interstitial fluid pressure occurs.(see Fig. (3.6)). According to these results, it is predicted that the tumor which is completely filled by necrotic core has no vasculature and its interstitial fluid pressure is zero.

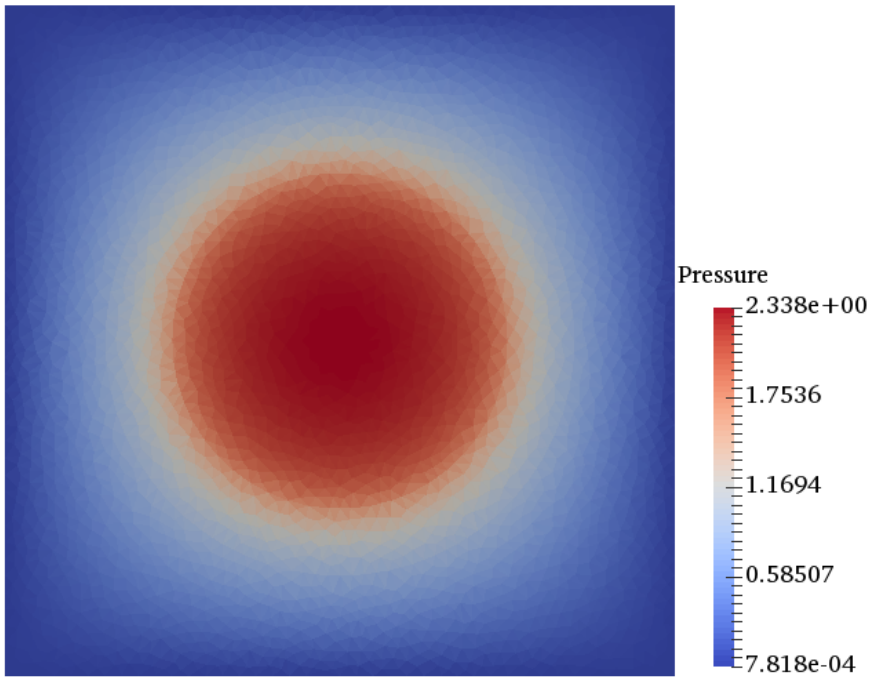

(a) Non-constant interstitial hydraulic conductivity - necrotic radius: 0.005

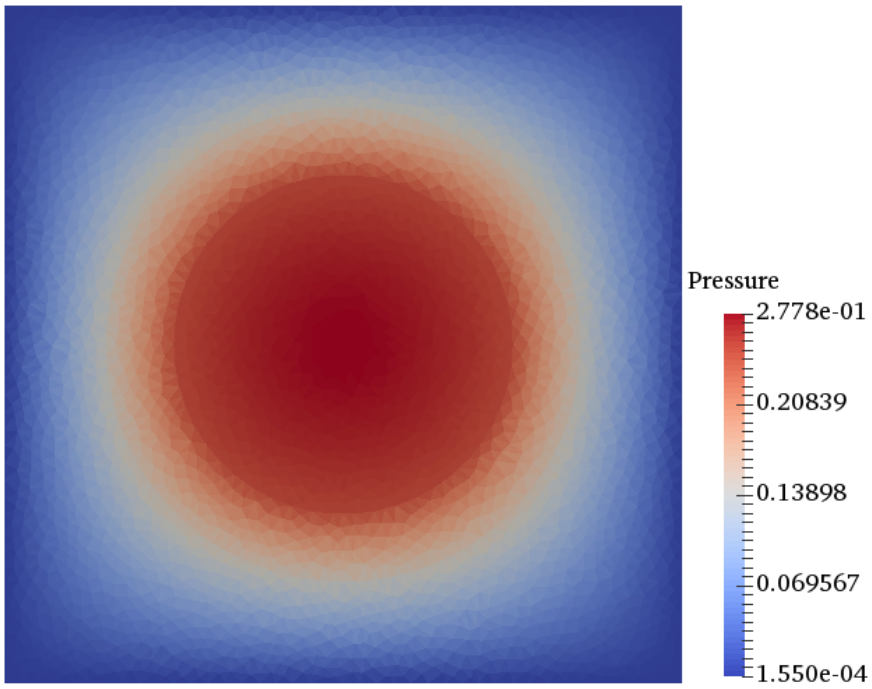

(b) Constant interstitial hydraulic conductivity - necrotic radius: 0.005

Figure 3.5: Difference of TIFP between (a) Liu model, (b) Baxter model, in spherical case.

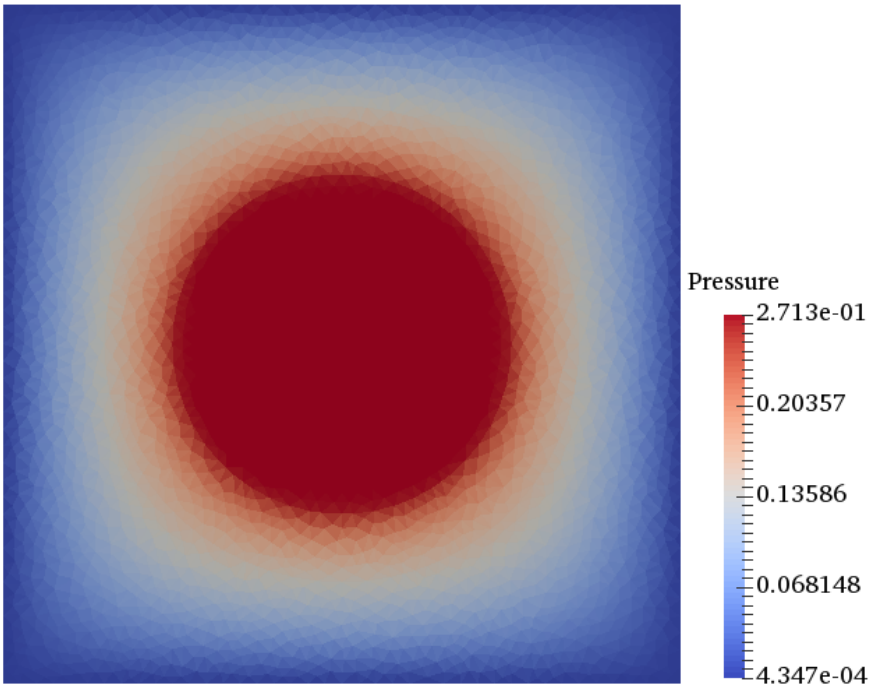

(a) Non-constant interstitial hydraulic conductivity - necrotic radius: 0.22

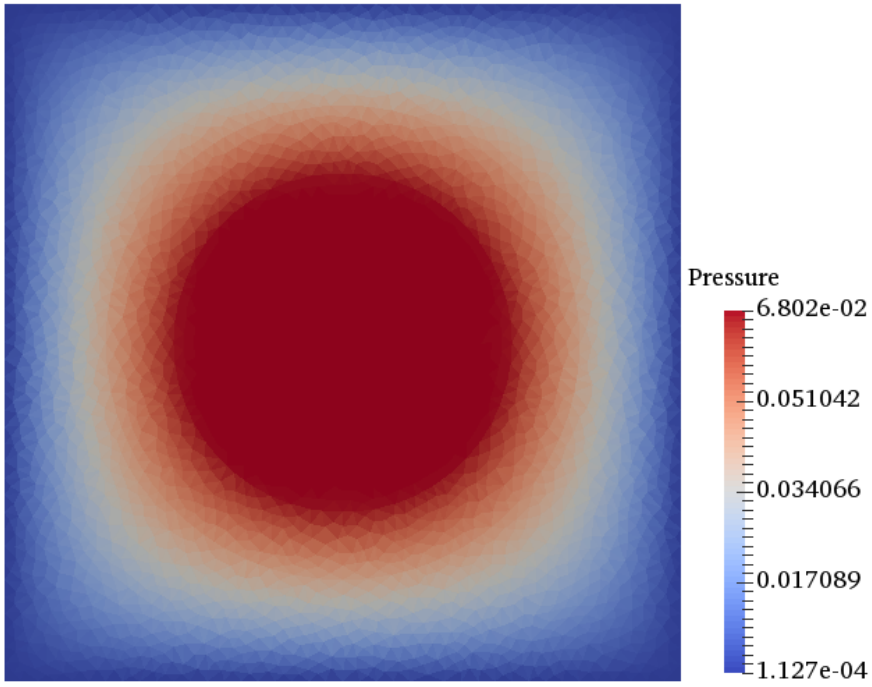

(b) Constant interstitial hydraulic conductivity - necrotic radius: 0.22

Figure 3.6: Differences of TIFP between (a) Liu model (b) Baxter model, in planar case.

Now, we consider non-constant interstitial hydraulic conductivity and change the dimensionless radius of necrotic core in the range of $[0.005, 0.22]$. As shown in Fig.(3.7), the dimensionless tumor interstitial fluid pressure faces a decreasing behaviour by raising the dimensionless radius of necrotic core radius. In addition, the maximum interstitial fluid pressure is observed in the center of the tumor (necrotic core).

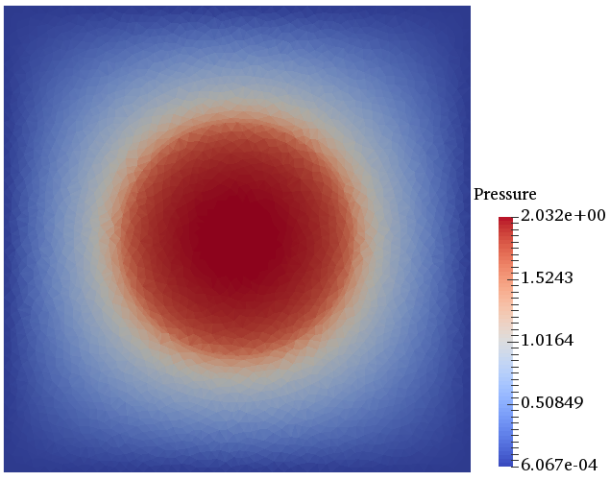

(a) necrotic radius: 0.05

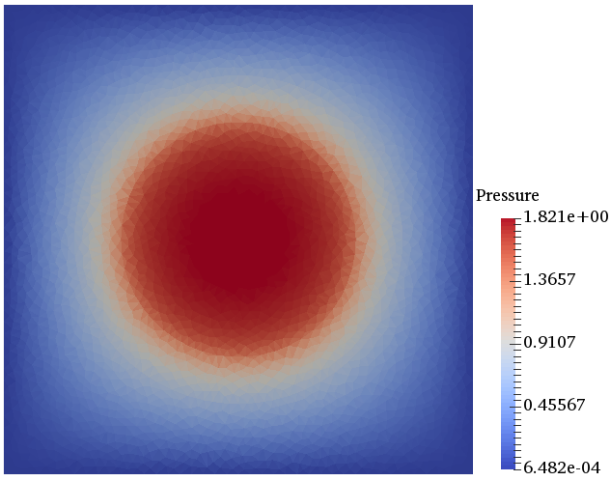

(b) necrotic radius: 0.07

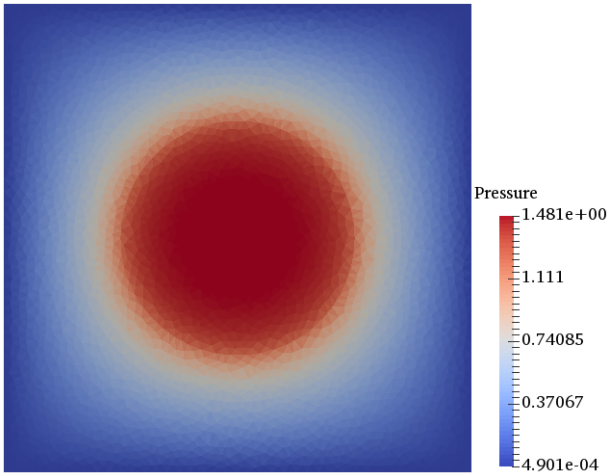

(c) necrotic radius: 0.10

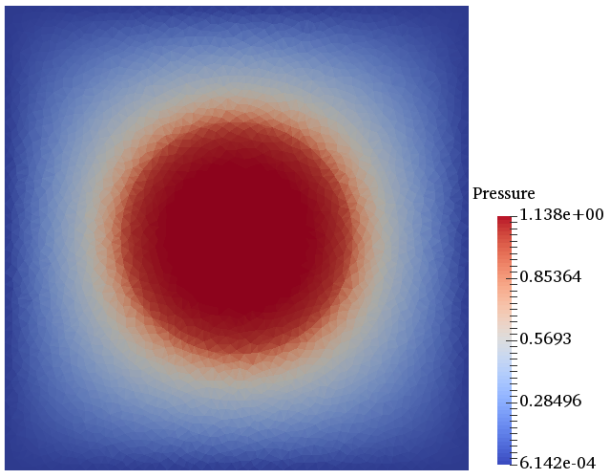

(d) necrotic radius: 0.13

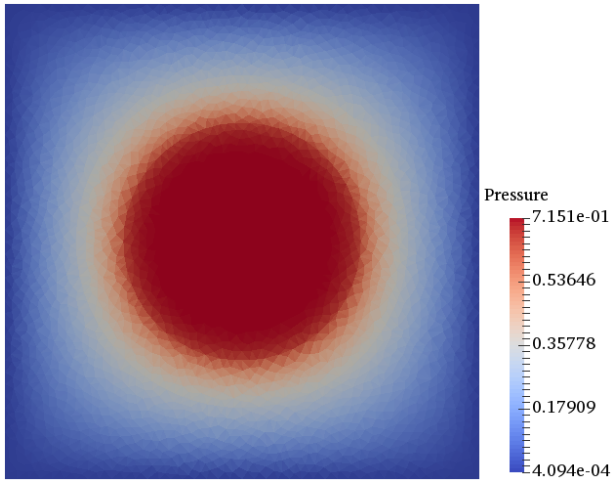

(e) necrotic radius: 0.17

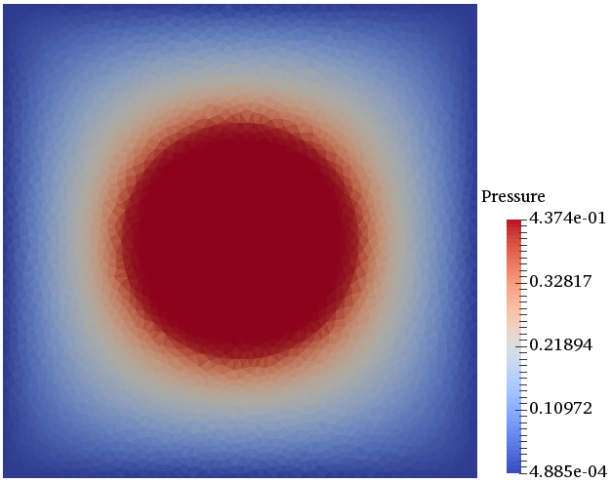

(f) necrotic radius: 0.20

Figure 3.7: Differences of TIFP with non-constant interstitial hydraulic conductivity for the specified radius of necrotic core and fixed radii of periphery and intermediary (The Liu model).

The table of specified dimensionless radii of necrotic core and corresponding values of maximum dimensionless interstitial fluid pressure extracted from visualizations (Fig.(3.7)), for non-constant interstitial hydraulic conductivity, are presented in Fig.(3.8). Moreover, in the same figure, the curve of the behaviour of the pressure versus radius of necrotic core is drawn up, which is decreasing by increasing the size of the necrotic core.

Dimenssionless Radius of Necrotic core	Maximum Dimenssionless Pressure
0.005	2.338
0.05	2.032
0.07	1.821
0.1	1.481
0.13	1.138
0.17	0.715
0.2	0.437
0.22	0.271

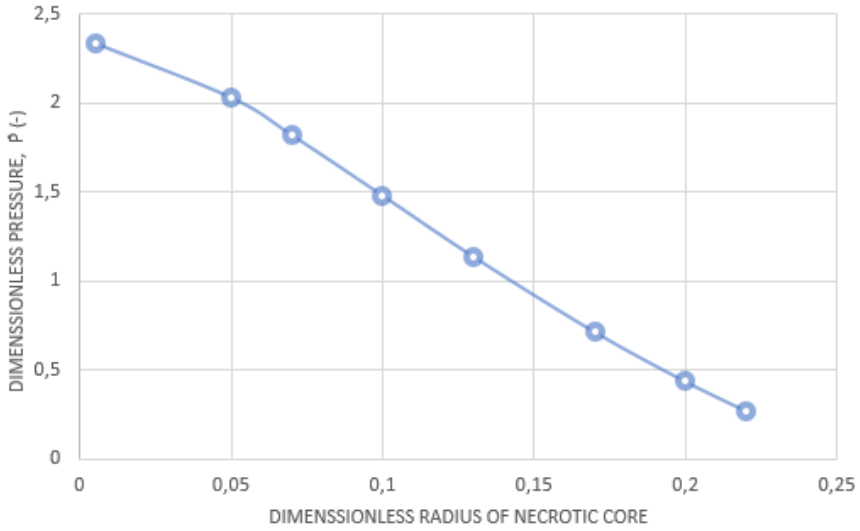

Figure 3.8: The trend of the maximum TIFP by increasing the size of the necrotic core for non-constant interstitial hydraulic conductivity.

Now, consider constant interstitial hydraulic conductivity. The distributions of TIFP by increasing the radius of necrotic core in the range of $[0.005, 0.22]$ are visualized in Fig.(3.9). As shown in Fig.(3.9), the maximum value of TIFP is decreasing by increasing the size of necrotic core.

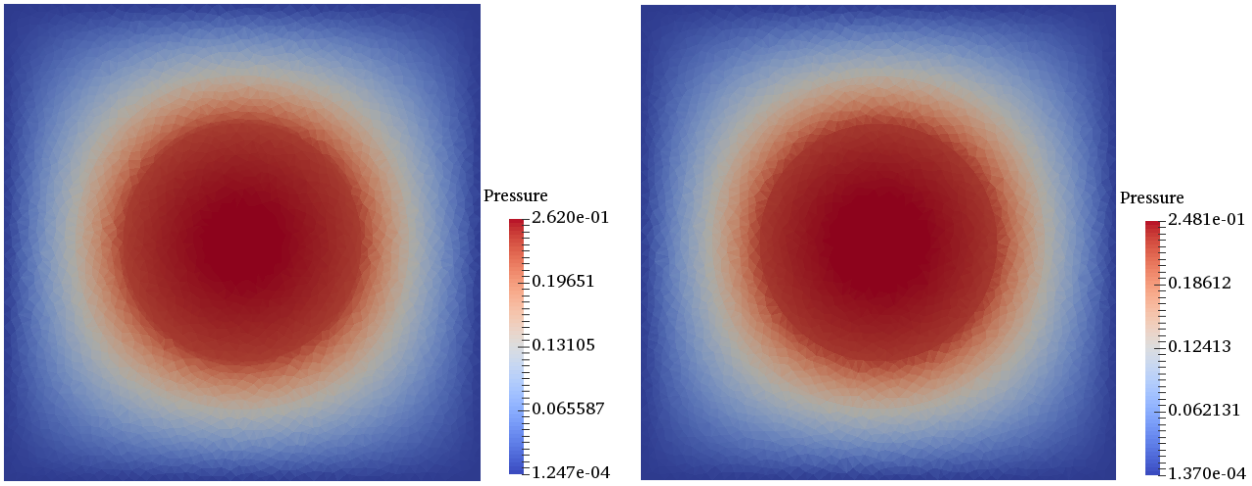

(a) necrotic radius: 0.05

(b) necrotic radius: 0.07

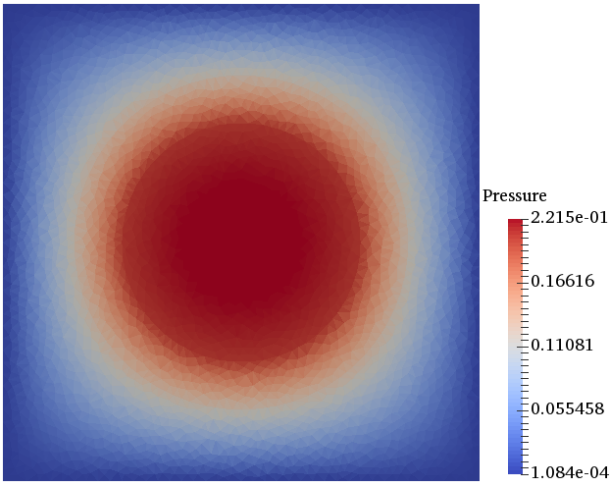

(c) necrotic radius: 0.10

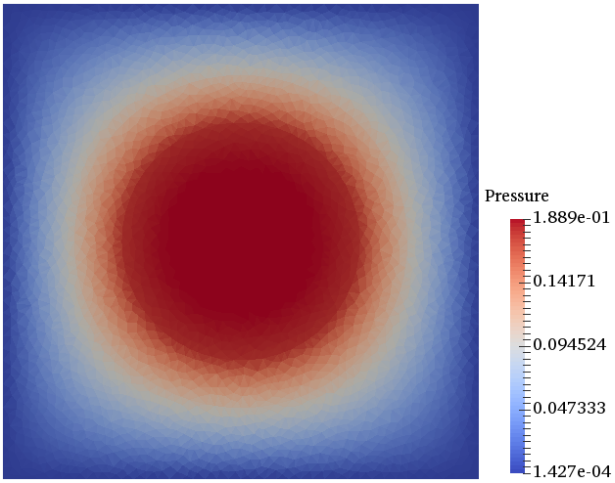

(d) necrotic radius: 0.13

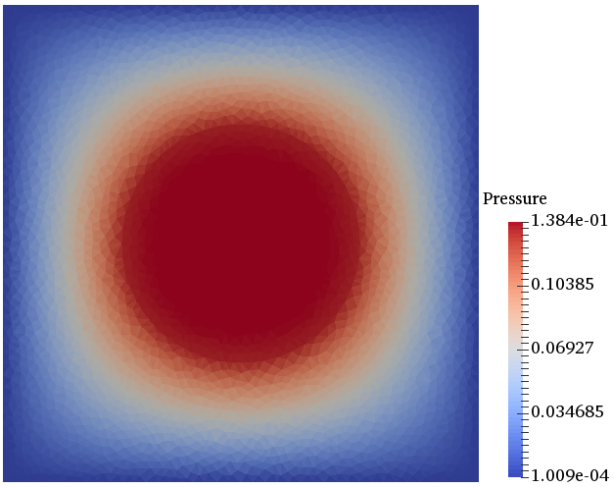

(e) necrotic radius: 0.17

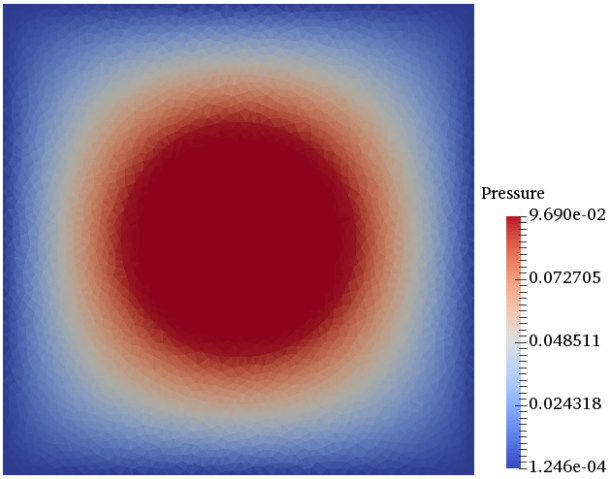

(f) necrotic radius: 0.20

Figure 3.9: Differences of TIFP with constant interstitial hydraulic conductivity for the specified radius of necrotic core and fixed radii of periphery and intermediary (The Baxter model).

The table of specified dimensionless radii of necrotic core and corresponding values of maximum dimensionless interstitial fluid pressure extracted from visualizations (Fig.(3.9)) are presented in Fig.(3.10). Moreover, the decreasing trend of the interstitial pressure for increasing radius of necrotic core is presented in the same Fig.(3.10).

Dimenssionless Radius of Necrotic core	Maximum Dimenssionless Pressure
0.005	0.277
0.05	0.262
0.07	0.248
0.1	0.221
0.13	0.188
0.17	0.138
0.2	0.096
0.22	0.068

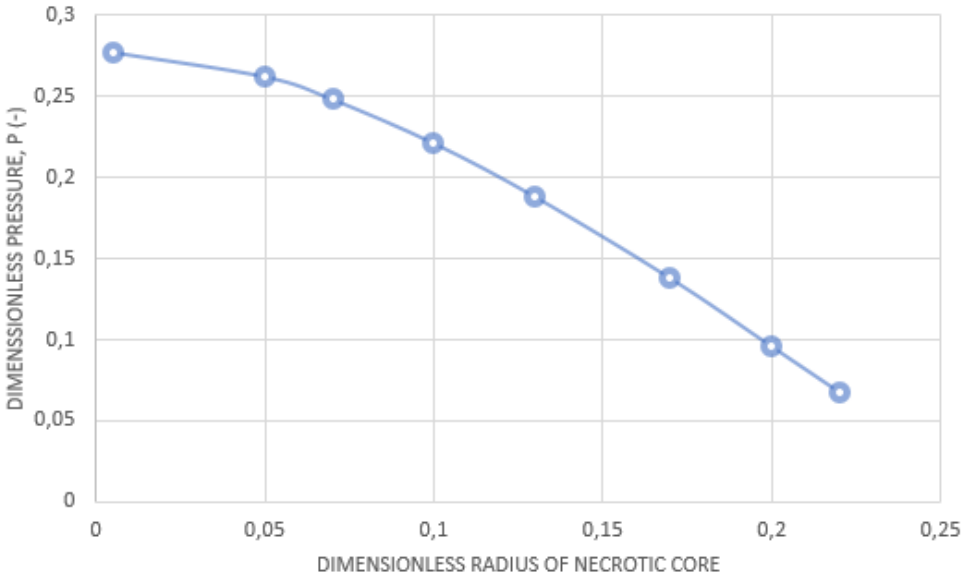

Figure 3.10: The trend of the maximum TIFP by increasing the size of the necrotic core for non-constant interstitial hydraulic conductivity.

3.2.1 Comparative analysis on the effect of constant and non-constant interstitial hydraulic conductivity on TIFP distribution

By merging the presented results of Figs.(3.8) and (3.10) in Fig.(3.11) the effect of constant and non-constant interstitial hydraulic conductivity on the maximum value of tumor interstitial fluid pressure ,by increasing the size of necrotic core, can be investigated. As shown in Fig.(3.11), there is a big gap between the values of the maximum interstitial fluid pressure for constant and non-constant interstitial hydraulic conductivity in the tumor which contains very small necrotic core in the central region. While, for large size of necrotic core with the dimensionless radius of 0.22 the maximum values of TIFP are the same for constant and non-constant interstitial hydraulic conductivity. Overall, by contributing non-constant interstitial hydraulic conductivity, the maximum value of TIFP is much higher than that for constant interstitial hydraulic conductivity. In addition the trend of pressure for non-constant is more sharp compare to the pressure trend for constant interstitial hydraulic conductivity, which decreases very smoothly. In addition, the behaviours shown in Fig.(3.11) illustrate that without paying attention to the type of the interstitial hydraulic conductivity, increasing the size of necrotic core decreases the interstitial fluid pressure. As a result, the size of necrotic core plays an important role in determining the pressure distribution.

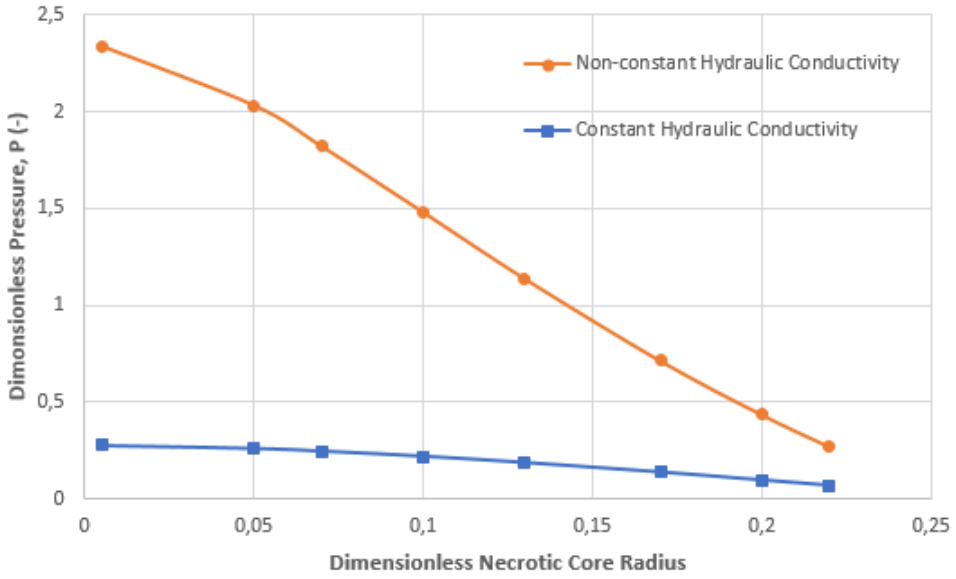

Figure 3.11: Comparison between the TIFP trends for Liu model and Baxter model by increasing the size of necrotic core.

3.3 Effect of periphery and intermediary regions sizes on TIFP distribution

The concentration of the vessels affects the interstitial fluid pressure. As it is assumed only vessel capillaries, contains arterial and venous capillaries (explained in section(2.2.1)), are found in the periphery region , so changing the enlargement of periphery causes big changes in the TIFP distribution. In addition, as assumptions in section (2.2.1), the intermediary region only contains lymphatics. In this section we only focus on determining the TIFP distribution for non-constant interstitial hydraulic conductivity and about 6200 number of triangular grids will be considered.

3.3.1 Systematic change of the periphery radius

Here, we fix dimensionless radii of necrotic core and intermediary circles to 0.10 and 0.35, respectively and change the size of the periphery region by adjusting a value from the range of $[0.10, 0.35]$ as a dimensionless radius of periphery. Fig.(3.12) shows distributions of TIFP for different specified dimensionless radii of periphery. In addition, the values of maximum interstitial fluid pressure corresponding to each radius of periphery is collected in Fig.(3.13). As shown, for small size of periphery, the maximum dimensionless value of TIFP is 0.199; while, the value of 1.967 is observed for big radius of periphery. This result was predicted because of the fact that plenty of blood vessels can be seen in periphery. For small size of periphery, less functional blood vessel observed and less fluid filtered from arterial capillaries so the pressure is lower compare to the big size of periphery.

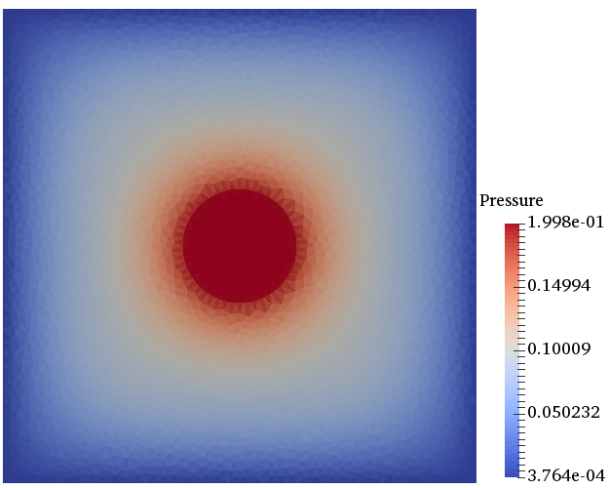

(a) periphery radius: 0.12

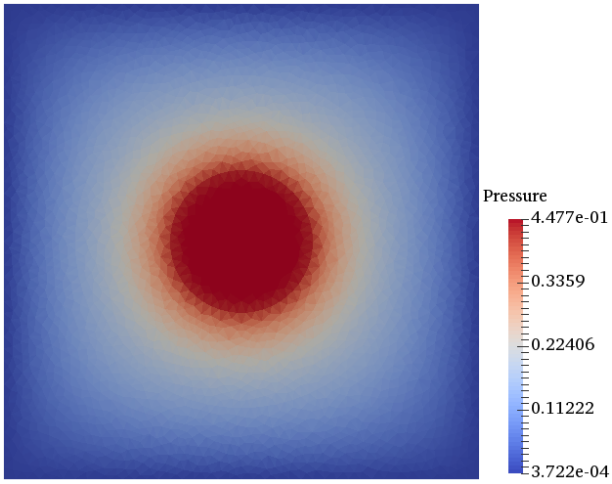

(b) periphery radius: 0.15

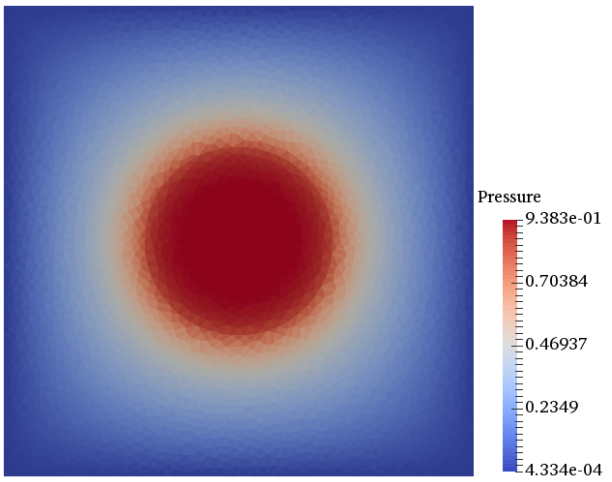

(c) periphery radius: 0.20

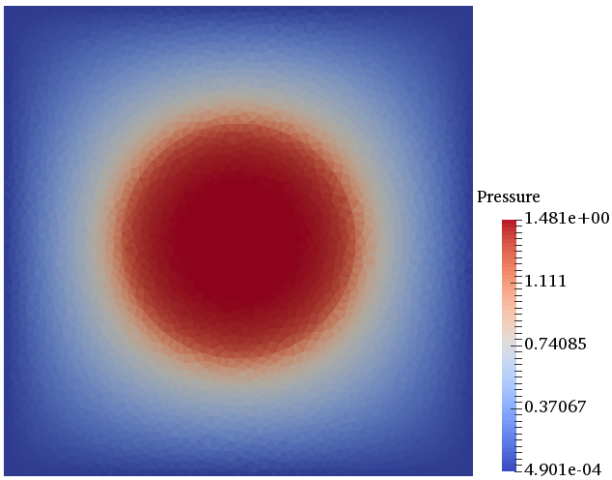

(d) periphery radius: 0.25

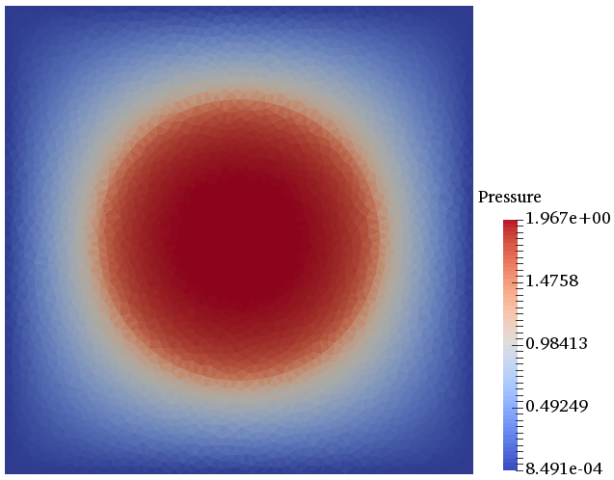

(e) periphery radius: 0.30

Figure 3.12: Differences of TIFP for different specified radius of periphery region and fixed radii of necrotic core and intermediary regions.

Fig.(3.13) shows that increasing the size of periphery region leads to increased TIFP. Since the periphery region only contains blood vessels, increasing the radius of periphery means increasing the abundance of the blood vessels in the tumor which causes the production of more leaky blood vessels and consequently forming the pressure barrier.

Dimenssionless Radius of Periphery	Maximum Dimenssionless Pressure
0.12	0.199
0.15	0.447
0.20	0.938
0.25	1.481
0.3	1.967

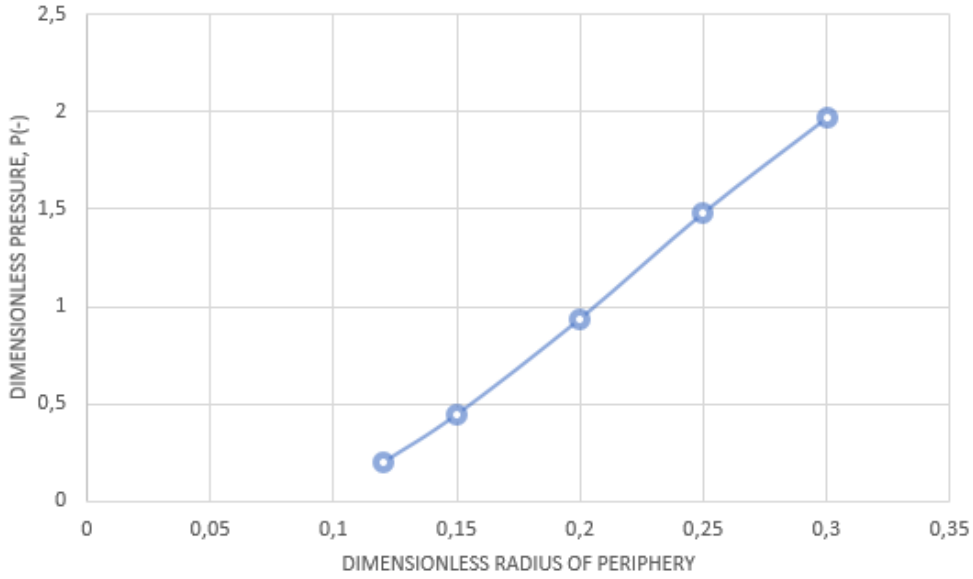

Figure 3.13: The trend of TIFP by increasing the size of periphery region.

3.3.2 Systematic change of the intermediary radius

To investigate the effect of the size of intermediary region, we set 0.10 as the dimensionless radius of necrotic core and 0.25 as the dimensionless radius of periphery circle. As in our model, the normal tissue is restricted by a 1.0×1.0 square and the center coordinates of circles is $(0.5, 0.5)$, we can adjust the values of intermediary region from the range of $[0.25, 0.5]$. The visualizations of the TIFP distribution for different specified dimensionless radii of intermediary are shown in Fig.(3.14).

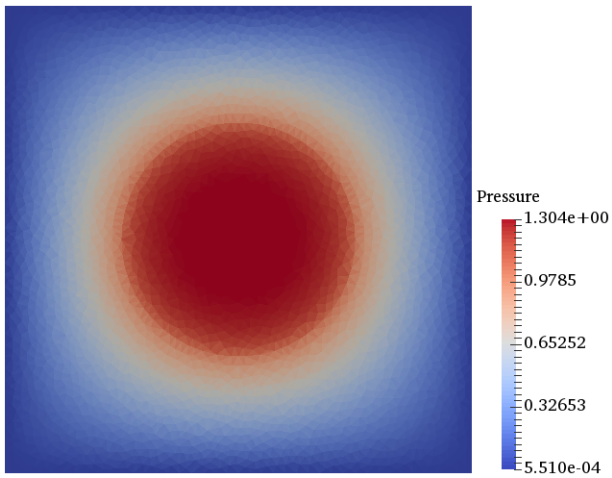

(a) intermediary radius: 0.27

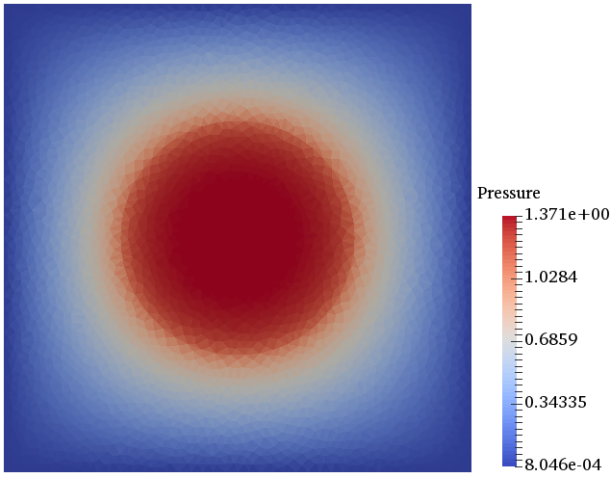

(b) intermediary radius: 0.30

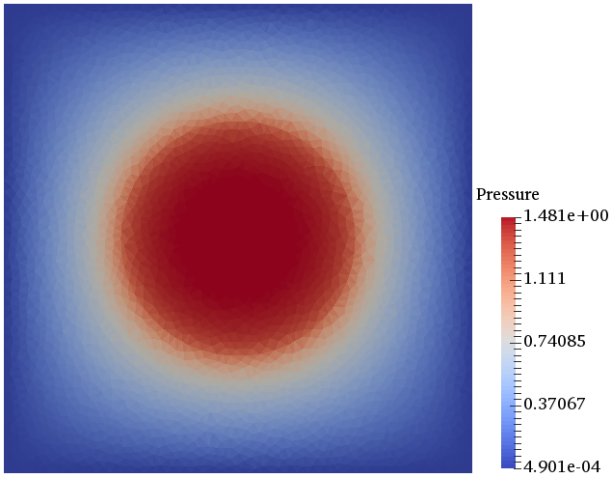

(c) intermediary radius: 0.35

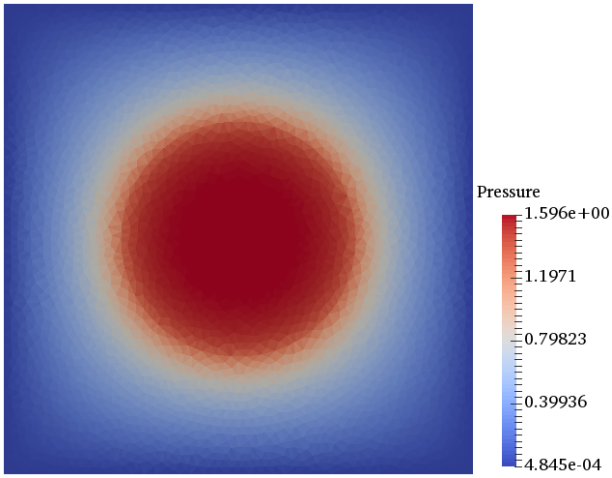

(d) intermediary radius: 0.40

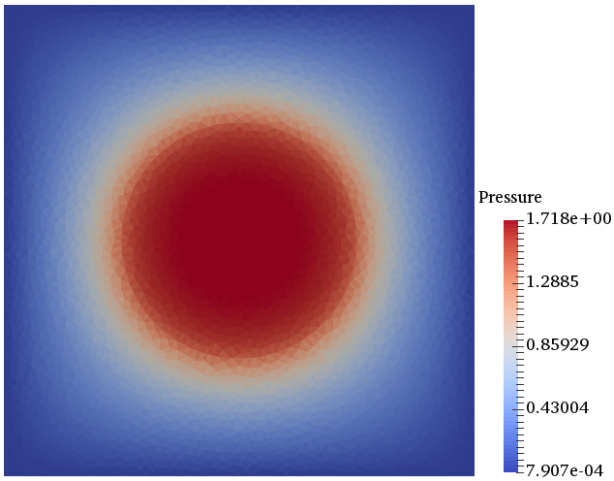

(e) intermediary radius: 0.45

Figure 3.14: Differences of TIFP for different specified radius of intermediary and fixed radii of necrotic core and periphery regions.

The collection of the values of maximum dimensionless interstitial fluid pressure corresponding to each

value of intermediary radius from Fig.(3.14) builds up the curve of the pressure trend that is shown in Fig.(3.15). The maximum tumor interstitial fluid pressure increases by increasing the size of the intermediary region.

Dimenssionless Radius of Intermediary	Maximum Dimenssionless Pressure
0.27	1.304
0.3	1.371
0.35	1.481
0.4	1.596
0.45	1.718

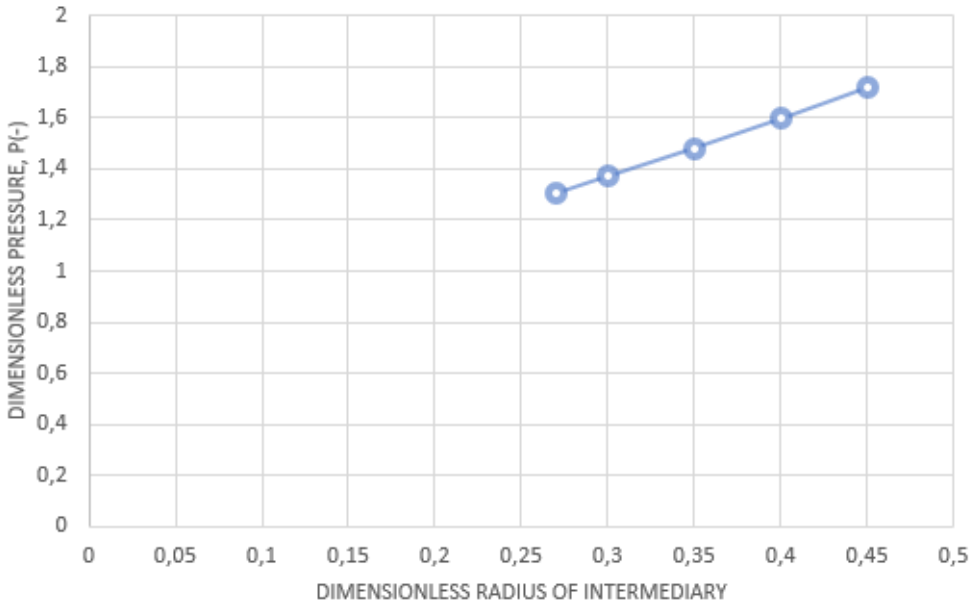

Figure 3.15: The trend of TIFP by increasing the size of intermediary region.

3.3.3 Comparison between the TIFP trends for different sizes of periphery and intermediary regions

The obtained values of the maximum TIFP from Figs.(3.13) and (3.15) are shown in Fig.(3.16). As shown, increasing the radii of periphery and intermediary causes increasing TIFP. However, because of the effect of vessel capillaries on the pressure distribution, the trend of pressure curvature for increased periphery radius is significantly sharper than increased intermediary radius. It means that decreasing the size of periphery region results lower interstitial fluid pressure. Specially, since we here focus on a heterogeneous tumor (containing necrotic core), cooperation between the necrotic core and the periphery decides the value of pressure inside the tumor. The larger necrotic core causes the existence of the smaller periphery region, thus, lower interstitial fluid pressure happens. Changing the size of intermediary does not have a significant

effect on the interstitial fluid pressure (see Fig.(3.16)).

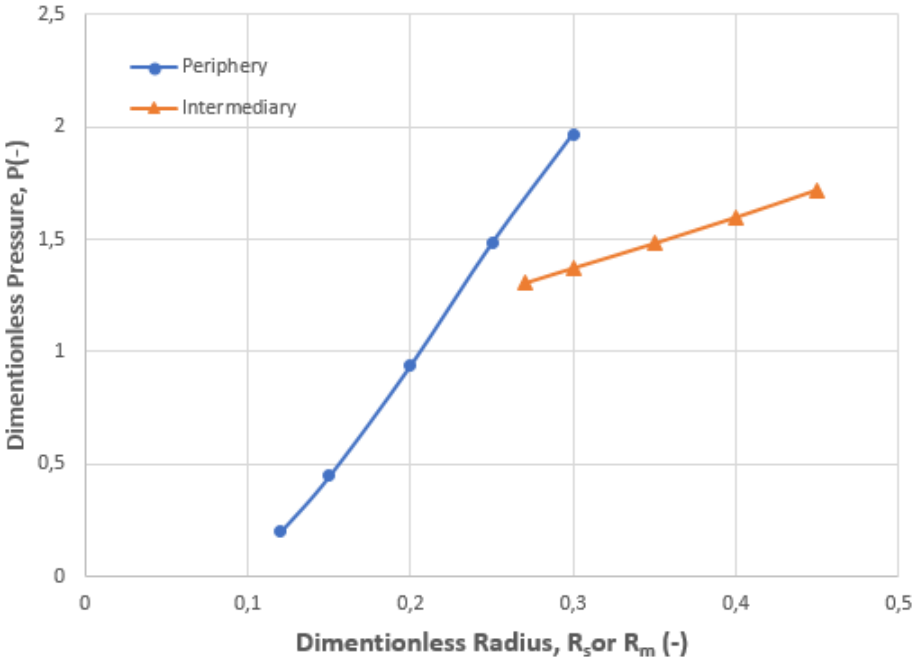

Figure 3.16: The effects of the size of periphery and intermediary on the trend of TIFP.

3.4 Effect of capillary hydraulic conductivity on TIFP distribution

Generally, as described in section(2.2.1)), there are three categories of capillaries in a tissue; arterial, venous and lymphatic capillaries. In this layout of tumor, blood vessel capillaries only exist in the periphery region and normal tissue. Blood vessel capillaries contain arterial and venous capillaries. The hydraulic conductivity of arterial and venous capillaries represent the abundance of blood vessels inside the tissue. Thus, the values of these hydraulic conductivity affect the production of blood vessels in the tissue. For example, increasing the hydraulic conductivity of arterial capillaries increases the amount of arterioles. On the other hand, the intermediary region only contains lymphatic capillaries. In this section, we are investigating the effect of arterial, venous and lymphatic capillaries on determining the TIFP distribution. In addition, as the values of the capillary (arterial, venous and lymphatic) hydraulic conductivity are different inside and outside a tumor, we use multiples to change these values.

3.4.1 Increasing the hydraulic conductivity of arterial capillaries

The visualizations of the TIFP distribution by increasing the hydraulic conductivity of arterial capillaries is shown in Fig.(3.17). More fluid can leak out of the arterial capillary by increasing the arterial hydraulic conductivity. As there is no lymphatic capillary in the periphery region, the leaked fluid remain in the tumor interstitium and it makes difficulty for fluid to flow through interstitium. Thus, interstitial pressure raises. It is proved by the increased maximum values of interstitial fluid pressure for increasing arterial hydraulic conductivity shown in Fig.(3.17).

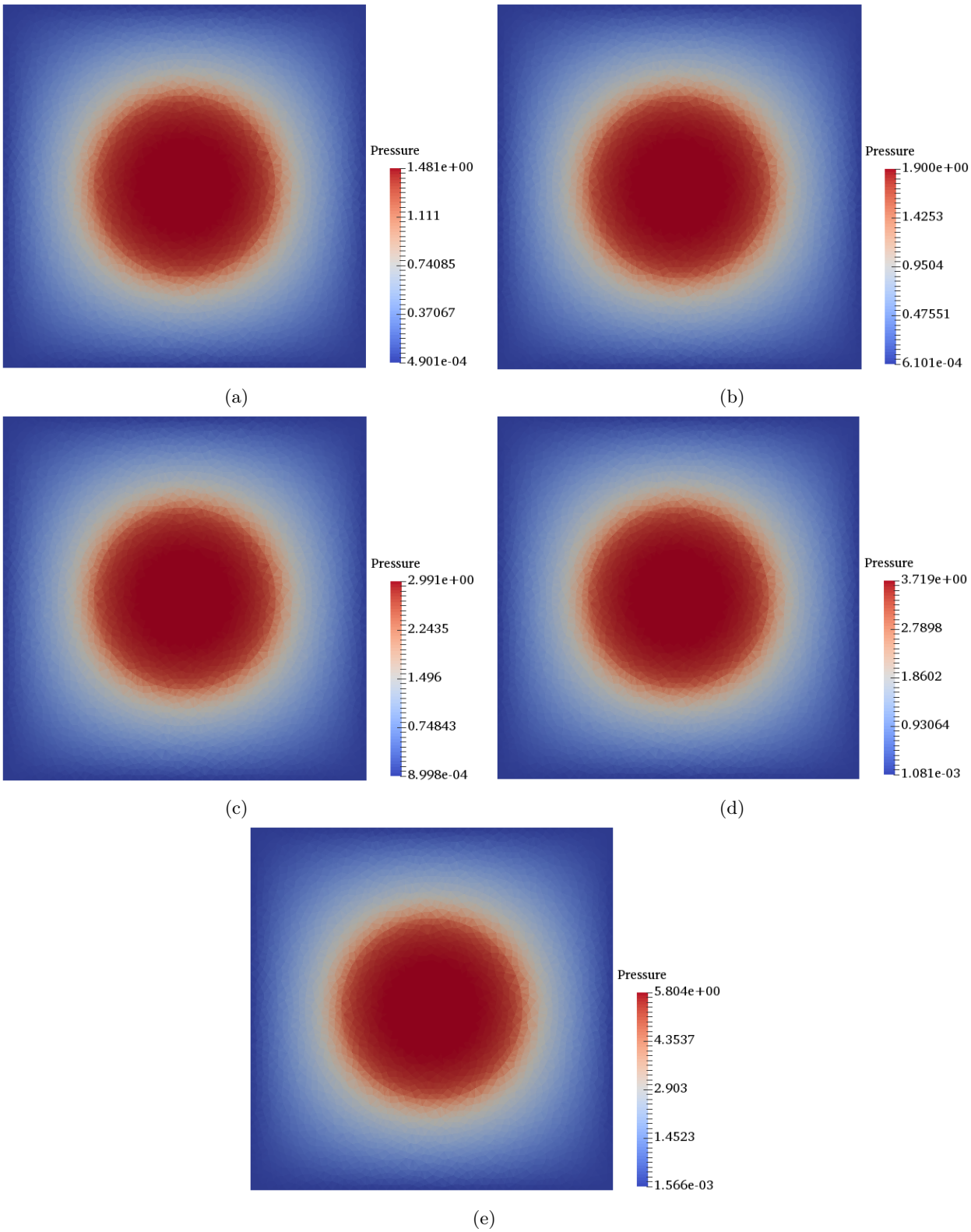

Figure 3.17: Differences between the TIFP distributions for increasing arterial hydraulic conductivity.

Fig.(3.18) shows that increasing the arterial hydraulic conductivity increases the value of maximum interstitial fluid pressure.

Multiplier of arterial hydraulic conductivity	Dimensionless interstitial pressure
1	1.481
1.25	1.9
1.75	2.991
2	3.719
2.5	5.804

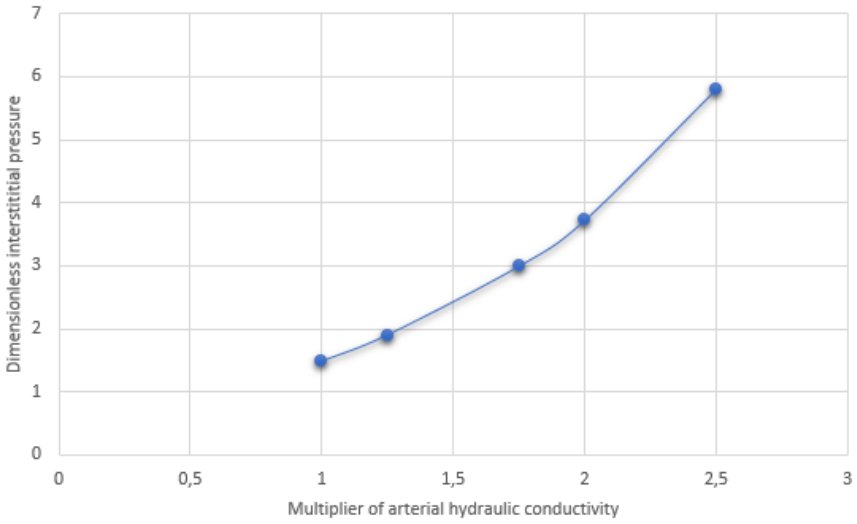

Figure 3.18: The trend of the maximum TIFP by increasing the arterial hydraulic conductivity.

3.4.2 Increasing the hydraulic conductivity of venous capillaries

The distributions of the TIFP for increasing venous hydraulic conductivity is shown in Fig.(3.19). In addition, the values of the maximum interstitial pressure corresponding to each venous hydraulic conductivity and the behaviour is illustrated in Fig.(3.20). Increased value of the venous hydraulic conductivity leads to increased value of the maximum interstitial fluid pressure.

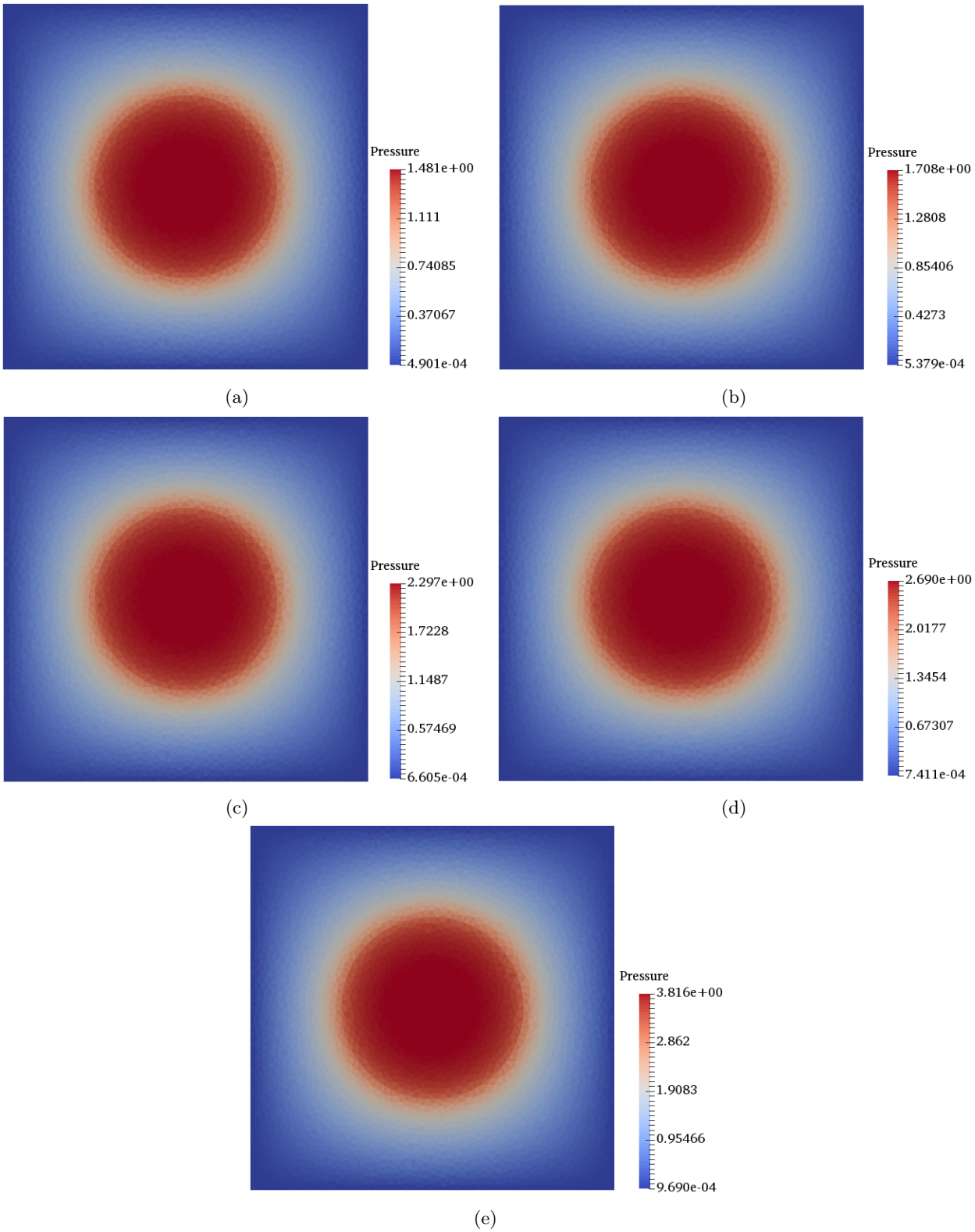

Figure 3.19: Differences between the TIFP distributions for increasing venous hydraulic conductivity.

Multiplier of venous hydraulic conductivity	Dimensionless interstitial pressure
1	1.481
1.25	1.708
1.75	2.297
2	2.69
2.5	3.816

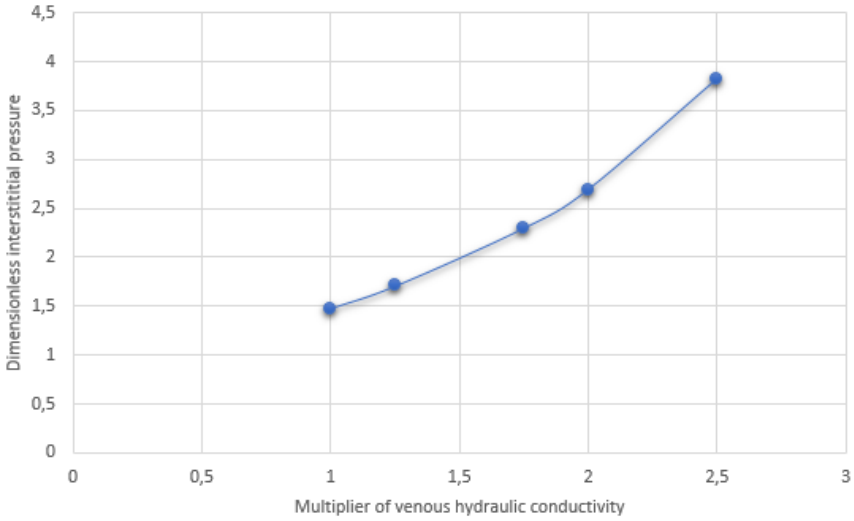

Figure 3.20: The trend of the maximum TIFP by increasing the venous hydraulic conductivity.

3.4.3 Changing the hydraulic conductivity of lymphatic capillaries

As in this study it is assumed that the lymphatic capillaries are observed only in the intermediary region which is outside of the tumor, investigating its influence on the distribution of the interstitial fluid pressure specially in the tumor is interesting. This would mean that excess fluid is not removed from the system as efficiently as with higher values of lymphatic hydraulic conductivity.

3.4.3.1 Decreasing the values of lymphatic hydraulic conductivity

Outcomes of visualizations are shown in Fig.(3.21). According to table (3.22), the value of the maximum interstitial fluid is decreasing by reducing the values of lymphatic hydraulic conductivity.

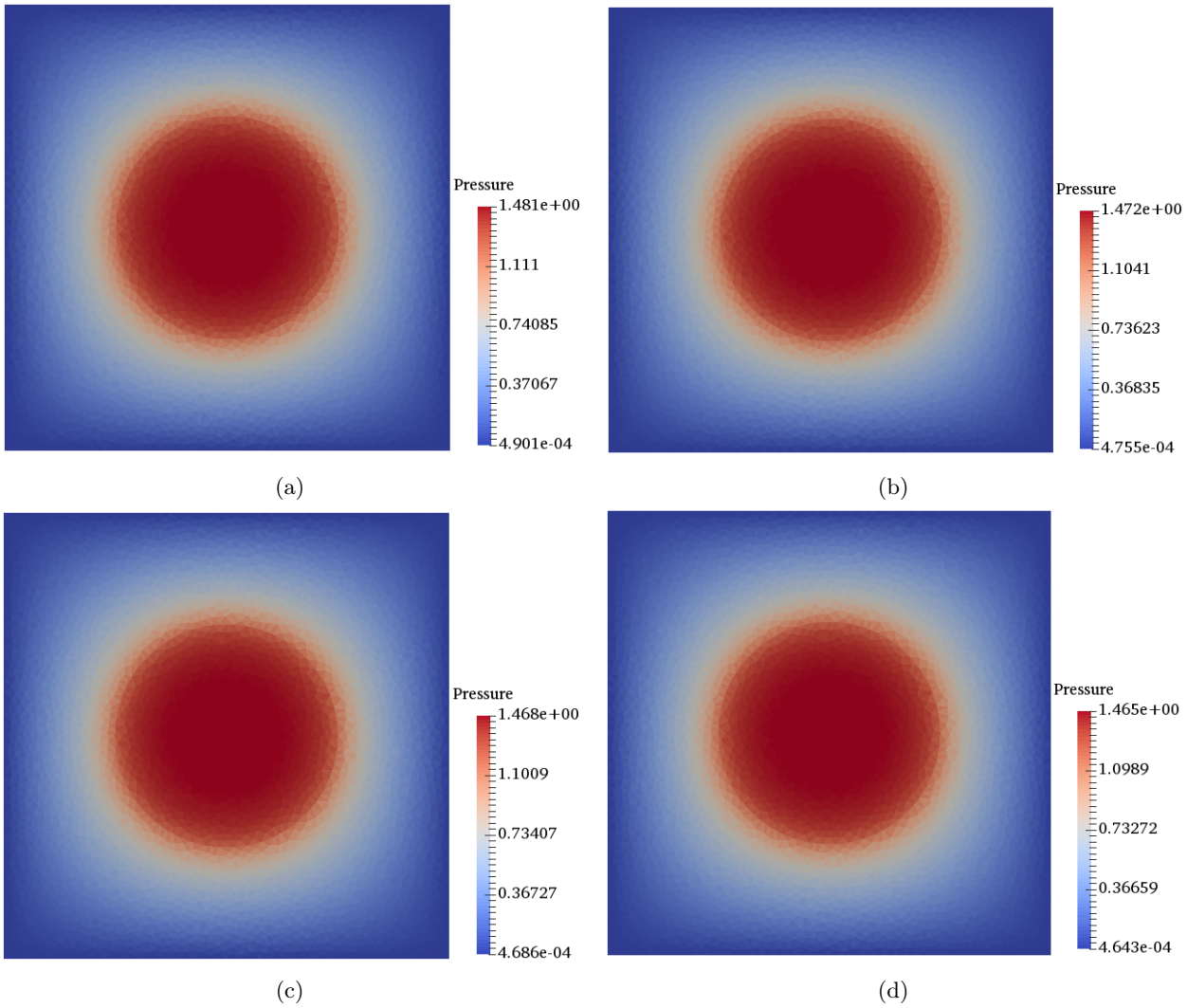

Figure 3.21: The effect of decreased value of lymphatic hydraulic conductivity on the maximum value of TIFP.

Multiplier of lymphatic hydraulic conductivity	Dimensionless interstitial pressure
1	1.481
0.66	1.472
0.5	1.468
0.4	1.465

Figure 3.22: Governed data of maximum TIFP from the visualizations for decreasing lymphatic hydraulic conductivity

3.4.3.2 Increasing the values of lymphatic hydraulic conductivity

The TIFP distributions for increasing lymphatic hydraulic conductivity and the obtained maximum values of interstitial pressure corresponding to each multiplier of lymphatic hydraulic conductivity are shown in Fig.(3.23) and table (3.24), respectively. The values in table (3.24) prove that the maximum value of TIFP is increasing by raising the value of lymphatic hydraulic conductivity.

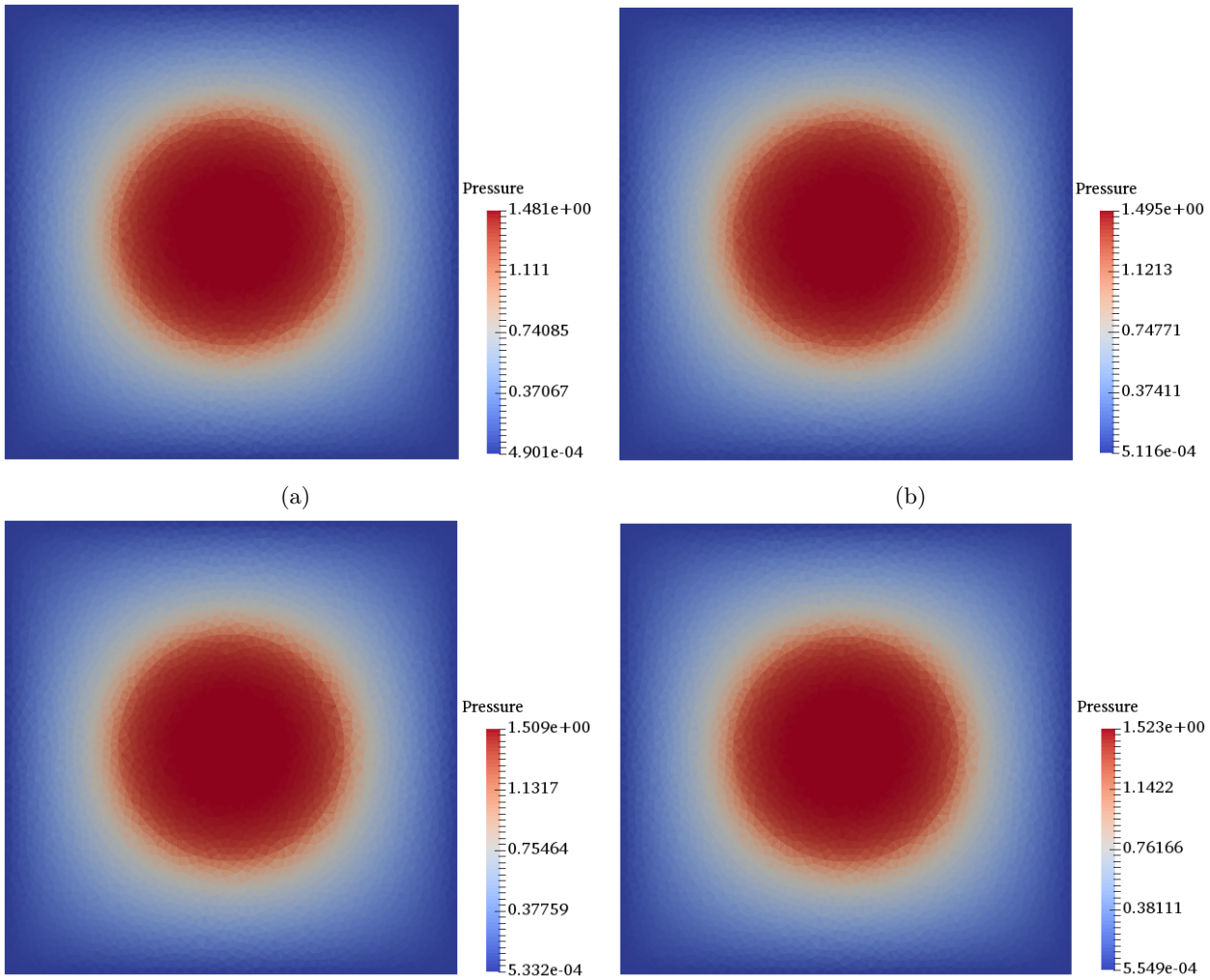

Figure 3.23: The effect of increased value of lymphatic hydraulic conductivity on the maximum value of TIFP.

Multiplier of lymphatic hydraulic conductivity	Dimensionless interstitial pressure
1	1.481
1.5	1.495
2	1.509
2.5	1.523

Figure 3.24: Governed data of maximum TIFP from the visualizations for increasing lymphatic hydraulic conductivity

The effect of the value of lymphatic hydraulic conductivity on the interstitial fluid pressure is illustrated in Fig.(3.25) which shows linearly increasing trend by increasing lymphatic hydraulic conductivity.

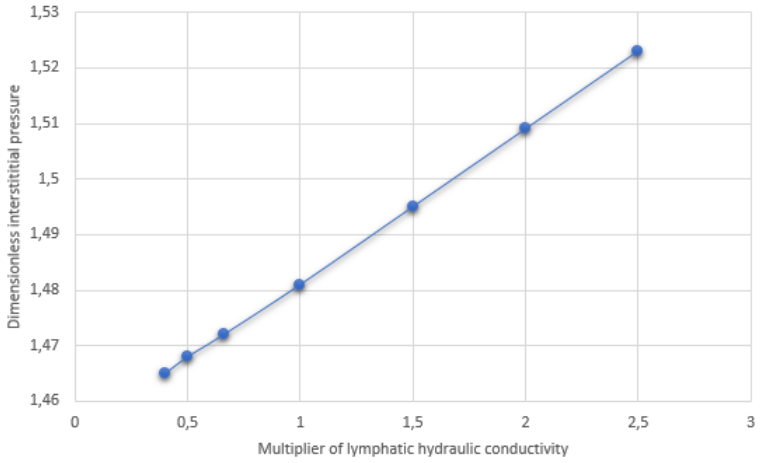

Figure 3.25: The trend of the maximum TIFP by increasing the lymphatic hydraulic conductivity.

Only a minor effect was observed by increasing the lymphatic hydraulic conductivity.

3.4.4 Comparison between the effects of arterial, venous and lymphatic hydraulic conductivity on TIFP

As shown in Fig.(3.26), for the largest values of arterial, venous and lymphatic hydraulic conductivity (which are defined as L_A, L_V and L_L, respectively, through Chapter 2) there are big gaps between the value of maximum interstitial fluid pressure. Increasing the arterial hydraulic conductivity (L_A) has significant effect on the interstitial fluid pressure and its trend is quite steep. In contrast, the effect of changing lymphatic hydraulic conductivity (L_L) on determining the tumor interstitial fluid pressure is almost negligible. Meanwhile, increased value of venous hydraulic conductivity, L_V, definitely increases the interstitial pressure but not as efficient as increased L_A. Which means that when we increase L_A and L_V in the same way, the obtained pressure for increased L_A is higher than increased L_V (see Fig.(3.26)). Inside the arterial capillary, the hydrostatic pressure of the capillary is more than osmotic pressure. Therefore, filtration occurs (fluid filtered out to the interstitial). While inside the venous capillary, the osmotic pressure is more than hydrostatic pressure and excess fluid absorbed into the venous capillary (Fig.2.17). Thus, venous capillary can drain off excess fluid.

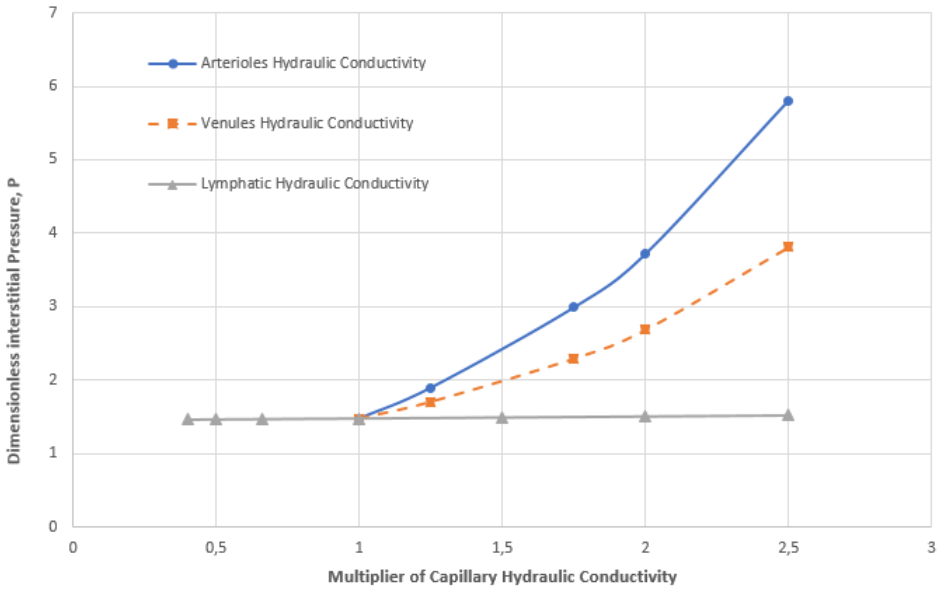

Figure 3.26: Comparison between the trends of pressure resulted from changed values of arterial, venous and lymphatic hydraulic conductivity.

3.5 Including sources of vessels in the periphery region

In previous sections, all results were investigated for a tumor with a uniform distribution of vessels which causes it to have symmetric visualizations. In the study in section (3.4), where the effect of arterial, venous and lymphatic hydraulic conductivities were investigated, it was found that arterial hydraulic conductivity has the strongest impact on TIFP.
As described in section (2.2.1), inside the tumor, the vessel capillaries, including arterial and venous capillaries, are observed in the periphery region. For the sake of simplicity, we assume that a circle with specific radius and center coordinates can be added in the periphery region which represents the source of blood vessel capillaries. So, lets call the added circle a source circle as a source of blood vessels.
In this case, it can be predicted that the visualization reveals non-uniform distribution of TIFP because of non-uniform distribution of blood vessels. This will represent a more realistic situation, as a more asymmetry TIFP distribution is more likely to be found in a real tumor. By changing the values of arterial hydraulic conductivity in the source circle, we can inquire its effect on determining the TIFP distribution.

First, we add the circle with the radius of 0.0375 and the center coordinates of $(0.675, 0.5)$), as a source of blood vessel capillary, in the periphery region, with fixed radii of necrotic core, periphery and intermediary circles as 0.10, 0.25 and 0.35 with the same center coordinates $(0.5, 0.5)$. Note that all parameters are considered dimensionless. In Fig.(3.27), it is shown that the TIFP distributions for the case with specified radii of necrotic core, periphery and intermediary circles (Fig.(3.7c)) (lets call this a 'base case') and added new circle are almost the same and the minor difference is because of the process of producing triangular grids. This is as expected and serves as a test for the programming.

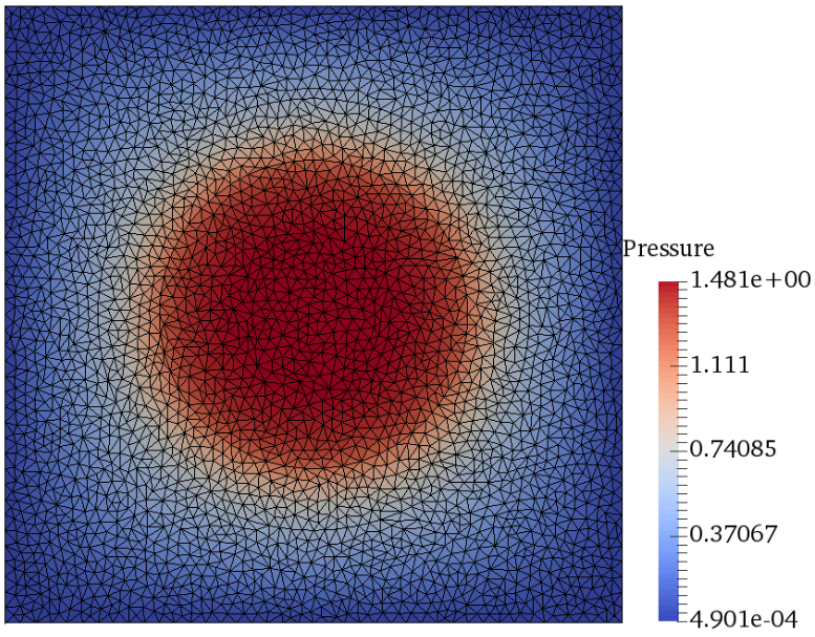

(a) The 'base case'

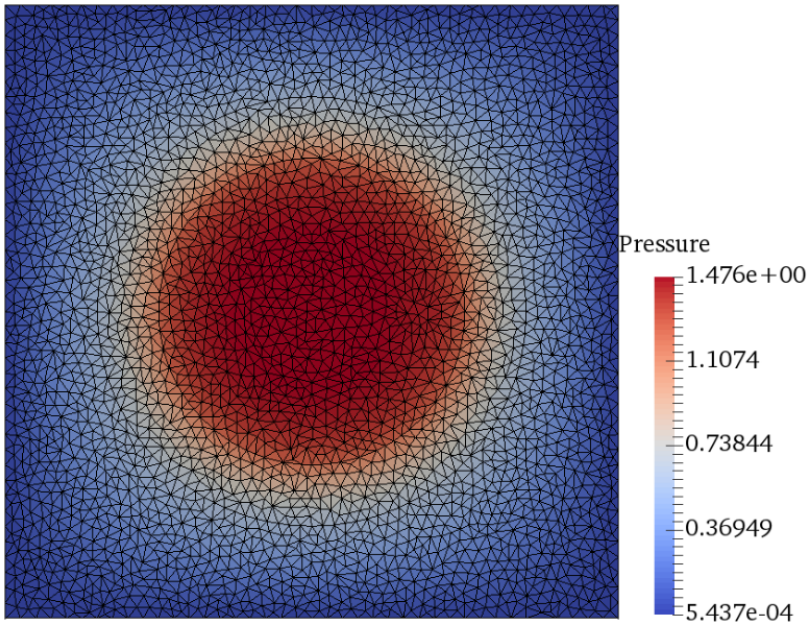

(b) Added new circle in periphery

Figure 3.27: The TIFP distribution (a) base case,(b) added one new circle in the periphery (consider the same arterial hydraulic conductivity throughout tumor for both cases).

Now, we investigate the effect of the value of arterial hydraulic conductivity in the added circle on the hole TIFP distribution. The results for low and high value of arterial hydraulic conductivity are shown in Figs.(3.28a) and (3.28b), respectively. Referring to Fig.(3.28), in contrast with symmetry distribution of blood vessels ('base case', for example), the maximum interstitial fluid pressure does not appear in the center of the tumor. Thus, the place and the concentration of blood vessels affect the interstitial pressure distribution.
Moreover, decreasing the L_A in the added source circle decreases the maximum interstitial pressure compare to the 'base case' in which dimensionless pressure is equal to 1.481, see Fig.(3.7c). In contrast, increased L_A causes increased maximum interstitial pressure. As shown in Fig.(3.28b), for increased arterial hydraulic conductivity, L_A, the maximum pressure occurs inside the added source circle. While for decreased L_A, the maximum interstitial pressure appeared in the region in the opposite side of the source circle Fig.(3.28a). As shown in Fig.(3.28), by adjusting high arterial hydraulic conductivity for the source circle, almost the restricted region of source area and its surrounding get highest pressure; while, the low arterial hydraulic conductivity causes the observation of high interstitial fluid pressure in wider region.

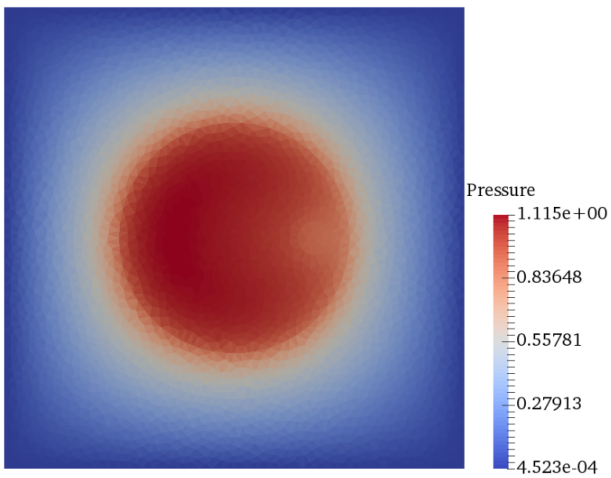

(a) decreased hydraulic conductivity of arterioles, L_A

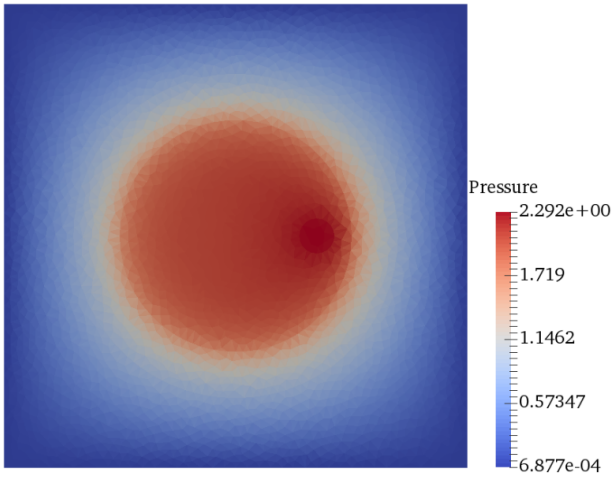

(b) increased hydraulic conductivity of arterioles, L_A

Figure 3.28: The effect of a source circle and its hydraulic conductivity L_A on the interstitial pressure.

Now, we change the position of the source circle in the periphery region by changing the center coordinates to $(0.3762, 0.3762)$ with the same radius of 0.0375. We have the same story for this new source circle (see Fig.(3.29)). The comparison of the two figures of (3.28) and (3.29) shows that the location of the source circle does not affect the value of the maximum interstitial fluid pressure (dimensionless pressure); so that, for the decreased value of arterial hydraulic conductivity, the maximum interstitial pressure gets the same value in both positions, which is equal to 1.11, and for increased L_A, regardless with the position of the sources, the maximum value of TIFP is equal to 2.29.

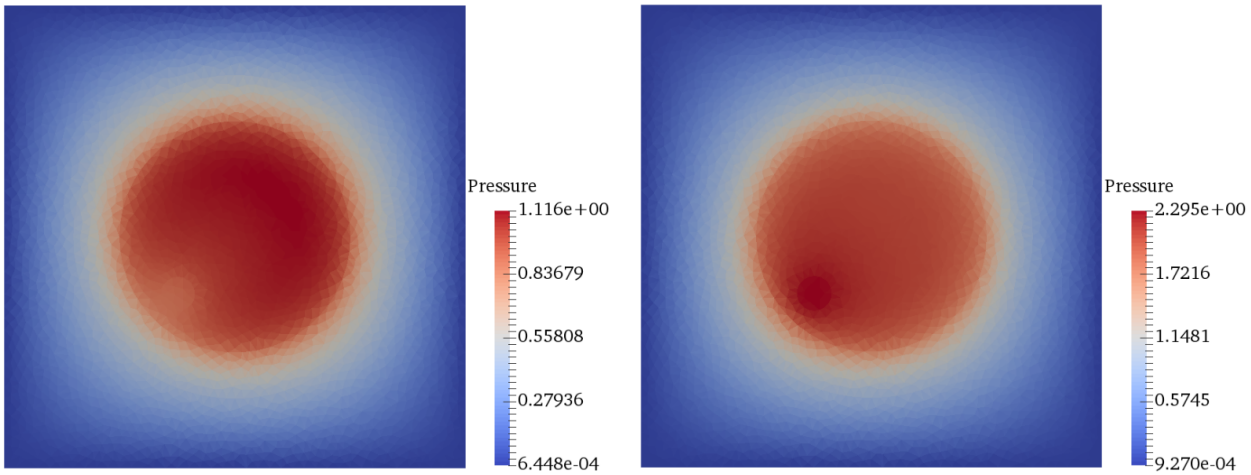

(a) decreased hydraulic conductivity of arterioles, L_A (b) increased hydraulic conductivity of arterioles, L_A

Figure 3.29: The effect of a source circle and its corresponding hydraulic conductivity L_A on the interstitial pressure.

Next, in the periphery region, we raise the number of source circles by including both previous circles with specified center coordinates and radii, with fixed radii of necrotic core, periphery and intermediary region. As shown in Fig.(3.30), adding two source circles to the 'base case' (3.7c), similar to observations in Fig.(3.27)), gives almost the same TIFP distribution.

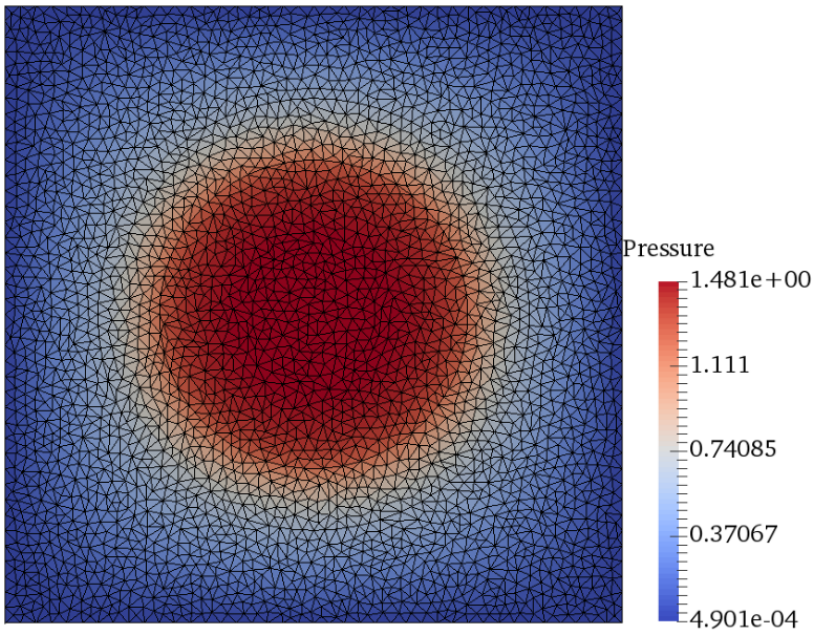

(a) The 'base case'

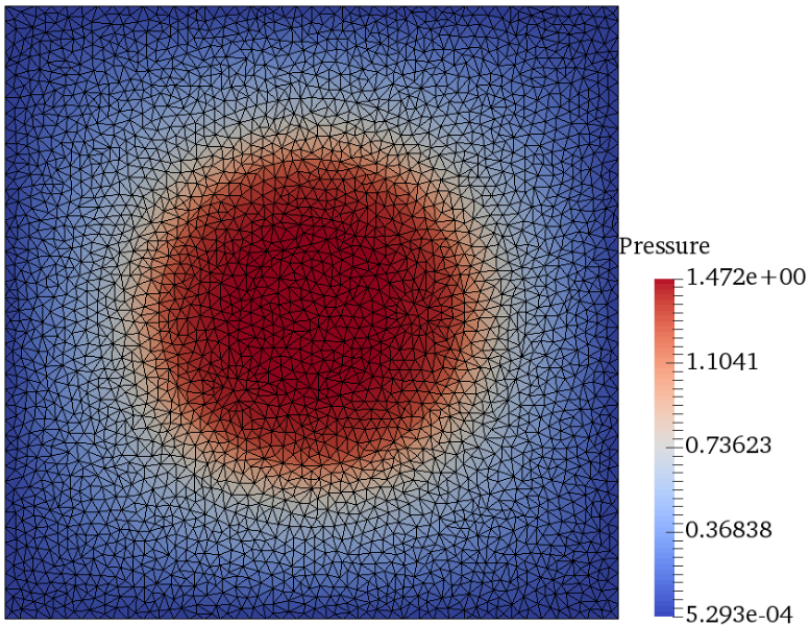

(b) Added two new source circles in the periphery

Figure 3.30: The TIFP distribution with the same adjusting of arterial hydraulic conductivity for (a) the base case, (b) added two new circles.

As shown in fig.(3.31a), decreasing the arterial hydraulic conductivities in both source circles reduces the abundance of blood vessels inside the circles and their surroundings. Referring to Fig.(3.31a), decreased L_A, in both sources, significantly decrease the maximum value of interstitial fluid pressure to the value of 0.79, compare to the base case (Fig.(3.7c)) in which the maximum value of interstitial fluid pressure is equal to 1.481. In contrast, increasing the arterial hydraulic conductivity in both circles increases the distribution of blood vessels inside the circles and it helps the tumor to get more nutrition and oxygen. Thus, relying to Fig.(3.31b), a strong increase of the maximum value of interstitial fluid pressure forms with the value of 3.0 by increasing the value of L_A in both source circles. Moreover, Figs.(3.31c) and (3.31d) illustrate that

increased L_A in one of the source circles and decreased L_A in the other one affect the tumor interstitial fluid pressure distribution; while, the same value of 1.83 is obtained for the maximum interstitial fluid pressure which is observed in the source with the higher arterial hydraulic conductivity.

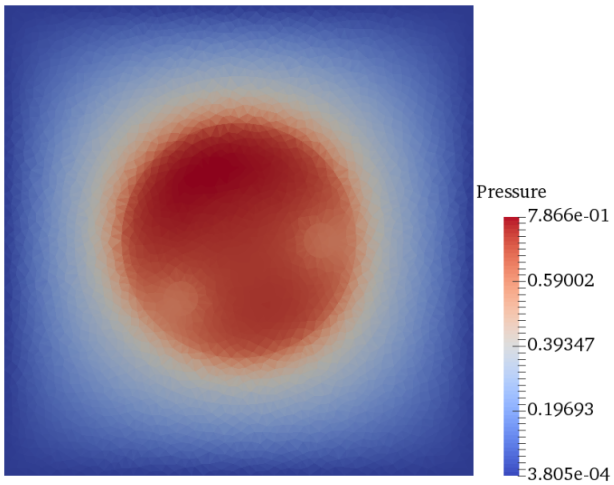

(a) decreased L_A in both vessel sources

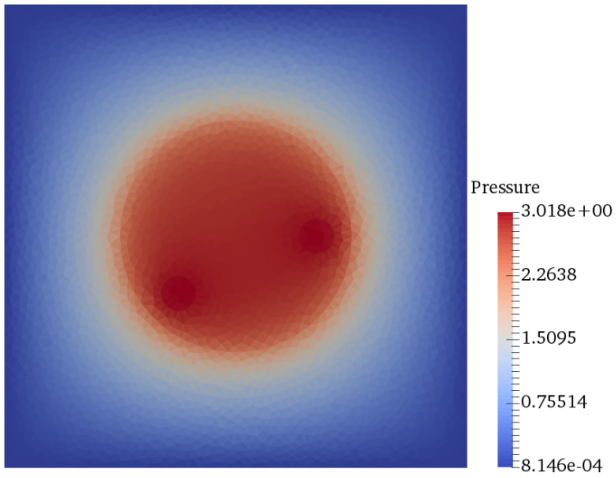

(b) increased L_A in both vessel sources

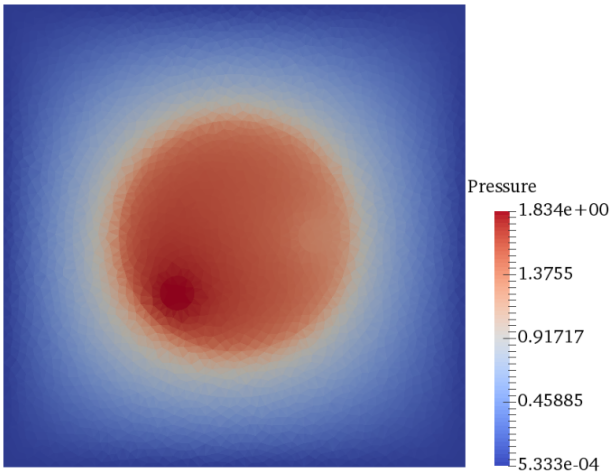

(c) decreased L_A in the source circle with the center coordinate of $((0.675, 0.5))$ and increased L_A in the source circle with the center coordinate of $(0.3762, 0.3762)$

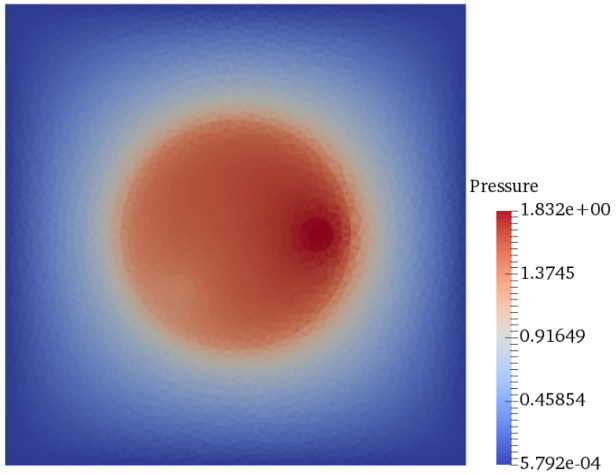

(d) decreased L_A in the source circle with the center coordinate of $(0.3762, 0.3762)$ and increased L_A in the source circle with the center coordinate of $((0.675, 0.5))$

Figure 3.31: The effects of two source circles in the periphery region and their corresponding arterial hydraulic conductivities on the TIFP distribution.

As shown in Fig.(3.31), the case with increased arterial hydraulic conductivity in both source circles gets the highest maximum interstitial pressure compare to other three cases. While, Fig.(3.31a) proves the obtaining of the lowest value of the maximum interstitial pressure by decreasing the arterial hydraulic conductivity in both source circles. As a result, the amount of source circles and their corresponding arterial hydraulic conductivity strongly affect the TIFP distribution.

3.6 Discussion of the model results with regards to venule and lymphatic effects on TIFP

When interpreting the results in section 3.4.4 according to expected behaviour, one would assume that venules and lymphatics would drain off fluid from the system and thereby decrease the TIFP.
When we find the opposite behaviour, we had to question the mathematical formulation given by Liu. Consider the mass-balance equation described in Eq.(2.1.4) (section 2.1.1); and focus on $J_S = S_A L_A[p_A - p(\vec{r}) - \sigma_A(\pi_A - \pi_{Ai})] + S_V L_V[p_V - p(\vec{r}) - \sigma_V(\pi_V - \pi_{Vi})]$, defined by Liu et al. in Eq.(2.2.5), which is the net flow rate filtered out of blood vessel capillary (source), and $J_L = L_L S_L(p_i - p_L)$, defined in Eq.(2.2.6), is the net flow rate absorbed into lymphatic capillary (sink). In the formulations, through arterial capillary, p_A should be bigger than p_i to function as filter (source) and, in contrast, through venous and lymphatic capillaries, p_i should be greater than p_V and p_L to form absorption (sink). By noticing this fact, the formulations presented by Liu et al. are correct.

Then we focus on the boundary conditions and baseline parameter values used in our numerical model.The observed model behaviour is in accordance with the model, but the chosen values for pressures in the venules and in the lymphatic vessels can not be correct (based on the model behaviour).
The boundary condition is such that the pressure is zero at the outer boundaries, so the TIFP are rather close to zero in the normal tissue. So, to have a sink behaviour for venous and lymphatic capillaries, we should change the signs of the values of venules hydrostatic and osmotic pressures, in addition to the lymphatic hydrostatic pressure in the Table (3.1), to have reasonable biophysical parameters in the model.
The results with this new implementation is demonstrated in the following sections.
Notice that these negative pressures are still in accordance with physics; since the pressure in this model is not unique, we can always add constant to the pressure and still get the same velocity field.
With these pressures for venules and lymphatics, we would expect that the pressure should decrease for increasing values of venous and lymphatic hydraulic conductivities.

3.6.1 Increased venous hydraulic conductivity

Increasing the hydraulic conductivity of venous capillaries would simulate a situation where the venules remove excess fluid more effective than with lower conductivity. In Fig.(3.34) the distributions of TIFP for increasing venous hydraulic conductivity are shown. The corresponding maximum value of dimensionless interstitial fluid pressure to each multiplier of venous hydraulic conductivity is written in Fig.(3.33a). As shown in Fig.(3.33b), a decreasing behaviour of pressure is observed by increasing the value of venous hydraulic conductivity.

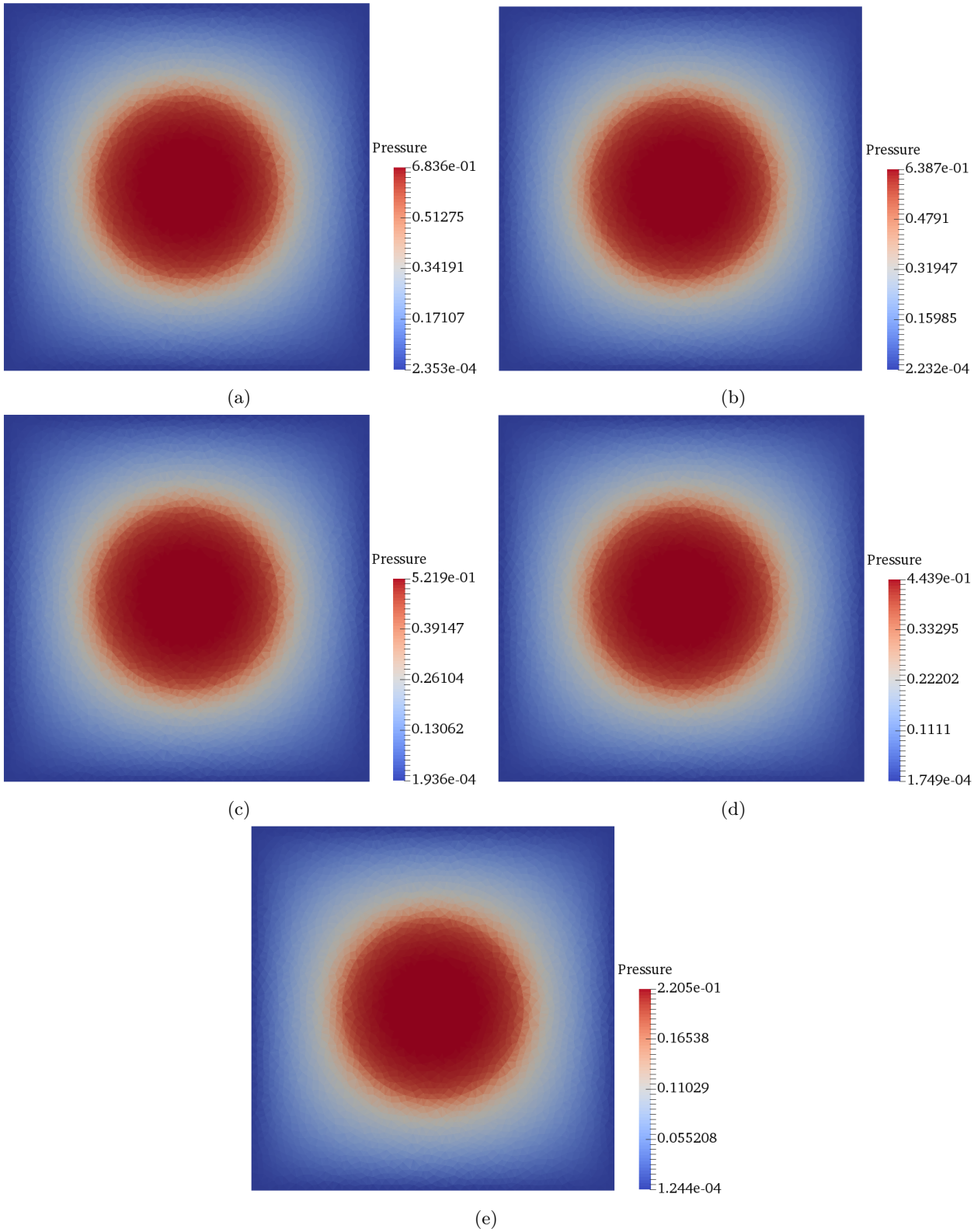

Figure 3.32: The differences between TIFP distributions for increasing venous hydraulic conductivity.

Multiplier of venous hydraulic conductivity	Dimensionless interstitial pressure
1	0.683
1.25	0.638
1.75	0.521
2	0.443
2.5	0.220

(a)

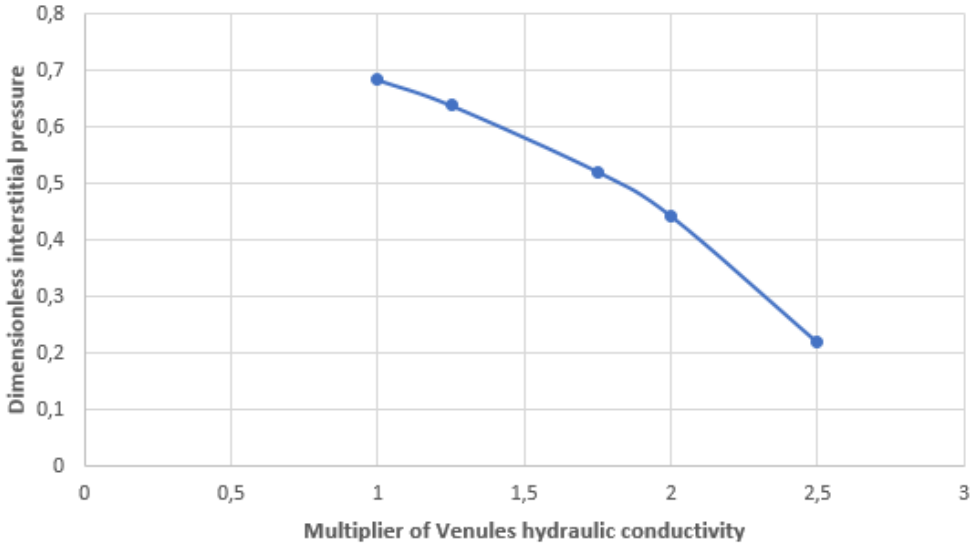

(b)

Figure 3.33: The trend of the interstitial pressure for increasing value of venous hydraulic conductivity.

In the model, most of the fluid is located in the periphery region, so the result is in accordance with what we expected.

3.6.2 Increased lymphatic hydraulic conductivity

As an assumption of the model, lymphatic capillaries are observed only in the intermediary region, which is outside of the tumor. Excess fluid is removed from the system by lymphatic capillaries. So, investigating the efficiency of high lymphatic hydraulic conductivity on the interstitial fluid pressure is interesting.
The visualizations of TIFP distribution for increasing value of lymphatic hydraulic conductivity is shown in Fig.(3.34). The values of maximum interstitial fluid pressure for each value of lymphatic hydraulic conductivity is written in Table (3.35a). As shown in Fig.(3.35b), increasing the value of lymphatic hydraulic conductivity weakly decreases the value of maximum interstitial fluid pressure.

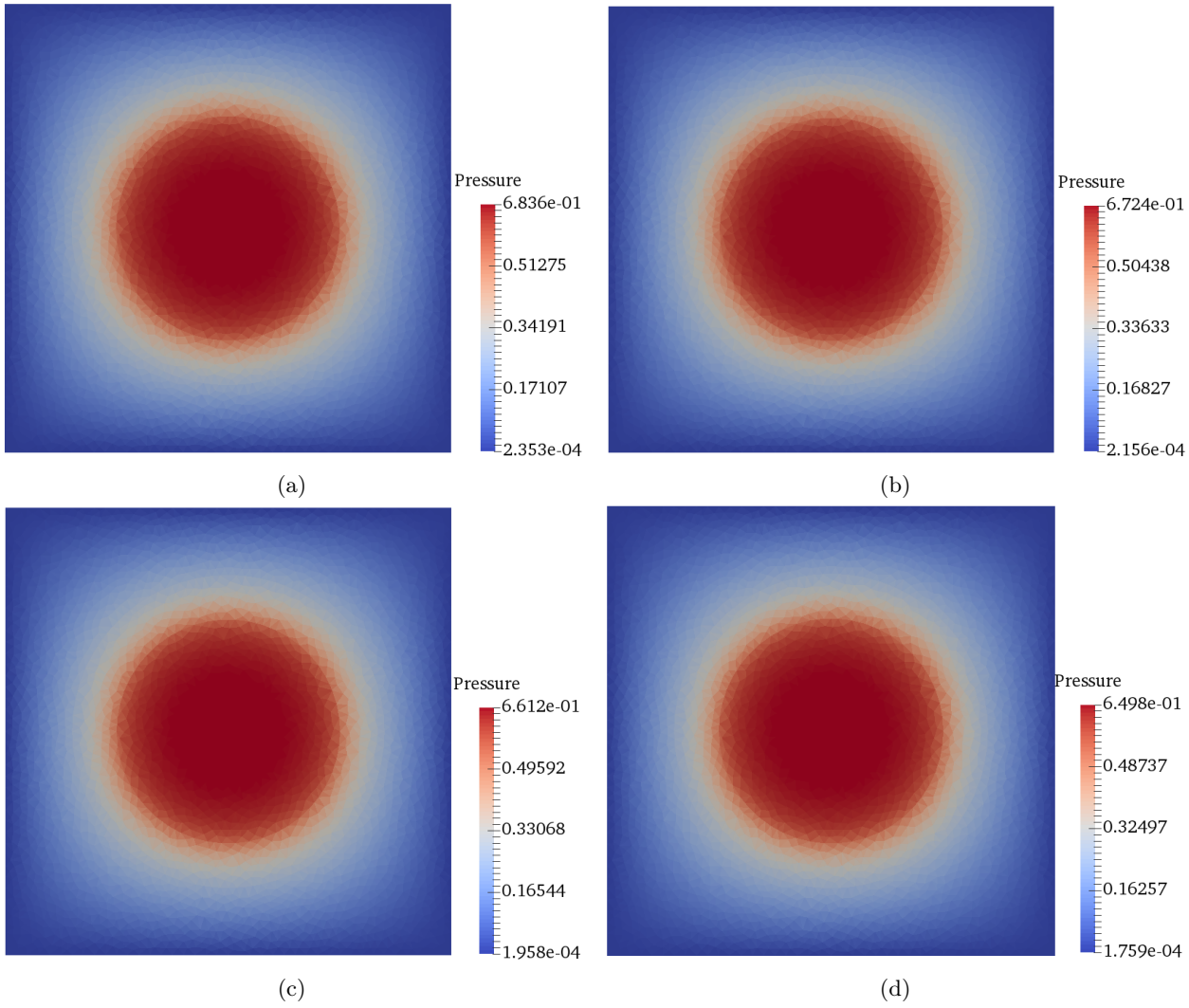

Figure 3.34: The differences between TIFP distributions for increasing value of lymphatic hydraulic conductivity.

Multiplier of lymphatic hydraulic conductivity	Dimensionless interstitial pressure
1	0.683
1.5	0.672
2	0.661
2.5	0.649

(a)

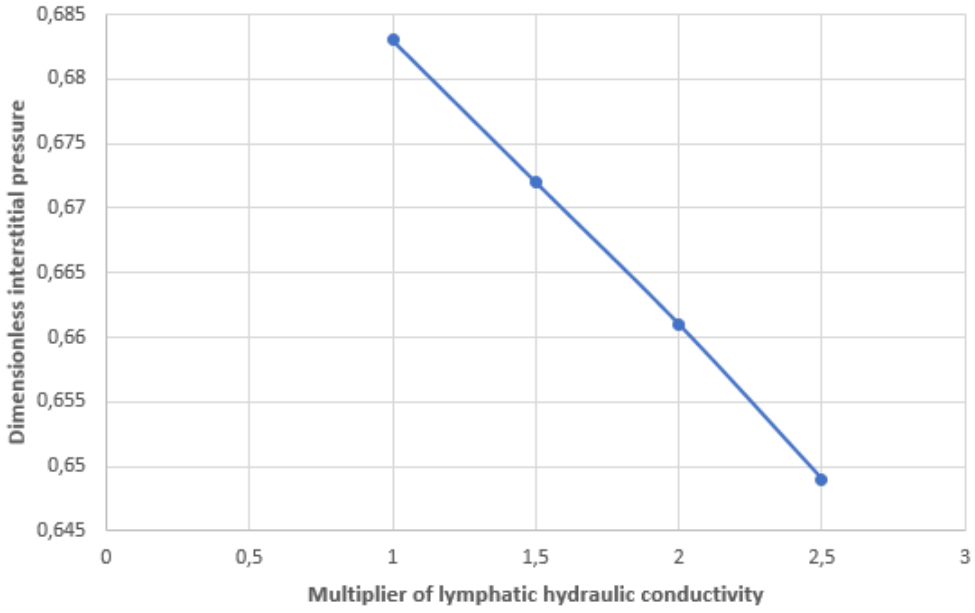

(b)

Figure 3.35: The behaviour of the interstitial pressure by increasing the value of lymphatic hydraulic conductivity.

The differences between the behaviours of interstitial fluid pressure for increasing values of venous and lymphatic hydraulic conductivity are illustrated in Fig.(3.36). Since venous capillaries function the same as the lymphatic capillaries, as predicted, the trend of the TIFP for increased values of venous and lymphatic hydraulic conductivities have the same directions. As shown in Fig.(3.36), the effect of increased lymphatic hydraulic conductivity is less than that of increased venous hydraulic conductivity.

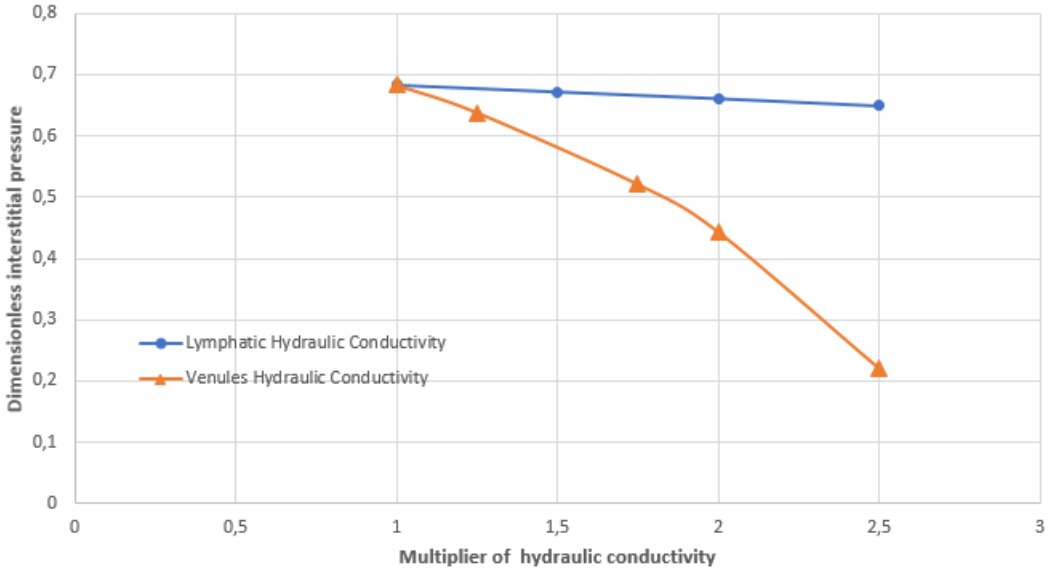

Figure 3.36: Comparison between the pressure trends for increased venous hydraulic conductivity and increased lymphatic hydraulic conductivity.

Chapter 4

Concluding remarks

Overall, the numerical simulation study did give valuable insights in TIFP behaviour. Targeting a heterogeneous tumor surrounded by normal tissue, with the tumor categorization into three different regions of necrotic core, periphery and intermediary, and considering corresponding continuous variation of the interstitial hydraulic conductivity, allows for investigation of the TIFP distribution in a more real tumor. The necrotic core region has an uniform structure which is reflected in the uniform TIFP. In this region the interstitial hydraulic conductivity is constant. Similarly, the interstitial hydraulic conductivity in the normal tissue has constant value which is lower than the constant value of the necrotic core region. Since fluid and tumor matrix composition and the amount of cancerous cells vary thorough the periphery and intermediary regions, the interstitial hydraulic conductivity is spatially dependent. Our method gives the possibility to investigate the actual TIFP distribution.

4.1 Main conclusions

In a tumor, with symmetric distribution of blood vessel capillaries, TIFP gets its maximum value in the central region and it is decreasing to the minimum value of TIFP in the normal tissue.
Increasing the size of the necrotic core has a strong impact on decreasing the value of TIFP. Consequently, decreasing the size of the periphery region, as an area with plenty of blood vessels and fluid, causes decreased TIFP. The size of the intermediary region, as an area "outside" of the tumor consisting of only lymphatic vessels, has minor effect on the TIFP distribution.

Moreover, the investigations show that arterial, venous and lymphatic hydraulic conductivities affect the TIFP distribution. Increasing the arterial hydraulic conductivity significantly increases the TIFP. While, as venules and lymphatics function as sink terms and they absorb excess interstitial fluid, increasing the value of venous and lymphatic hydraulic conductivity decreases the TIFP.

In the periphery region, adding a region as the blood vessel source influences on TIFP distribution. An asymmetric distribution of blood vessel capillaries leads to an asymmetric distribution of TIFP. In this case, maximum value of TIFP is observed in the area with higher arterial hydraulic conductivity and its surrounding.
The amount of the blood vessel sources and their corresponding arterial hydraulic conductivity significantly affect the distribution of TIFP. If we have only one source of blood vessel, regardless with the position in the periphery region, its value of arterial hydraulic conductivity influence on the TIFP distribution. The highest interstitial fluid pressure is observed when all the sources get their highest value of arterial hydraulic conductivity. In contrast, if all sources get the lowest value of arterial hydraulic conductivity, very low interstitial pressure will be formed.

Finally, the findings discussed in section (3.6), indicate that some of the simulation studies should be repeated with the new parameter values. But due to lack of time, this is not included in the master thesis work. We

do not expect that the observed trends will be significantly changed by repeating these simulations. It will however, be crucial for the planned journal publication.

4.2 Future work

The model results needs to be further confirmed, both by further testing and confirmation of the model. The model should also be developed further to involve transport of substances across the cancerous matrix. Next, it will be important to compare the numerical results with experimental findings for different cases. In [22], it is suggested that a numerical model can aid the development of methods that invasively measure TIFP in a given tumor (via DCE-MRI). Further investigations of how the numerical model can have clinical contributions in cancer diagnostics, monitoring and treatment planning will be important.

Appendices

Appendix 1

Spherical Coordinates

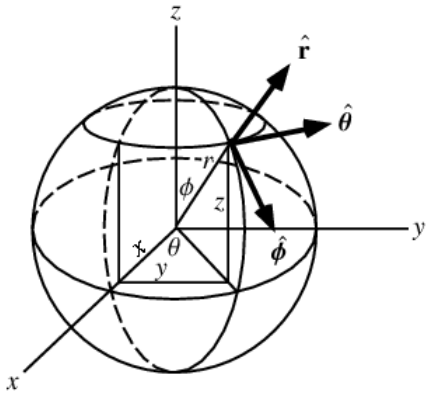

Figure 4.1: Spherical polar coordinates[46].

The spherical coordinates (r, θ, ϕ) are related to the Cartesian coordinates (x, y, z) by:

$$r = \sqrt{x^2 + y^2 + z^2}$$

$$\theta = \arctan(\sqrt{x^2 + y^2}, z)$$

$$\phi = \arctan(y, x)$$

and,

$$x = r \sin\theta \cos\phi$$

$$y = r \sin\theta \sin\phi$$

$$z = r \cos\theta$$

with the unit vectors of:

$$\hat{r} = \frac{\vec{r}}{r} = \frac{x\hat{x} + y\hat{y} + z\hat{z}}{r} = \hat{x} \sin\theta \cos\phi + \hat{y} \sin\theta \sin\phi + \hat{z} \cos\theta$$

$$\hat{\phi} = \frac{\hat{z} \times \hat{r}}{\sin\theta} = \hat{x} \sin\phi + \hat{y} \cos\phi$$

$$\hat{\theta} = \hat{\phi} \times \hat{r} = \hat{x} \cos\theta \cos\phi + \hat{y} \cos\theta \sin\phi - \hat{z} \sin\theta$$

The del operator from the definition of the gradient:
Assume that u is a function of the spherical coordinate. The value of u changes by an infinitesimal amount du

when the point of observation is changed by $d\vec{r}$. That change may be determined from the partial derivatives as:

$$du = \frac{\partial u}{\partial r}dr + \frac{\partial u}{\partial \theta}d\theta + \frac{\partial u}{\partial \phi}d\phi$$

In addition, another definition for gradient is

$$du = \vec{\nabla}u.d\vec{r}$$

therefore,

$$\frac{\partial u}{\partial r}dr + \frac{\partial u}{\partial \theta}d\theta + \frac{\partial u}{\partial \phi}d\phi = \vec{\nabla}u.d\vec{r}$$

in a spherical coordinates,

$$\frac{\partial u}{\partial r}dr + \frac{\partial u}{\partial \theta}d\theta + \frac{\partial u}{\partial \phi}d\phi = (\vec{\nabla}u)_r dr + (\vec{\nabla}u)_\theta r d\theta + (\vec{\nabla}u)_\phi r\sin\theta d\phi$$

Thus,

$$(\vec{\nabla}u)_r = \frac{\partial u}{\partial r}, (\vec{\nabla}u)_\theta = \frac{1}{r}\frac{\partial u}{\partial \theta}, (\vec{\nabla}u)_\phi = \frac{1}{r\sin\theta}\frac{\partial u}{\partial \phi}$$

from which we find

$$\vec{\nabla} = \hat{r}\frac{\partial}{\partial r} + \frac{\hat{\theta}}{r}\frac{\partial}{\partial \theta} + \frac{\hat{\phi}}{r\sin\theta}\frac{\partial}{\partial \phi}$$

Laplacian:

$$\nabla^2 u = \vec{\nabla}.(\vec{\nabla}u) = [\hat{r}\frac{\partial}{\partial r} + \frac{\hat{\theta}}{r}\frac{\partial}{\partial \theta} + \frac{\hat{\phi}}{r\sin\theta}\frac{\partial}{\partial \phi}].[\hat{r}\frac{\partial u}{\partial r} + \frac{\hat{\theta}}{r}\frac{\partial u}{\partial \theta} + \frac{\hat{\phi}}{r\sin\theta}\frac{\partial u}{\partial \phi}]$$

$$\nabla^2 u = \hat{r}.\frac{\partial}{\partial r}(\hat{r}\frac{\partial u}{\partial r} + \frac{\hat{\theta}}{r}\frac{\partial u}{\partial \theta} + \frac{\hat{\phi}}{r\sin\theta}\frac{\partial u}{\partial \phi}) + \frac{\hat{\theta}}{r}.\frac{\partial}{\partial \theta}(\hat{r}\frac{\partial u}{\partial r} + \frac{\hat{\theta}}{r}\frac{\partial u}{\partial \theta} + \frac{\hat{\phi}}{r\sin\theta}\frac{\partial u}{\partial \phi}) + \frac{\hat{\phi}}{r\sin\theta}.\frac{\partial}{\partial \phi}(\hat{r}\frac{\partial u}{\partial r} + \frac{\hat{\theta}}{r}\frac{\partial u}{\partial \theta} + \frac{\hat{\phi}}{r\sin\theta}\frac{\partial u}{\partial \phi})$$

With the help of partial derivatives, we find the Laplacian operator which can be written as:

$$\nabla^2 = \frac{1}{r^2}\frac{\partial}{\partial r}(r^2\frac{\partial}{\partial r}) + \frac{1}{r^2\sin\theta}\frac{\partial}{\partial \theta}(\sin\theta\frac{\partial}{\partial \theta}) + \frac{1}{r^2\sin^2\theta}\frac{\partial^2}{\partial \phi^2}$$

Appendix 2

We here look at the following equation,

$$p'' + \frac{2}{r}p' - kp = 0$$

Change the problem to the first degree problem by using the well known technique in [15]:

$$u' + u^2 + \frac{2}{r}u - k = 0 \qquad (b)$$

The Ricatti equation is:

$$y' = -y^2 - \frac{2}{x}y + k \qquad (c)$$

One of the solutions of the Ricatti equation is:

$$y_1 = -\frac{1}{x} + \sqrt{k}$$

So,

$$y = -\frac{1}{x} + \sqrt{k} + \frac{1}{\nu} \qquad (d)$$

and

$$y' = \frac{1}{x^2} + \frac{-\nu'}{\nu^2} \qquad (e)$$

By applying (d) and (e) in the Ricatti equation, we have:

$$\frac{1}{x^2} - \frac{-\nu'}{\nu^2} = -(\frac{1}{x^2} + k + \frac{1}{\nu^2} - 2\frac{\sqrt{k}}{x} + 2\frac{\sqrt{k}}{\nu} - 2\frac{1}{x\nu}) - \frac{2}{x}(-\frac{1}{x} + \sqrt{k} + \frac{1}{\nu}) + k$$

$\Rightarrow$

$$-\frac{\nu'}{\nu^2} = -\frac{1}{\nu^2} - 2\frac{\sqrt{k}}{\nu}$$

$\Rightarrow$

$$\nu' = 1 + 2\sqrt{k}\nu \qquad (f)$$

Solving the equation (f):

$$\frac{d\nu(x)}{dx} = 1 + 2\sqrt{k}\nu$$

$\Longrightarrow$

$$\frac{1}{1 + 2\sqrt{k}\nu(x)}\frac{d\nu(x)}{dx} = 1$$

integrating from both sides by the substitution of $h = 2\sqrt{k}\nu(x) + 1$ and $\partial h = 2\sqrt{\partial}\nu(t)$,

$$\int \frac{1}{1 + 2\sqrt{k}\nu(x)}\frac{d\nu(x)}{dx} = \int \frac{1}{2\sqrt{k}h}dh = \frac{1}{2\sqrt{k}}\int \frac{1}{h}dh = \frac{1}{2\sqrt{k}}\ln h + c$$

$\Longrightarrow$

$$\frac{\ln(2\sqrt{k}\nu(x) + 1)}{2\sqrt{k}} + c = x + c'$$

Finally,

$$\nu(x) = \frac{e^{2\sqrt{k}(c_1 + x)} - 1}{2\sqrt{k}}$$

Putting this solution in equation (d):

$$y = -\frac{1}{x} + \sqrt{k} + \frac{2\sqrt{k}}{e^{2\sqrt{k}(c_1 + x)} - 1}$$

Change the parameters to the origin ones as $y = u, x = r, k = \frac{\alpha^2}{R^2}$.
According to equation (a), we have:

$$p = \exp\int u dr = \exp\int(-\frac{1}{r} + \frac{\alpha}{R} + \frac{2\frac{\alpha}{R}}{e^{2\frac{\alpha}{R}(c_1 + r)} - 1})dr \qquad (g)$$

$$\int -\frac{1}{r}dr = -\ln r + c$$

$$\int \frac{\alpha}{R}dr = \frac{\alpha}{R}r + c'$$

$$\int(\frac{2\frac{\alpha}{R}}{e^{2\frac{\alpha}{R}(c_1 + r)} - 1})dr = \frac{2\alpha}{R}\int(\frac{1}{e^{2\frac{\alpha}{R}(c_1 + r)} - 1})dr$$

To solve $\int(\frac{1}{e^{2\frac{\alpha}{R}(c_1 + r)} - 1})dr$, use the substitution of $u = \frac{2\alpha c_1 + 2\alpha r}{R}$. So, $\frac{du}{dr} = \frac{2\alpha}{R} \Rightarrow dr = \frac{R}{2\alpha}du$. So,

$$\int (\frac{1}{e^{2\frac{\alpha}{R}(c_1+r)}-1})dr = \frac{R}{2\alpha}\int \frac{1}{e^u-1}du$$

Again use the substitution $v = \frac{1}{e^u-1} \Rightarrow \frac{dv}{du} = -\frac{e^u}{(e^u-1)^2} \Rightarrow du = -\frac{(e^u-1)^2}{e^u}dv$.
In addition, $ve^u - v = 1 \Rightarrow e^u = \frac{1+v}{v} = 1 + \frac{1}{v}$. So,

$$\int \frac{1}{e^u-1}du = -\int \frac{1}{v+1}dv = -\ln(v+1) = -\ln(\frac{1}{e^u-1}+1)$$

$\Longrightarrow$

$$\frac{R}{2\alpha}\int \frac{1}{e^u-1}du = -\frac{R}{2\alpha}\ln(\frac{1}{e^u-1}+1)$$

$\Longrightarrow$

$$\int (\frac{1}{e^{2\frac{\alpha}{R}(c_1+r)}-1})dr = -\frac{R}{2\alpha}\ln(\frac{1}{e^{2\alpha(\frac{c_1+r}{R})}-1}+1) + C_2$$

On the other hand,

$$\ln(\frac{1}{e^{\frac{2\alpha c_1+2\alpha r}{R}}-1}+1) = \ln(\frac{1+e^{\frac{2\alpha c_1+2\alpha r}{R}}-1}{e^{\frac{2\alpha c_1+2\alpha r}{R}}-1}) =$$

$$\ln(1+e^{\frac{2\alpha c_1+2\alpha r}{R}}-1) - \ln(e^{\frac{2\alpha c_1+2\alpha r}{R}}-1) = \ln(e^{\frac{2\alpha c_1+2\alpha r}{R}}) - \ln(e^{\frac{2\alpha c_1+2\alpha r}{R}}-1) = 2\alpha(\frac{c_1+r}{R}) - \ln(e^{2\alpha(\frac{c_1+r}{R})}-1)$$

Reffering to equation (g):

$$p = \exp\{-\ln r + \frac{\alpha r}{R} + \frac{2\alpha}{R}(-\frac{R}{2\alpha}(\frac{2\alpha(c_1+r)}{R} - \ln(e^{2\alpha(\frac{c_1+r}{R})}-1) + c_2)\}$$

$\Longrightarrow$

$$p = \exp\{-\ln r + \frac{\alpha r}{R} - \frac{2\alpha(c_1+r)}{R} + \ln(e^{2\alpha(\frac{c_1+r}{R})}-1) + \frac{2\alpha c_2}{R}\}$$

Appendix 3

The solution for spherical case can be written as

$$\begin{cases} p = \frac{1}{r}e^{\sqrt{\alpha}(2c_2+r)} - \frac{1}{r}e^{\sqrt{\alpha}(2c_1+2c_2-r)} + p_e \quad (R_0 < r < R_s)\ , \\ \\ p = \frac{1}{r}e^{\sqrt{\beta}(2c_4+r)} - \frac{1}{r}e^{\sqrt{\beta}(2c_3+2c_4-r)} + p_L \quad (R_s < r < R_m). \end{cases} \tag{4.2.1}$$

Refer to the first boundary condition Eq.(2.2.12),

$$\frac{1}{R_0}e^{\sqrt{\alpha}(2c_2+R_0)} - \frac{1}{R_0}e^{\sqrt{\alpha}(2c_1+2c_2-R_0)} + p_e = p_0$$

so,

$$e^{\sqrt{\alpha}(2c_2+R_0)} - e^{\sqrt{\alpha}(2c_1+2c_2-R_0)} + p_e = (p_0-p_e)R_0$$

so,

$$e^{\sqrt{\alpha}(2c_1+2c_2-R_0)} = -(p_0-p_e)R_0 + e^{\sqrt{\alpha}(2c_2+R_0)} \tag{1}$$

And,

$$-K'[-\frac{1}{R_0^2}e^{\sqrt{\alpha}(2c_2+R_0)} + \frac{\sqrt{\alpha}}{R_0}e^{\sqrt{\alpha}(2c_2+R_0)} + \frac{1}{R_0^2}e^{\sqrt{\alpha}(2c_1+2c_2-R_0)} + \frac{\sqrt{\alpha}}{R_0}e^{\sqrt{\alpha}(2c_1+2c_2-R_0)}] = 0$$

so,

$$-\frac{1}{R_0}e^{\sqrt{\alpha}(2c_2+R_0)}+\sqrt{\alpha}e^{\sqrt{\alpha}(2c_2+R_0)}+\frac{1}{R_0}e^{\sqrt{\alpha}(2c_1+2c_2-R_0)}+\sqrt{\alpha}e^{\sqrt{\alpha}(2c_1+2c_2-R_0)}=0 \tag{2}$$

put the value of $e^{\sqrt{\alpha}(2c_1+2c_2-R_0)}$ in Eq.(2). So,

$$-\frac{1}{R_0}e^{\sqrt{\alpha}(2c_2+R_0)}+\sqrt{\alpha}e^{\sqrt{\alpha}(2c_2+R_0)}+\frac{1}{R_0}(-(p_0-p_e)R_0+e^{\sqrt{\alpha}(2c_2+R_0)})+\sqrt{\alpha}(-(p_0-p_e)R_0+e^{\sqrt{\alpha}(2c_2+R_0)})=0$$

then,

$$-\frac{1}{R_0}e^{\sqrt{\alpha}(2c_2+R_0)}+\sqrt{\alpha}e^{\sqrt{\alpha}(2c_2+R_0)}-(p_0-p_e)+\frac{e^{\sqrt{\alpha}(2c_2+R_0)}}{R_0}-\sqrt{\alpha}(p_0-p_e)R_0+\sqrt{\alpha}e^{\sqrt{\alpha}(2c_2+R_0)}=0$$

So,

$$e^{\sqrt{\alpha}(2c_2+R_0)}[-\frac{1}{R_0}+\sqrt{\alpha}+\frac{1}{R_0}+\sqrt{\alpha}]=\sqrt{\alpha}(p_0-p_e)R_0+(p_0-p_e)$$

so,

$$e^{\sqrt{\alpha}(2c_2+R_0)}=\frac{(p_0-p_e)(\sqrt{\alpha}R_0+1)}{2\sqrt{\alpha}}$$

Define C_2 and C_1 as follows:

$$C_2=e^{\sqrt{\alpha}(2c_2)}=\frac{(p_0-p_e)(\sqrt{\alpha}R_0+1)}{2\sqrt{\alpha}}e^{-\sqrt{\alpha}R_0} \tag{3}$$

therefore,

$$e^{\sqrt{\alpha}(2c_1+2c_2-R_0)}=\frac{(-R_0+\sqrt{\alpha}R_0+1)(p_0-p_e)}{2\sqrt{\alpha}}$$

$$C_1=e^{\sqrt{\alpha}(2c_1+2c_2)}=\frac{(-R_0+\sqrt{\alpha}R_0+1)(p_0-p_e)}{2\sqrt{\alpha}}e^{\sqrt{\alpha}R_0} \tag{4}$$

Due to The second boundary condition, Eq.(2.2.13):

$$\frac{1}{R_m}e^{\sqrt{\beta}(2c_4+R_m)}-\frac{1}{R_m}e^{\sqrt{\beta}(2c_3+2c_4-R_m)}+p_L=p_\infty$$

so,

$$e^{\sqrt{\beta}(2c_4+R_m)}-e^{\sqrt{\beta}(2c_3+2c_4-R_m)}=(p_\infty-p_L)R_m$$

so,

$$e^{\sqrt{\beta}(2c_3+2c_4-R_m)}=-(p_\infty-p_L)R_m+e^{\sqrt{\beta}(2c_4+R_m)} \tag{5}$$

And,

$$-K[-\frac{1}{R_m^2}e^{\sqrt{\beta}(2c_4+R_m)}+\frac{\sqrt{\beta}}{R_m}e^{\sqrt{\beta}(2c_4+R_m)}+\frac{1}{R_m^2}e^{\sqrt{\beta}(2c_3+2c_4-R_m)}+\frac{\sqrt{\beta}}{R_m}e^{\sqrt{\beta}(2c_3+2c_4-R_m)}]=0$$

so,

$$-\frac{1}{R_m}e^{\sqrt{\beta}(2c_4+R_m)}+\sqrt{\beta}e^{\sqrt{\beta}(2c_4+R_m)}+\frac{1}{R_m}e^{\sqrt{\beta}(2c_3+2c_4-R_m)}+\sqrt{\beta}e^{\sqrt{\beta}(2c_3+2c_4-R_m)}=0 \tag{6}$$

Place the value of $e^{\sqrt{\beta}(2c_3+2c_4-R_m)}$ in Eq.(5):

$$-\frac{1}{R_m}e^{\sqrt{\beta}(2c_4+R_m)}+\sqrt{\beta}e^{\sqrt{\beta}(2c_4+R_m)}-(p_\infty-p_L)+\frac{e^{\sqrt{\beta}(2c_4+R_m)}}{R_m}-\sqrt{\beta}(p_\infty-p_L)+\sqrt{\beta}e^{\sqrt{\beta}(2c_4+R_m)}=0$$

so,

$$e^{\sqrt{\beta}(2c_4+R_m)}(-\frac{1}{R_m}+\sqrt{\beta}+\frac{1}{R_m}+\sqrt{\beta})=(p_\infty-p_L)+\sqrt{\beta}R_m(p_\infty-p_L)$$

so,

$$e^{\sqrt{\beta}(2c_4+R_m)} = \frac{(p_\infty - p_L)(1+\sqrt{\beta}R_m)}{2\sqrt{\beta}}$$

Define C_4 and C_3:

$$C_4 = e^{\sqrt{\beta}(2c_4)} = \frac{(p_\infty - p_L)(1+\sqrt{\beta}R_m)}{2\sqrt{\beta}} e^{-\sqrt{\beta}R_m} \tag{7}$$

as a result:

$$C_3 = e^{\sqrt{\beta}(2c_3+2c_4)} = \frac{(-R_m+\sqrt{\beta}R_m+1)(p_\infty - p_L)}{2\sqrt{\beta}} e^{\sqrt{\beta}R_m} \tag{8}$$

Apply the third boundary condition, Eq.(2.2.14):

$$\frac{1}{R_s}e^{\sqrt{\alpha}(2c_2+R_s)} - \frac{1}{R_s}e^{\sqrt{\alpha}(2c_1+2c_2-R_s)} + p_e = \frac{1}{R_s}e^{\sqrt{\beta}(2c_4+R_s)} - \frac{1}{R_s}e^{\sqrt{\beta}(2c_3+2c_4-R_s)} + p_L$$

so,

$$\frac{1}{R_s}e^{\sqrt{\alpha}(2c_2)}e^{\sqrt{\alpha}R_s} - \frac{1}{R_s}e^{\sqrt{\alpha}(2c_1+2c_2)}e^{-\sqrt{\alpha}R_s} + p_e = \frac{1}{R_s}e^{\sqrt{\beta}(2c_4)}e^{\sqrt{\beta}R_s} - \frac{1}{R_s}e^{\sqrt{\beta}(2c_3+2c_4)}e^{\sqrt{\beta}R_s} + p_L$$

so,

$$\frac{1}{R_s}C_2e^{\sqrt{\alpha}R_s} - \frac{1}{R_s}C_1e^{-\sqrt{\alpha}R_s} + p_e = \frac{1}{R_s}C_4e^{\sqrt{\beta}R_s} - \frac{1}{R_s}C_3e^{-\sqrt{\beta}R_s} + p_L$$

And,

$$K[-\frac{1}{R_s^2}C_4e^{\sqrt{\beta}R_s} + \frac{\sqrt{\beta}}{R_s}C_4e^{\sqrt{\beta}R_s} + \frac{1}{R_s^2}C_3e^{-\sqrt{\beta}R_s} + \frac{\sqrt{\beta}}{R_s}C_3e^{-\sqrt{\beta}R_s}] =$$

$$K'[-\frac{1}{R_s^2}C_2e^{\sqrt{\alpha}R_s} + \frac{\sqrt{\alpha}}{R_s}C_2e^{\sqrt{\alpha}R_s} + \frac{1}{R_s^2}C_1e^{-\sqrt{\alpha}R_s} + \frac{\sqrt{\alpha}}{R_s}C_1e^{-\sqrt{\alpha}R_s}]$$

so,

$$K[C_4e^{\sqrt{\beta}R_s}(-\frac{1}{R_s}+\sqrt{\beta}) + C_3e^{-\sqrt{\beta}R_s}(\frac{1}{R_s}+\sqrt{\beta})] = K'[C_2e^{\sqrt{\alpha}R_s}(-\frac{1}{R_s}+\sqrt{\alpha}) + C_1e^{-\sqrt{\alpha}R_s}(\frac{1}{R_s}+\sqrt{\alpha})]$$

so,

$$C_4e^{\sqrt{\beta}R_s}(-\frac{1}{R_s}+\sqrt{\beta}) + C_3e^{-\sqrt{\beta}R_s}(\frac{1}{R_s}+\sqrt{\beta}) = C_2\frac{K'}{K}e^{\sqrt{\alpha}R_s}(-\frac{1}{R_s}+\sqrt{\alpha}) + C_1\frac{K'}{K}e^{-\sqrt{\alpha}R_s}(\frac{1}{R_s}+\sqrt{\alpha})$$

Substitute the values of C_i constants $i = 1, 2, 3, 4$:

$$\frac{(p_\infty - p_L)(1+\sqrt{\beta}R_m)}{2\sqrt{\beta}}e^{-\sqrt{\beta}R_m}e^{\sqrt{\beta}R_s}(-\frac{1}{R_s}+\sqrt{\beta}) + \frac{(-R_m+\sqrt{\beta}R_m+1)(p_\infty - p_L)}{2\sqrt{\beta}}e^{\sqrt{\beta}R_m}e^{-\sqrt{\beta}R_s}(\frac{1}{R_s}+\sqrt{\beta}) =$$

$$\frac{(p_0 - p_e)(\sqrt{\alpha}R_0+1)}{2\sqrt{\alpha}}e^{-\sqrt{\alpha}R_0}\frac{K'}{K}e^{\sqrt{\alpha}R_s}(-\frac{1}{R_s}+\sqrt{\alpha}) + \frac{(-R_0+\sqrt{\alpha}R_0+1)(p_0 - p_e)}{2\sqrt{\alpha}}e^{\sqrt{\alpha}R_0}\frac{K'}{K}e^{-\sqrt{\alpha}R_s}(\frac{1}{R_s}+\sqrt{\alpha})$$

Define below parameters which are constants:

$$A = \frac{1}{R_s}\frac{(\sqrt{\alpha}R_0+1)}{2\sqrt{\alpha}}e^{-\sqrt{\alpha}R_0}e^{\sqrt{\alpha}R_s}$$

$$B = \frac{1}{R_s}\frac{(-R_0+\sqrt{\alpha}R_0+1)}{2\sqrt{\alpha}}e^{\sqrt{\alpha}R_0}e^{-\sqrt{\alpha}R_s}$$

$$C = \frac{1}{R_s}\frac{(1+\sqrt{\beta}R_m)}{2\sqrt{\beta}}e^{-\sqrt{\beta}R_m}e^{\sqrt{\beta}R_s}$$

$$D = \frac{1}{R_s}\frac{(-R_m+\sqrt{\beta}R_m+1)}{2\sqrt{\beta}}e^{\sqrt{\beta}R_m}e^{-\sqrt{\beta}R_s}$$

$$E = \frac{(1+\sqrt{\beta}R_m)}{2\sqrt{\beta}} e^{-\sqrt{\beta}R_m} e^{\sqrt{\beta}R_s} (-\frac{1}{R_s} + \sqrt{\beta})$$

$$F = \frac{(-R_m+\sqrt{\beta}R_m+1)}{2\sqrt{\beta}} e^{\sqrt{\beta}R_m} e^{-\sqrt{\beta}R_s} (\frac{1}{R_s} + \sqrt{\beta})$$

$$G = \frac{(\sqrt{\alpha}R_0+1)}{2\sqrt{\alpha}} e^{-\sqrt{\alpha}R_0} \frac{K'}{K} e^{\sqrt{\alpha}R_s} (-\frac{1}{R_s} + \sqrt{\alpha})$$

$$H = \frac{(-R_0+\sqrt{\alpha}R_0+1)}{2\sqrt{\alpha}} e^{\sqrt{\alpha}R_0} \frac{K'}{K} e^{-\sqrt{\alpha}R_s} (\frac{1}{R_s} + \sqrt{\alpha})$$

As a result,

$$(p_0 - p_e)A - (p_0 - p_e)B + p_e = (p_\infty - p_L)C - (p_\infty - p_L)D + p_L$$

$\Longrightarrow$

$$-(C-D)p_\infty + (A-B)p_0 = -(-A+B+1)p_e + (-C+D+1)p_L \tag{9}$$

and

$$(p_\infty - p_L)E + (p_\infty - p_L)F = (p_0 - p_e)G + (p_0 - p_e)H$$

$\Longrightarrow$

$$(E+F)p_\infty - (G+H)p_0 = -(G+H)p_e + (E+F)p_L \tag{10}$$

By considering the two Eqs.(9),(10), the parameters p_L and p_e are calculable. Therefore,

$$p_L = \frac{[(G+H)(C-D) + (-A+B+1)(E+F)]p_\infty - [(G+H)(A-B) + (G+H)(-A+B+1)]}{[-(G+H)(-C+D+1) + (-A+B+1)(E+F)]}$$

and

$$p_e =$$

if $R_0 < r < R_s$,

$$p = \frac{1}{r} e^{\sqrt{\alpha}(2c_2)} e^{\sqrt{\alpha}r} - \frac{1}{r} e^{\sqrt{\alpha}(2c_1+2c_2)} e^{-\sqrt{\alpha}r} + p_e$$

$\Longrightarrow$

$$p = \frac{1}{r} \frac{(p_0 - p_e)(\sqrt{\alpha}R_0+1)}{2\sqrt{\alpha}} e^{-\sqrt{\alpha}R_0} e^{\sqrt{\alpha}r} - \frac{1}{r} \frac{(-R_0+\sqrt{\alpha}R_0+1)(p_0-p_e)}{2\sqrt{\alpha}} e^{\sqrt{\alpha}R_0} e^{-\sqrt{\alpha}r} + p_e$$

And if $R_s < r < R_m$,

$$p = \frac{1}{r} e^{\sqrt{\beta}(2c_4+r)} - \frac{1}{r} e^{\sqrt{\beta}(2c_3+2c_4-r)} + p_L$$

$\Longrightarrow$

$$p = \frac{1}{r} \frac{(p_\infty - p_L)(1+\sqrt{\beta}R_m)}{2\sqrt{\beta}} e^{-\sqrt{\beta}R_m} e^{\sqrt{\beta}r} - \frac{1}{r} \frac{(-R_m+\sqrt{\beta}R_m+1)(p_\infty - p_L)}{2\sqrt{\beta}} e^{\sqrt{\beta}R_m} e^{-\sqrt{\beta}r} + p_L$$

List of Symbols

ϕ_L	Lymphatic drainage term (sec^{-1})
ϕ_V	Fluid source term (sec^{-1})
π_A	Arterioles osmotic pressure (mmHg)
π_i	Interstitial osmotic pressure (mmHg)
π_V	Venules osmotic pressure (mmHg)
K	Interstitial hydraulic conductivity (cm^2/mmHg.sec)
L_A	Arterial hydraulic conductivity (cm^2/mmHg.sec)
L_L	Hydraulic conductivity of the lymphatic wall (cm^2/mmHg.sec)
L_P	Hydraulic conductivity of the microvascular wall (cm^2/mmHg.sec)
L_{PL}	Hydraulic conductivity of the lymphatic wall (cm^2/mmHg.sec)
p_A	Arterioles hydrostatic pressure (mmHg)
p_i	Interstitial pressure (mmHg)
p_L	Lymphatic hydrostatic pressure (mmHg)
p_V	Venules hydrostatic pressure (mmHg)
S	Surface area (cm^2)
V	Unit volume (cm^3)
IFP	Interstitial Fluid Pressure
NFP	Net fluid pressure
TIFP	Tumor Interstitial Fluid Pressure

Bibliography

[1] D.W. Bailey D. L. Townsend, P. E. Valk, and M. N. Maisey. *Positron emission tomography*. Springer, 2005.

[2] P. Baluk et al. "Abnormalities of basement membrane on blood vessels and endothelial sprouts in tumors". In: *The American journal of pathology* 163.5 (2003), pp. 1801–1815.

[3] L. T. Baxter and R. K. Jain. "Transport of fluid and macromolecules in tumors. I. Role of interstitial pressure and convection". In: *Microvascular Research* (1988), pp. 77–104.

[4] L. T. Baxter and R. K. Jain. "Transport of fluid and macromolecules in tumors. II. Role of heterogeneous perfusion and lymphatics". In: *Microvascular Research* 40.2 (1990), pp. 246–263. ISSN: 0026-2862. DOI: 10.1016/0026-2862(90)90023-K.

[5] J. M. Brown and A. J. Giaccia. "The Unique Physiology of Solid Tumors: Opportunities (and Problems) for Cancer Therapy". In: *Cancer Research* 58.7 (1998), pp. 1408–1416. ISSN: 0008-5472.

[6] University of california. *osmotic pressure*. URL: https://chem.libretexts.org/LibreTexts/University_of_California_Davis/UCD_Chem_002B/UCD_Chem_2B.

[7] *Capillary bed*. 2011. URL: https://medicine.academic.ru/1306/Capillary.

[8] H Darcy. "Les Fontaines Publiques de la Ville de Dijon, Dalmont, Paris (1856)". In: *Google Scholar* (2007).

[9] R. Droual. *Capillary pressure*. URL: http://droualb.faculty.mjc.edu.

[10] M.M. Escribese and D. Barber. "New insight into cancer immunotherapy". In: *Allergologia et Immunopathologia* 45.Supplement 1 (2017). Sagunto's Second Scientific Meeting on Immunotherapy. Regulation and Current Situation., pp. 50–55. ISSN: 0301-0546. DOI: 10.1016/j.aller.2017.09.013.

[11] M. A. Felmlee, M. E. Morris, and D. E. Mager. "Mechanism-based pharmacodynamic modeling". In: *Computational Toxicology: Volume I* (2012), pp. 583–600.

[12] H. A. Friis and M. G. Edwards. "A family of MPFA finite-volume schemes with full pressure support for the general tensor pressure equation on cell-centered triangular grids." In: *Comput. Phys.* (2011), pp. 205–231.

[13] Cooper G.M. *Elements of human cancer*. Jones and Bartlett Publishers., 1992.

[14] *Hydraulic conductivity*. 2017. URL: https://en.wikipedia.org/wiki/Hydraulic_conductivity.

[15] E.L. Ince, I.N. Sneddon, and L. T. Baxter. "The solution of ordinary differential equations". In: *Longman mathematical texts*. Ed. by Kenneth L. Audus and T. J. Raub. New York: Longman science and technical, 1987.

[16] R. K. Jain and L. T. Baxter. "Mechanisms of Heterogeneous Distribution of Monoclonal Antibodies and Other Macromolecules in Tumors: Significance of Elevated Interstitial Pressure". In: *Cancer Research* (1988).

[17] N. James. *Interstitial fluid*. 2017. URL: http://study.com/academy/lesson/interstitial-fluid-definition-pressure-composition.html.

[18] S. H. Jang et al. "Drug delivery and transport to solid tumors". In: *Pharmaceutical research* 20.9 (2003), pp. 1337–1350.

[19] W. C. Krumbein. "The Flow of Homogeneous Fluids through Porous Media. M. Muskat". In: *The Journal of Geology* 46.6 (1938), pp. 902–903. DOI: 10.1086/624705.

[20] L.J. Liu et al. "Phenomenological model of interstitial fluid pressure in a solid tumor". In: *Physical Review E* 84.2 (2011), p. 021919.

[21] M. Schlesinger L.J. Liu. "Interstitial hydraulic conductivity and interstitial fluid pressure for avascular or poorly vascularized tumors". In: *Journal of Theoretical Biology* (2015).

[22] Liu L.J. et al. "Estimation of Tumor Interstitial Fluid Pressure, TIFP, Noninvasively." In: *Journal of Theoretical Biology* (2016).

[23] U.S. National Library of Medicine. *How do cancer cells grow and spread?* 2016. URL: https://www.ncbi.nlm.nih.gov/pubmedhealth/PMH0072594/.

[24] M. Charjouei Moghadam et al. "Numerical simulation of the tumor interstitial fluid transport: Consideration of drug delivery mechanism". In: *Microvascular Research* 101 (2015), pp. 62–71.

[25] J. Lagergren N. Beerenwinkel C. D Greenman. "Computational Cancer Biology: An Evolutionary Perspective". In: *PLOS Computational Biology* 12.2 (Feb. 2016), pp. 1–12. DOI: 10.1371/journal.pcbi.1004717.

[26] Creech J. O. et al. "Chemotherapy of cancer: regional perfusion utilizing an extracorporeal circuit". In: *Annals of surgery* 148.4 (1958), p. 616.

[27] *Oncotic pressure*. 2017. URL: https://en.wikipedia.org/wiki/Oncotic_pressure.

[28] World Health Organization. *International Classification of Diseases (ICD-10)*. World Health Organization, 1991.

[29] *Osmotic pressure*. 2017. URL: https://en.wikipedia.org/wiki/Osmotic_pressure.

[30] L. Pecorino. *Molecular biology of cancer*. Oxford university press, 2008.

[31] I. Prieto et al. "The role of immunonutritional support in cancer treatment: Current evidence". In: *Clinical Nutrition* (2017).

[32] M. Sefidgar et al. "Effect of tumor shape, size, and tissue transport properties on drug delivery to solid tumors". In: *Journal of biological engineering* 8.1 (2014), p. 12.

[33] M. Sefidgar et al. "Numerical modeling of drug delivery in a dynamic solid tumor microvasculature". In: *Microvascular research* 99 (2015), pp. 43–56.

[34] J. Shewchuk. *Triangle grid generator*. URL: https://www.cs.cmu.edu/~quake/triangle.html.

[35] Silverstein. *Conquering a Deadly Disease*. 2006.

[36] Chen P. Soltani M. "Numerical Modeling of Fluid Flow in Solid Tumors". In: (2011).

[37] M. Soltani et al. "Spatiotemporal distribution modeling of PET tracer uptake in solid tumors". In: *Annals of Nuclear Medicine* 31.2 (2017), pp. 109–124. ISSN: 1864-6433. DOI: 10.1007/s12149-016-1141-4.

[38] Daniel E. Spratt et al. "A Systematic Review and Framework for the Use of Hormone Therapy with Salvage Radiation Therapy for Recurrent Prostate Cancer". In: *European Urology* (2017). ISSN: 0302-2838. DOI: 10.1016/j.eururo.2017.06.027.

[39] E. H Starling. "On the absorption of fluids from the connective tissue spaces". In: *Classic Papers in Critical Care* 19 (1896), p. 303.

[40] V.J. Stella and N.L. Pochopin. "Lipophilic prodrugs and the promotion of intestinal lymphatic drug transport". In: *Lymphatic Transport of Drugs*. CRC Press Boca Raton, FL, 1992, pp. 181–210.

[41] TutorVista.com. *Capillary hydrostatic pressure*. 2017. URL: http://www.tutorvista.com/biology/capillary-hydrostatic-pressure.

[42] Cancer research UK. *What is cancer?* 2014. URL: http://www.cancerresearchuk.org/about-cancer/what-is-cancer/how-cancers-grow.

[43] Johns Hopkins Medicine university. *What are tumors?* 2016. URL: http://pathology.jhu.edu/pc/BasicTypes1.php?area=ba.

[44] The Pennsylvania State University. *Hydrostatic and osmotic pressure of blood capillaries*. 2017. URL: https://online.science.psu.edu/bisc004_activeup002/node/5410.

[45] K. Wang, F. M. Kievit, and M. Zhang. "Nanoparticles for cancer gene therapy: Recent advances, challenges, and strategies". In: *Pharmacological Research* 114.Supplement C (2016), pp. 56–66. ISSN: 1043-6618. DOI: 10.1016/j.phrs.2016.10.016.

[46] E.W Weisstein. 2017. URL: http://mathworld.wolfram.com/SphericalCoordinates.html.

[47] W. Zhan, W. Gedroyc, and X. Y. Xu. "The effect of tumour size on drug transport and uptake in 3-D tumour models reconstructed from magnetic resonance images". In: *PloS one* 12.2 (2017), e0172276.